



Advanced nanomedicine for drug delivery and biotherapy

Edited by Karine Andrieux, Sophia Antimisiaris, Bice Conti
and Emilie Roger

Imprint

Beilstein Journal of Nanotechnology
www.bjnano.org
ISSN 2190-4286
Email: journals-support@beilstein-institut.de

The *Beilstein Journal of Nanotechnology* is published by the Beilstein-Institut zur Förderung der Chemischen Wissenschaften.

Beilstein-Institut zur Förderung der
Chemischen Wissenschaften
Trakehner Straße 7–9
60487 Frankfurt am Main
Germany
www.beilstein-institut.de

The copyright to this document as a whole, which is published in the *Beilstein Journal of Nanotechnology*, is held by the Beilstein-Institut zur Förderung der Chemischen Wissenschaften. The copyright to the individual articles in this document is held by the respective authors, subject to a Creative Commons Attribution license.



From shield to spear: Charge-reversible nanocarriers in overcoming cancer therapy barriers

Madhuri Yeduvaka¹, Pooja Mittal², Ameer Boyalakuntla¹, Usman Bee Shaik³, Himanshu Sharma⁴, Thakur Gurjeet Singh⁵, Siva Nageswara Rao Gajula^{*6} and Lakshmi Vineela Nalla^{*1}

Review

Open Access

Address:

¹Department of Pharmacology, GITAM School of Pharmacy, GITAM (Deemed to be University), Rushikonda, Visakhapatnam, Andhra Pradesh, India, ²GITAM School of Pharmacy, GITAM University, Rudraram, Patancheru, Sangareddy District, Hyderabad, India, ³GITAM School of Pharmacy, GITAM (Deemed to be University), Visakhapatnam, Andhra Pradesh, India, ⁴Chitkara College of Pharmacy, Chitkara University, Rajpura, Punjab-140401, India, ⁵Centre for Research Impact & Outcome, Chitkara College of Pharmacy, Rajpura- 140401, Punjab, India and ⁶Department of Pharmaceutical Analysis, GITAM School of Pharmacy, GITAM (Deemed to be University), Visakhapatnam, Andhra Pradesh, India

Email:

Siva Nageswara Rao Gajula^{*} - sgajula@gitam.edu;
Lakshmi Vineela Nalla^{*} - lnalla@gitam.edu

* Corresponding author

Keywords:

cancer; charge reversible nanocarriers; nanocarriers; targeted therapy; tumour microenvironment

Beilstein J. Nanotechnol. **2026**, *17*, 159–175.
<https://doi.org/10.3762/bjnano.17.10>

Received: 07 August 2025
Accepted: 05 December 2025
Published: 14 January 2026

This article is part of the thematic issue "Advanced nanomedicine for drug delivery and biotherapy".

Associate Editor: Y. Corvis



© 2026 Yeduvaka et al.; licensee Beilstein-Institut.
License and terms: see end of document.

Abstract

Cancer remains a significant global health burden, responsible for 16.8% of all deaths and 30.3% of premature mortality due to noncommunicable diseases, and continues to be one of the leading causes of death worldwide despite medical progress. Conventional treatment methods such as surgery, chemotherapy, and radiotherapy often face challenges such as systemic toxicity, drug resistance, and poor tumour selectivity. In response to these limitations, nanotechnology-based drug delivery systems have gained prominence for enhancing solubility, improving molecular stability, enabling controlled drug release, and prolonging systemic circulation, offering superior therapeutic outcomes over traditional approaches. Among these innovations, charge-reversible nanocarriers have attracted considerable attention due to their ability to overcome physiological and pathological barriers in the tumour microenvironment (TME) by altering their surface charge in response to specific stimuli, which enhances drug targeting while reducing off-target effects. These carriers leverage triggers such as changes in pH, enzymatic activity, redox conditions, temperature, light, ultrasound, X-rays, and magnetic fields to enable intelligent and controlled release of therapeutics. This review examines the crucial role of surface charge in cellular uptake and intracellular transport, highlighting recent advances that demonstrate improved targeting, reduced systemic toxicity, enhanced cellular internalisation, and the potential for integrated approaches,

including combination therapies and theranostics. Despite these promising developments, challenges related to nanocarrier stability, safety, manufacturing scalability, and regulatory approval still impede clinical translation. Nevertheless, emerging trends in nanocarrier design, the advancement of personalised medicine, and integration with therapies (e.g., immunotherapy) underscore the transformative potential of charge-reversible nanocarriers in revolutionising cancer treatment and improving patient outcomes.

Review

1 Introduction

Cancer remains a foremost global health challenge, characterized by uncontrolled cellular proliferation and the ability to invade and metastasize to distant sites. Unlike normal cells, cancer cells bypass regulatory mechanisms to form tumours and spread via lymphatic or circulatory systems, such as malignant breast epithelial cells metastasizing to axillary lymph nodes [1]. Leukaemias and other haematological malignancies spread differently, affecting the bone marrow, lymph nodes, and the blood [2]. According to the latest GLOBOCAN and World Health Organization data, cancer ranks as the leading cause of death among individuals aged 30 to 69 in 177 countries, accounting for 16.8% of all deaths globally and 30.3% of premature mortality from noncommunicable diseases [3]. Traditional cancer treatments, such as chemotherapy, hormonal therapy for hormone-sensitive cancers, and radiation therapy, primarily aim to eliminate rapidly dividing cancer cells. However, these conventional approaches often face limitations in specificity and long-term efficacy [4-6]. In recent years, significant advancements have transformed the therapeutic landscape with the introduction of gene therapy, stem cell therapy, targeted therapy, and immunotherapy modalities that enable more precise and personalized cancer management [7]. In parallel, complementary strategies such as photodynamic therapy and hyperthermia further enhance treatment effectiveness, collectively reflecting the ongoing evolution of cancer therapeutics [8]. Despite their efficacy, conventional therapies often cause severe side effects. Chemotherapy induces anaemia and immunosuppression, radiation triggers fatigue and psychological strain, surgery carries risks of organ damage, and hormone therapy disrupts endocrine balance, highlighting the pressing need for innovative solutions. An example would be smart nanocarrier drug delivery systems that enhance targeting precision and mitigate adverse effects [9,10].

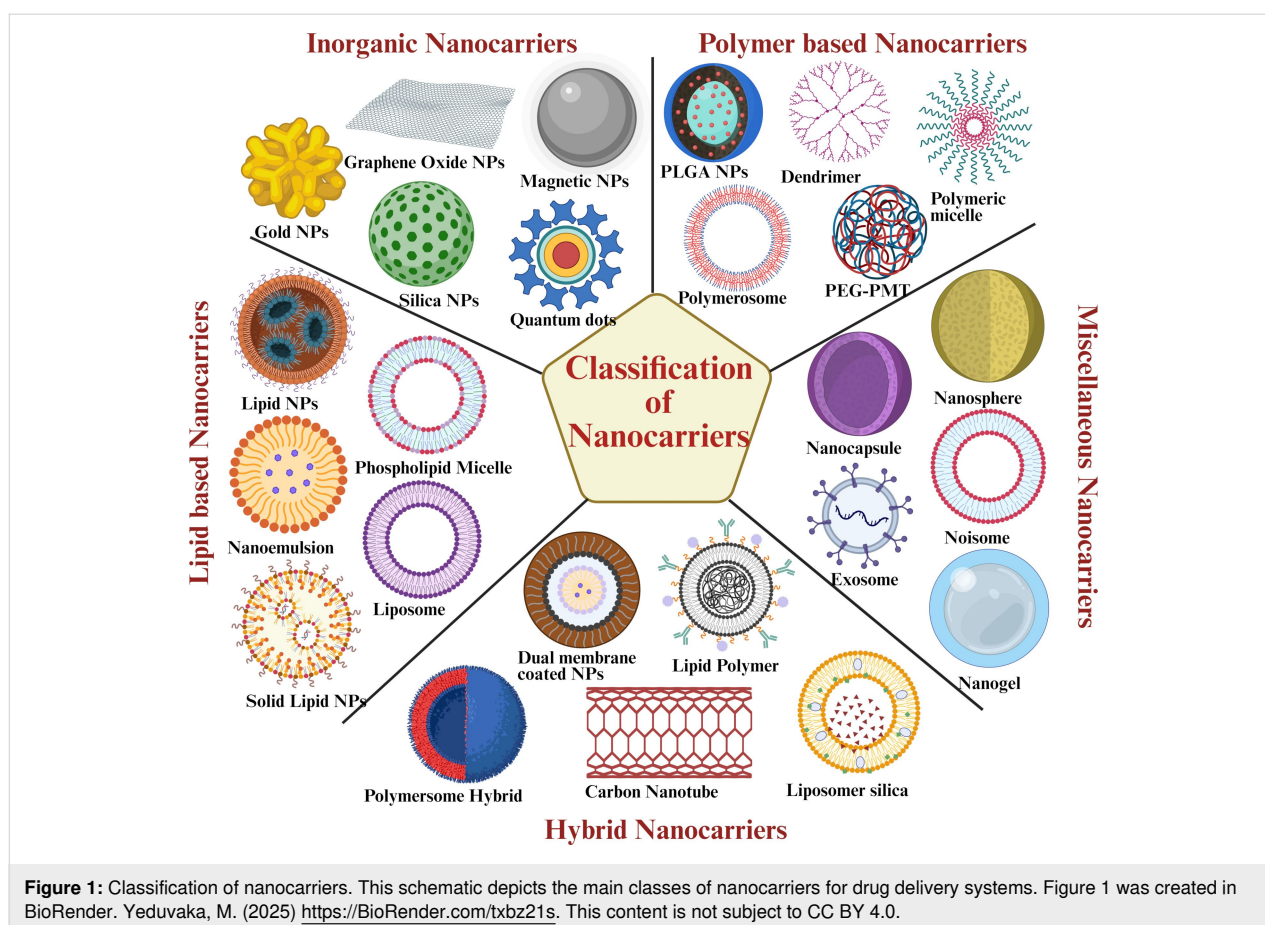
Nanotechnology-based drug delivery systems have revolutionised cancer treatment by improving drug solubility, stability, and biodistribution while protecting fragile biomolecules such as proteins and nucleic acids [11]. Through targeted and sustained release, these systems enhance therapeutic efficacy, prolong circulation, and reduce systemic toxicity compared to conventional formulations [12,13]. As illustrated in Figure 1, nanocarriers encompass diverse types including polymeric nanoparticles, liposomes, micelles, dendrimers, lipid-

based carriers, carbon-based nanomaterials, and gold nanoparticles.

They exhibit versatile structures (1–100 nm) with diverse morphologies (e.g., spherical, tubular, or conical shapes [14]). With advancements in nanocarrier-based cancer therapy, recent research has increasingly emphasised refining their physicochemical traits, especially surface charge, to boost therapeutic outcomes. A notable development in this context is the emergence of charge-reversible nanoscale drug delivery systems (CR-NDDSs) [15]. These systems can switch their surface charge in response to tumour microenvironment (TME) triggers such as pH changes, redox states, or enzymatic activity, enhancing drug stability, facilitating cellular uptake, and enabling targeted drug release. This responsive functionality gives CR-NDDSs a distinct edge over conventional nanocarriers, representing a significant leap toward more precise and efficient cancer treatments [16]. This review aims to present an in-depth analysis of charge-reversible nanocarriers (CRNs) in cancer treatment, emphasising their underlying mechanisms, benefits, and therapeutic value. It also explores existing challenges and prospects to advance their translation into clinical cancer treatments.

2 Concept of charge-reversible nanocarriers

Surface charge plays a vital role in the efficiency and functionality of nanocarriers used for drug delivery [13]. Among various physicochemical parameters, the surface charge is essential for determining nanocarrier interactions with biological membranes, cellular uptake, and biodistribution [17]. With a positive charge, the nanocarrier tends to be absorbed by high plasma proteins and cleared faster from the bloodstream. In contrast, those with neutral or negative charge exhibit longer circulation times, reduced immune clearance, and improved therapeutic efficacy. Further, positively charged nanocarriers exhibit enhanced cellular uptake due to their electrostatic interaction with negatively charged cell membranes; however, they may also induce cytotoxicity and rapid clearance by the mononuclear phagocyte system [18]. Moreover, surface charge influences aggregation behaviour, colloidal stability, and protein corona formation, directly impacting the therapeutic efficacy of nanocarriers. Optimising surface charge is essential for enhancing the therapeutic efficacy and safety profiles of



nanocarriers in clinical applications [15]. The functional mechanism of CRNs (Figure 2) is designed to enhance the selectivity and efficacy of anticancer drug delivery systems, along with their behaviour in response to the acidic environment of biofilms within the TME, where the nanoparticles are activated by pH changes and demonstrate their potential for site-specific drug delivery [19].

This strategy also enables controlled drug release, as the pH-sensitive charge reversal triggers site-specific drug unloading in acidic tumour microenvironments or intracellular compartments like endosomes and lysosomes [20]. Bobrin et al. studied that a PEI-based polymeric nanocarrier demonstrated charge reversal from negative (pH 7.4) to positive (pH 6.8) under tumour pH. This transformation facilitated tumour cell uptake and site-specific unloading of siRNA within lysosomes via protonation-induced release [21]. Similarly, a study presented a polymer nanocarrier with acid-triggered charge reversal achieving >60% drug release within 48 h at lysosomal pH 5.0, compared to less than 10% release at physiological pH 7.4. The system used tethered imidazole groups for protonation-driven charge inversion, ensuring precise intracellular payload unloading [22]. Furthermore, the neutral charge state during

systemic circulation helps to reduce cytotoxicity by minimising nonspecific protein adsorption and immune system activation. A study by Yuan et al. showed that zwitterionic and neutral nanoparticles possess highly hydrated, charge-balanced surfaces that minimize serum protein adsorption, complement activation, and cytokine release (IL-6, TNF- α). In murine models, these particles exhibited reduced systemic inflammation and enhanced circulation stability [23]. Neutral PEG or hydroxyl-modified nanoparticles demonstrated significantly lower protein binding, opsonization, and phagocytic uptake compared to their charged counterparts, thereby reducing immune clearance and cytotoxicity [24].

Overall, these findings demonstrate that surface charge modulation through pH-sensitive or neutral/zwitterionic designs enhances therapeutic precision, circulation stability, and biocompatibility by enabling controlled drug release while minimising immune recognition and cytotoxicity. CRNs exhibit diverse mechanisms, applications, and advantages that enhance their performance in targeted and controlled drug delivery (Table 1). The detailed mechanism of CRNs in response to various environmental stimuli is described in Figure 3.

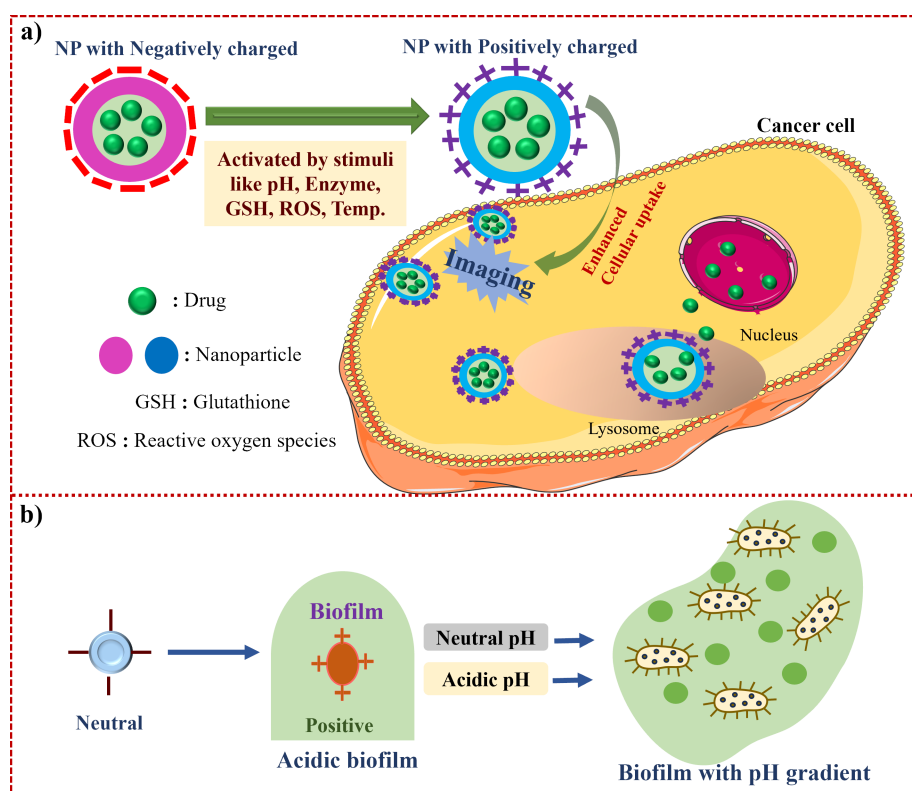


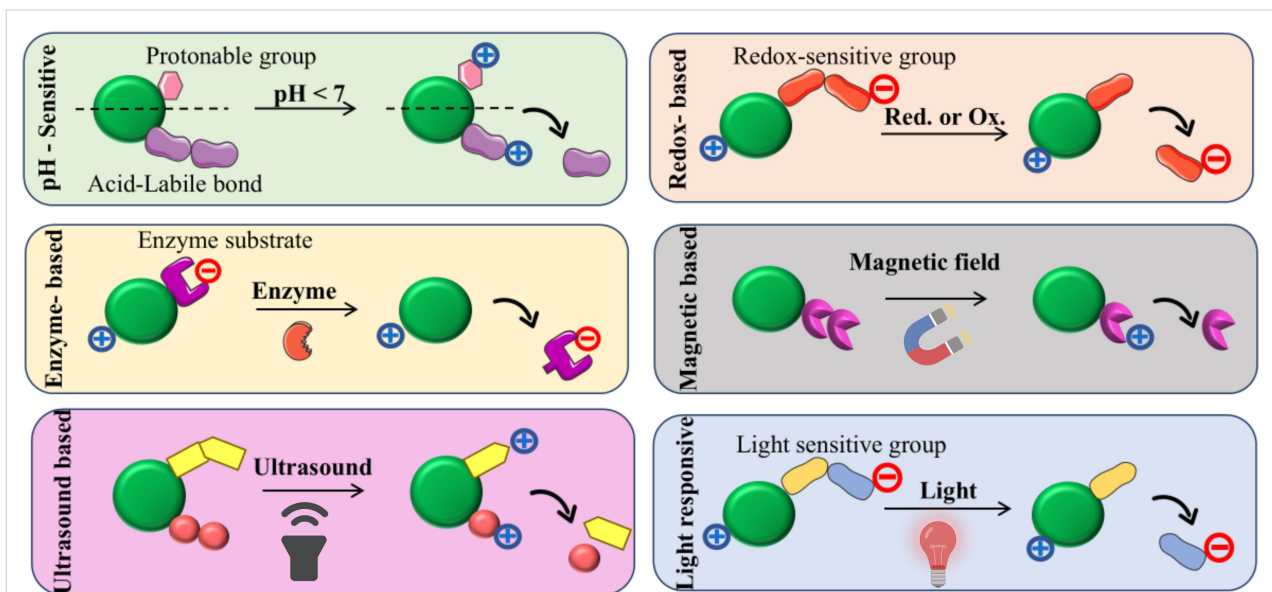
Figure 2: Schematic representation of charge-reversible nanocarrier system for tumour therapy. a) In general mechanism of CRNs activated by various stimuli for targeted therapy, b) charge reversal of nanocarriers exhibiting responsiveness to the acidic environment in biofilms. The images of EMPTY CELL, NUCLEUS and PROTEIN were provided by Servier Medical Art (<https://smart.servier.com/>), licensed under CC BY 4.0 (<https://creativecommons.org/licenses/by/4.0/>).

Table 1: Types of charge-reversible nanocarriers, their mechanisms, applications, and advantages.

Type of charge-reversible nanocarrier	Mechanism of charge reversal	Application in drug delivery	Advantages	Examples	Ref.
pH-sensitive	protonation/deprotonation in acidic tumour environment (pH 6.5–6.8)	targeted drug release in acidic tumour sites and intracellular compartments	enhanced tumour penetration, improved cellular uptake, and minimised off-target effects	doxorubicin-loaded pH-sensitive liposomes; polymeric nanoparticles with pH-responsive bonds	[25-27]
enzyme-responsive	enzyme-mediated cleavage of functional groups or linkers	site-specific drug release where enzymes (e.g., MMPs) are overexpressed	high specificity, tumour-selective activation, improved efficacy	MMP-responsive peptide-modified nanoparticles	[28-30]
redox-sensitive	disulfide bond cleavage triggered by high glutathione (GSH) levels	intracellular drug release in reductive tumour environments	increased drug concentration in tumour cells, reduced systemic toxicity	GSH-responsive disulfide-linked polymeric micelles; DTPA-DOX nanoparticles	[31-33]
light-responsive	structural change or ROS generation upon light exposure (UV–NIR)	on-demand drug release via external light	spatial/temporal control, selective tumour targeting, phototherapy compatibility	spiropyran-based nanocarriers; UV-sensitive nanocarriers	[34-36]
ultrasound-responsive	cavitation or thermal effects trigger reversible interactions	enhanced drug penetration through deep tissues	noninvasive targeting, controlled release, and high biocompatibility	ultrasound-triggered liposomes or microbubbles	[37,38]

Table 1: Types of charge-reversible nanocarriers, their mechanisms, applications, and advantages. (continued)

X-ray-responsive	ROS generation and bond cleavage under X-ray exposure	drug release during radiotherapy for synergy	enhanced radiotherapy, reduced drug dosage, dual therapy	gold nanoparticle-based radiosensitizers	[39-41]
magnetic-responsive	localised hyperthermia via alternating magnetic field	magnetically guided, localised drug release	noninvasive precision therapy, MRI compatibility, controlled targeting	SPIONs-based magnetic liposomes	[42-44]

**Figure 3:** Illustrative mechanisms of various charge-reversible nanocarrier (CRN) types. Figure 3 was created in BioRender. Yeduvaka, M. (2025) <https://BioRender.com/2d2dp36>. This content is not subject to CC BY 4.0.

2.1 pH-responsive charge-reversible nanocarriers

When exposed to the acidic cancer microenvironment (pH 6.5–6.8), CRNs undergo a pH-sensitive change in their surface charge [4]. The breakdown of adenosine triphosphate to release protons in the cancer tissue, along with aerobic glycolysis, which generates lactic acid, results in a decrease in the pH of the TME, which is a widely observed phenomenon [22]. Typically, the pH of most solid tumours ranges between 5.7 and 7.8, differing significantly from the physiological blood pH of 7.4 [23]. These nanocarriers typically possess pH-sensitive chemical bonds or functional groups that undergo protonation or deprotonation, leading to a charge switch from negative to positive. This charge reversal enhances cellular uptake by facilitating better interaction with the negatively charged cell membrane, improving drug delivery efficiency [45]. For example, nanoparticles engineered with pH-responsive polymers facilitate the controlled release of therapeutic agents specifically within the acidic tumour microenvironment, thereby improving treatment efficacy. A notable study by Liu Y et al. described polymeric micellar nanoparticles incorporating hydrazone

bonds within their core–shell structure; these hydrazone linkages are selectively cleaved under acidic conditions, such as those found in endosomes and lysosomes. Upon bond cleavage, the nanoparticles undergo a surface charge shift by exposing cationic groups, which significantly enhances cellular adsorption and uptake. This charge-switching mechanism, exemplified by PEG-*b*-poly(L-lysine)-hydrazone-doxorubicin micelles from the cited study, enables targeted drug delivery with improved intracellular release and reduced systemic toxicity, highlighting the therapeutic advantage of pH-sensitive hydrazone bonds in nanocarrier design [46]. Another work involved polymers modified with weak acidic groups (e.g., carboxylic acids or phosphates). Under neutral pH, the surface was negatively charged, but in acidic tumour tissues or endosomes, protonation caused a charge reversal to positive, facilitating cell binding and internalisation, which improved drug accumulation within tumour cells [21]. These scientific findings exemplify the use of pH-sensitive bonds and functional groups that enable charge reversal, a strategy that significantly improves cellular interaction and drug delivery efficiency in tumour environ-

ments. Additionally, it should be noted that, unlike pH-responsive charge reversal, which is reversible due to protonation and deprotonation processes, other stimuli, such as enzymatic cleavage, redox reactions, or magnetic heating induce irreversible charge changes since they involve permanent chemical or structural modifications to the nanocarrier surface.

2.2 Enzyme-responsive nanocarriers

Enzymes are essential components that manage cellular function and various bodily processes. Certain enzymes, such as matrix metalloproteinases (MMPs), hyaluronidases (HAases), γ -glutamyltransferases (GGTs), aminopeptidases (APNs), esterases, and others, are found more regularly in cancer cells [32,47-49]. By encapsulating specific enzyme substrates in nanocarriers, novel drug delivery systems may respond to over-expressed enzymes both inside and outside cells. CRNs that are enzyme-responsive specifically utilise the enzyme presence in the TME to trigger drug release. A study by Liu et al. developed nanomicelles that respond to cathepsin B overexpressed in tumours, undergoing enzymatic cleavage of peptide bonds which causes nanocarrier destabilization, charge reversal, and size reduction. These transformations triggered drug release within the tumour tissue and improved nuclear targeting, optimizing therapeutic efficacy [50]. Thereafter, a study by Lin et al. developed MMP-2-responsive PEG-coated nanocarriers that, upon peptide cleavage, underwent PEG detachment, charge reversal, and size reduction, enhancing cellular uptake and tumour-specific drug release. This system effectively inhibited tumour growth with minimal systemic toxicity in mice [51]. These studies demonstrate how enzyme substrates embedded in nanocarriers enable the selective cleavage, charge reversal, and targeted delivery of drugs in response to cancer-associated enzymes.

2.3 Redox-sensitive nanocarriers

Redox-sensitive nanocarriers exploit the distinct intracellular environment of tumour cells, characterized by elevated levels of GSH and reactive oxygen species (ROS), to trigger on-demand drug release. These nanocarriers typically incorporate redox-sensitive chemical bonds, such as disulfide linkages, which remain stable in blood circulation but undergo cleavage in the reductive tumour microenvironment, leading to structural transformation and payload discharge. By taking advantage of the high GSH concentration and acidic extracellular pH of the tumour, these systems can achieve precise site-specific drug release and improved therapeutic efficacy while minimizing systemic toxicity [52]. For example, a nanocarrier constructed by conjugating 2,3-dimethylmaleic anhydride (DMA) and 3,3-dithiopropionic acid-modified doxorubicin (DTPA-DOX) onto poly(ethylene glycol)-*b*-poly(L-lysine) (PEG-*b*-PLL) encapsulates triptolide in its hydrophobic core. Under acidic tumour

extracellular pH, the DMA group triggers a charge reversal, improving cellular uptake, whereas the high intracellular GSH levels cleave the disulfide bond in DTPA-DOX, releasing the drug payload specifically inside tumour cells. This dual redox and pH-sensitive strategy ensures controlled and efficient delivery of multiple drugs in response to the biochemical cues of the tumour microenvironment, enhancing anticancer activity with reduced off-target effects [53].

2.4 Light-responsive nanocarriers

Light-sensitive nanocarriers represent an innovative approach to regulated drug delivery, utilizing photosensitive materials such as graphene, azobenzene, and gold nanorods [54]. Upon exposure to UV-vis or near-infrared (NIR) light, these materials undergo structural changes or generate ROS, triggering controlled release of their therapeutic cargo. This precise spatiotemporal control over drug release and therapeutic activity enhances treatment efficacy and minimises off-target effects, thus seamlessly complementing other stimuli-responsive delivery systems discussed earlier.

Earlier, a study by Hu et al. demonstrated that nanocarriers functionalized with photoisomerizable azobenzene groups, upon UV-vis or NIR light exposure, azobenzene undergoes reversible trans-cis isomerisation, inducing structural changes that regulate cargo release [55]. Additionally, Choi et al. demonstrated that nanocarriers incorporating graphene oxide (GO) loaded with photosensitizers generate ROS upon NIR irradiation, enabling effective tumour photodynamic therapy. The study highlights the excellent light absorption and ROS generation capacity of the material, allowing targeted tumour cell damage while sparing healthy tissues [56]. Similarly, a study reports thermo-responsive gold nanorod vesicles (USGRV-17-AAG) integrate NIR-II photothermal therapy and chemotherapy by encapsulating the HSP90 inhibitor 17-AAG within UCST-type polymer-modified gold nanorods. Upon 1064 nm irradiation, they exhibit 65.1% photothermal conversion efficiency and trigger heat-induced 17-AAG release, achieving 98.86% of tumour growth inhibition in mice [57]. Collectively, these studies validate that light-sensitive nanocarriers incorporating photosensitive materials are capable of controlled drug release and phototherapeutic tumour ablation with high specificity and minimised collateral damage.

2.5 Ultrasound-responsive nanocarriers

Ultrasound-responsive CRN is a novel technique for precise and effective gene or drug delivery. When exposed to ultrasonic treatment, the dynamic coordinating leakages, such as carboxyl-calcium interaction, on which these nanocarriers rely, may be reversibly broken and re-established. For example, a study by Li et al. designed calcium-ion-crosslinked sodium-

alginate-coated mesoporous silica nanoparticles (MSNs) for ultrasound-triggered drug delivery. High- or low-intensity focused ultrasound (HIFU/LIFU) induced reversible disruption of carboxyl–calcium bonds, enabling precise, on-demand release [58]. This confirms that ultrasound-responsive CRNs employing calcium-ion-crosslinked sodium-alginate coatings on mesoporous silica nanoparticles offer reversible, on-demand, and biocompatible drug release options. Such systems harness ultrasound-induced cavitation to disrupt and reform ionic bonds, showing considerable promise for cancer therapy and other clinical applications.

2.6 X-ray-responsive nanocarriers

These systems offer innovative mechanisms for targeted drug delivery systems and enhanced therapeutic efficiency. These nanoparticles are designed to release therapeutic agents upon exposure to X-rays, which can generate ROS [59] and activate drug release mechanisms. For instance, nitroimidazole-ligated gold nanoparticles release nitrate, a precursor for nitric oxide, when irradiated with clinically relevant X-rays. This release sensitises hypoxic cancer cells to radiation therapy by generating reactive oxygen and nitrogen species, thereby improving treatment outcomes [60]. Additionally, an X-ray-activated nanoscale platform can produce significant quantities of ROS-enhancing PDT effects in cancer treatment by conjugating photosensitizers to these nanoparticles; the efficiency of ROS generation increases under X-ray radiation compared to that under conventional methods. These dual-functionality CRNs improved drug delivery precision and enhanced the overall effectiveness of radiotherapy [61]. A study by Liu et al. developed the nanoscale coordination polymer Hf-nIm@PEG (HNP), which integrates hafnium ions (Hf^{4+}) with 2-nitroimidazole and a PEG-modified lipid shell, enabling multifunctional X-ray-responsive therapy. Upon low-dose of X-ray irradiation, Hf^{4+} deposits radiation energy to induce DNA damage while 2-nitroimidazole releases NO to block DNA repair, relieve hypoxia, and produce reactive nitrogen species (RNS) that trigger apoptosis. Moreover, Hf^{4+} activates the cGAS–STING immune pathway, enhancing antitumour immunity and achieving synergistic radio-immunotherapy against cancer [62].

2.7 Magnetic-responsive nanocarriers

Magnetic-responsive CRNs utilise magnetic fields to enhance drug delivery and therapeutic efficiency [63]. Superparamagnetic iron-oxide nanoparticles (SPIONs), which react to external magnetic fields and enable selective accumulation in tumour areas, are commonly used to create these nanocarriers [64]. These systems follow thermo-sensitive binding strategies that permit targeted drug release (e.g., DOX, geldanamycin) under alternating magnetic fields while preserving systemic safety [65]. Core–shell magnetic nanoparticles

($\text{Fe}_3\text{O}_4@P(\text{MEO}_2\text{MA}_{60}\text{-OEGMA}_{40})$) combine magnetic hyperthermia with controlled doxorubicin release, achieving localized heating ($\approx 42^\circ\text{C}$) under an alternating magnetic field to trigger drug release. They show minimal release at physiological temperature, near-complete release under hyperthermia, and excellent tumour-targeting efficacy with high biocompatibility [66]. Iron oxide nanocubes coated with a thermoresponsive polymer (TR-DOXO) enabled magnetic-hyperthermia-triggered doxorubicin release at temperatures of $\geq 44^\circ\text{C}$, effectively targeting resistant and quiescent cancer stem cells. Combined TR-DOXO and magnetic field treatment achieved complete tumour inhibition in mice, demonstrating strong hyperthermia–chemotherapy synergy [67]. The combination of magnetic targeting, thermal stimuli responsiveness, and charge-reversal mechanisms offers a powerful route to overcome multidrug resistance and enhance cancer treatment precision.

3 Role of charge-reversible nanocarriers in cancer therapy

Polymer-based CRNs have shown significant promise in improving cancer treatment by precisely regulating drug activity within the tumour microenvironment. Their capacity to switch surface charge in response to specific biological triggers enhances therapeutic effectiveness [68]. This section highlights the diverse functions of CRNs, such as enhanced targeting, minimised off-target effects, controlled drug release, and co-delivery strategies. Furthermore, their use in theranostics and promoting cellular uptake emphasises their potential in advancing personalised and more efficient cancer therapies. An overview of various CRNs employed in targeted cancer therapy is presented in Table 2, illustrating their key functionality, mechanism of drug release, and surface modification.

3.1 Targeted delivery

The charge-reversible NPs encapsulating diagnostic probes and therapeutic drugs result in efficient tumour-targeted delivery [86]. To achieve targeted delivery, charge reversal needs to be precisely controlled within a small pH range [87]. Chen et al. developed pH-activatable charge-reversal supramolecular nanocarriers, named $\text{MI}_7\text{-}\beta\text{-CD/SA}$ NPs, which show targeted delivery and controlled release of celastrol in tumour cells, enhancing drug accumulation and therapeutic effects while minimising toxicity to normal cells [69]. Wang et al. developed a pH/hypoxia synergistic nanocarrier technology, which, with the aid of azo and sulfamide-based zwitterions, achieved targeted medication release and deep tumour penetration [70]. Miao et al. designed a pH/reduction-sensitive, charge-reversal PMAABACy/CS/CS-DMMA nanohydrogel, with excellent biodegradability and biocompatibility, which holds strong potential as a doxorubicin drug carrier for targeted nuclear delivery in cancer therapy [71]. The charge-reversal

Table 2: Overview of charge-reversible nanocarriers in targeted cancer therapy.

Nanoparticle type	Targeted cancer therapy	Functional groups involved in charge reversal	Mechanism of drug release	Surface modification	Key results	Ref.
Role of CRNCs: targeted delivery						
pH-activatable supramolecular MI7-β-CD/SA NCs	hepatocellular carcinoma	protonation/deprotonation of the carboxyl (–COOH/–COO [–]) and imidazole (–NH ⁺ /neutral) groups on MI7-β-CD/SA nanoparticles	diffusion-based drug release	sodium alginate and imidazolyl-decorated cyclodextrin	- 90% cumulative release of celastrol at pH 5.0 - high apoptosis rate	[69]
pH/hypoxia-responsive COF-based NCs	anticancer drug delivery for solid tumours	protonation of imine (–C=N–) groups under acidic pH causes surface charge to switch	hypoxia reduction of azobenzene to amines	zwitterionic polymer (sulfamide-based)	- surface potential rose from –15.45 mV at pH 8.0 to 12.24 mV at pH 5.4 - charge switched from negative to positive at pH ≈6.5, attributed to protonation of imine groups	[70]
dual pH/redox-sensitive PMAABACy/CS/CS-DMMA NPs	doxorubicin to tumour cells	cleavage of DMMA–amide bonds at acidic pH exposes chitosan amines (–NH ₂), switching surface charge	GSH-triggered degradation of sulfide cross-links in the intracellular tumour environment	dimethylmaleic anhydride-modified chitosan (CS-DMMA)	- PMAABACy cores showed an initial negative zeta potential of –38.2 mV - after adsorption of the cationic CS layer, the potential reversed to +29.3 mV - following the addition of the CS-DMMA polyanion layer, the potential shifted back to negative, measuring –28.4 mV	[71]
mesoporous silica NPs (MSNs-COS-CMC)	cervical carcinoma	the carboxyl (–COOH) and amino groups on carboxymethyl chitosan (CMC) and chitosan oligosaccharide (COS) are responsible for the charge reversal	endocytic uptake and pH-triggered release for enhanced delivery	chitosan oligosaccharide and carboxymethyl chitosan	- higher cytotoxicity at acidic pH (6.5): IC ₅₀ = 0.6 μg/mL - much lower IC ₅₀ than at physiological pH (7.4): IC ₅₀ = 5.8 μg/mL - more potent than free DOX at pH 6.5: free DOX IC ₅₀ = 2.6 μg/mL	[72]
Role of CRNCs: reduced off-target effects						
GelMA-PEDOT-based NCs	breast cancer and other tumours	the thiophene groups (C–S–C) of the PEDOT backbone and the associated p-toluenesulfonate (–SO ₃ [–]) dopant ions undergoing charge reversal	controlled release via electrical or environmental triggers	functionalized with GelMA hydrogel and PEDOT polymer	- improved tumour uptake, reduced off-target toxicity, tuneable release	[73]
mesoporous silica-based NCs (MCM@CS@PEG-APT)	breast cancer	the amino groups on chitosan, which protonate to –NH ₃ ⁺ under acidic pH	increase DOX uptake and 73% release at pH 5.5 over 10 days	chitosan and polyethylene glycol coating for biocompatibility, with aptamer functionalization	- 99.42% DOX loading - 98% cell uptake - 42.7% co-delivery (DOX + DNA)	[74]

Table 2: Overview of charge-reversible nanocarriers in targeted cancer therapy. (continued)

mixed micelles with nimotuzumab (NTZ-DCMMs)	hepatocellular carcinoma	protonation of $-NH_2$ to $-NH_3^+$ and deprotonation of $-COOH$ to $-COO^-$ under varying pH causes surface charge reversal	reduction-sensitive cleavage of disulfide bonds in PEG- <i>b</i> -P(GMA-ss-DOX)	nimotuzumab (anti-EGFR antibody)	- enhanced tumour drug accumulation, inhibited growth, and reduced cardiotoxicity	[75]
mesoporous silica nanoparticles (MSNs)	HER2-positive breast cancer	amine ($-NH_2$) and carboxyl ($-COOH$) groups undergo protonation and deprotonation, driving the reversible charge reversal of the nanocarriers	controlled release via pH-sensitive poly(tannic acid) "gatekeeper"	poly(tannic acid) polymer shell with HER2 antibody conjugation	- efficient tumour inhibition with minimal side effects and low myocardial toxicity - 2.2× higher tumour targeting using pH-responsive nanocarriers - selective drug release: 67.9% at acidic pH vs 8.1% at physiological pH - improved cytotoxicity: $IC_{50} = 0.32 \mu\text{g/mL}$ (nanocarrier) vs $0.42 \mu\text{g/mL}$ (free drug).	[76]
Role of CRNCs: controlled drug release						
redox/pH dual-responsive HA-SH/CS nanoparticles	breast cancer	amino groups, which are protonated to $-NH_3^+$ in acidic environments	GSH-triggered disulfide bond cleavage and pH-triggered release at acidic intracellular environments	thiol-hyaluronic acid (HA-SH) and chitosan (CS) for charge reversibility and CD44 targeting	- high DOX-loading (45.7 wt %), rapid release (87.8 wt % at pH 4.5, 10 mM GSH), and improved cellular uptake	[77]
pH-responsive charge-reversal polyelectrolyte and integrin $\alpha\beta_3$ mono-antibody	DOX to cancer cells (U87 MG)	citraconic amide ($-CONH-C(COO^-)CH_3$) moieties on PAH-Cit, which hydrolyse to expose protonated amine groups on poly(allylamine)	releasing DOX from GO into the nucleus	functionalized GO with charge-reversal polyelectrolytes and integrin $\alpha\beta_3$ mono-antibodies	- high DOX loading, targeted U87 MG cell uptake via $\alpha\beta_3$, and effective nuclear delivery for enhanced therapy - at physiological pH (pH 7.4), PAH-Cit is positively charged - specifically, at pH 5.0, PAH-Cit reverses to a negatively charged state	[78]
pH-responsive charge-reversal and photo-crosslinkable polymer NPs	DOX with inhibitory effects on tumour cell growth	dimethylamino ($-N(CH_3)_2$) and carboxyl ($-COOH/-COO^-$) groups undergo protonation–deprotonation	pH-dependent release and UV-triggered photo-cleavage enable precise DOX control	coumarin-functionalized copolymer with reversible photo-reactions ($\lambda = 365 \text{ nm}$ cross-linking, $\lambda = 254 \text{ nm}$ cleavage)	- $pH \leq 4$: micelles show a positive zeta potential ($\approx +19.44 \text{ mV}$) - $pH 5.0-7.8$: zeta potential decreases and approaches 0 mV - around $pH 8.6$: zeta potential is near neutral ($\approx 0 \text{ mV}$) - $pH > 10$: nanoparticles exhibit a negative zeta potential ($\approx -27.88 \text{ mV}$)	[79]
pH-responsive charge-reversal polymer-coated mesoporous silica NPs	cervical carcinoma	charge reversal occurs via citraconic amide groups, which hydrolyse to primary amine groups under acidic conditions	acidic pH triggers charge reversal, facilitating drug release and endosome escape to ensure nuclear targeting	coating with poly(allylamine)-citraconic anhydride (PAH-cit) and (3-aminopropyl) triethoxysilane (APTES)	- efficient DOX delivery to nuclei, real-time confocal laser scanning microscopy imaging, and effective cancer cell killing with good biocompatibility	[80]

Table 2: Overview of charge-reversible nanocarriers in targeted cancer therapy. (continued)

Role of CRNCs: combination therapy (or) co-delivery						
dual-responsive shape-transformable charge-reversible nanomedicine system (DHP@BPP)	breast cancer and lung metastasis	imidazole groups of histidine residues undergo protonation, causing charge reversal	acidic TME protonates histidine, inducing DHP shedding and charge reversal; MMP-2 cleaves BPP to release BBR, and ROS from PPA under 650 nm laser enhances ICD	PEG-modified dPPA for tumour targeting; DHP electrostatically adsorbed onto BPP for charge reversal and extended circulation	- charge reversal in DHP@BPP NPs was quantitatively confirmed by a zeta potential shift from -16.4 to $+12.5$ mV at pH 6.5 - results in 1.62× deeper tumour penetration and significantly enhanced cellular uptake under acidic, MMP-2-rich conditions	[81]
metal–organic framework (MOF)-based polymer-coated hybrid NPs	breast cancer	charge reversal occurs via hydrolysis of ortho ester groups, exposing amine groups on the inner MOF core	polymer degrades to expose MOF core, enabling multi-drug release, nuclear targeting, and tumour penetration	polymer coating stabilises and masks charge, revealing cationic MOF core in acidic tumours	- surface charge stayed negative (-33 mV) at pH 7.4 - charge switched to positive ($+28$ mV) at tumour-relevant pH 5.0 within 4 h, indicating polymer degradation and exposure of the cationic MOF core. - MCF-7/ADR cells showed significantly higher uptake at acidic pH, with ≈ 3.5 -fold greater DOX fluorescence at pH 6.5 compared to pH 7.4	[31]
silk sericin-based nanoparticles (MR-SNC)	breast cancer	amino, carboxyl ($-\text{COOH}$), and hydroxyl ($-\text{OH}$) groups in sericin undergo ionization, causing pH-dependent charge reversal	pH-dependent release: maximum at mildly acidic pH (pH 6)	pH-triggered charge reversal boosts cellular uptake and drug release by disrupting sericin-electrostatic interactions	- optimal nanoparticle size (≈ 127 nm), reduced MCF-7 viability, enhanced uptake at pH 6, and induced DNA damage and apoptosis	[82]
dual-pH responsive DMMA-P-DOX/LAP polymeric nanoparticles	breast cancer	primary amine groups on e-poly-L-lysine undergo charge reversal via acid-labile β -carboxylic amide cleavage	pH-triggered drug release in endo/lysosomes disassembles nanoparticles, releasing LAP for a synergistic anti-tumour effect	a dual-pH responsive surface enhances tumour targeting and endosomal escape	- stable circulation, selective tumour accumulation, and significant tumour reduction/complete elimination in the MCF-7 cells	[83]
Role of CRNCs: improved cellular uptake						
dual pH-sensitive charge-reversal poly(β -L-malic acid) (PMLA)-based nanocomplex	anticancer activity	dimethylmaleic anhydride (DMMA) and amino groups undergo hydrolysis, exposing amines and reversing surface charge	at pH 6.8, DMMA hydrolyses, exposing TAT and reversing charge; at acidic pH, micelles release DOX	surface coated with pH-sensitive PEG-DMMA	- at pH 7.4, the nanocomplex maintained a negative surface charge of -16.33 mV while the surface charge reversed to $+10.81$ mV at pH 6.8	[84]

Table 2: Overview of charge-reversible nanocarriers in targeted cancer therapy. (continued)

charge-convertible carbon dots (CDs–Pt(IV)@PEG-(PAH/DMM A))	anticancer activity	DMMA groups hydrolyse in acidic pH, exposing amino groups that switch surface charge	at pH 6.8, the polymer shifts to positive, enhancing internalisation; reductive cytosol activates cisplatin prodrug	functionalized with PEG-(PAH/DMM A) for pH-responsive charge reversal and enhanced biocompatibility	- prolonged blood circulation enabling effective tumour targeting - enhanced therapeutic efficacy with reduced side effects - pH-responsive surface charge switching: At pH 7.4: zeta potential = –16.15 mV At pH 6.8: zeta potential shifts to +12.01 mV after 4 h at 37 °C	[85]
---	---------------------	--	---	---	--	------

DOX@MSNs-COS-CMC nanocarrier designed by Cui et al. for targeted delivery, demonstrated enhanced uptake and nuclear delivery in HeLa cells, reduced inflammatory cytokines, and improved tumour inhibition over free DOX, showing promise for cervical carcinoma therapy [72]. Cheah et al. developed a charge-responsive CPH material enabling electrically controlled protein release, reducing off-target effects through tuneable, site-specific delivery via GelMA-PEDOT interactions and degradation over 21 days [73]. Esmacili et al. developed a charge-reversible MCM@CS@PEG-APT (DOX-GFP) nanosystem that minimises off-target effects by pH-sensitive charge transition, enhancing tumour selectivity, reducing systemic toxicity, and ensuring efficient drug delivery in breast cancer therapy [74]. Yu et al. develop NTZ-DCMMs, charge-reversible nanocarriers with enhanced EGFR-targeted drug delivery, ensuring tumour-specific, redox-triggered DOX release, minimising off-target toxicity, cardiotoxicity, and enabling synergistic chemo-photodynamic therapy for hepatocellular carcinoma [75]. Chen et al. developed a reversible pH-responsive nanocarrier with poly(tannic acid)-coated MSNs that enables controlled drug release, HER2-targeting, and reduced off-target effects, enhancing efficacy while minimising secondary side effects in cancer therapy [76].

3.2 Controlled drug release

Biodegradable nanoparticles and micelles offer significant potential as nanosystems for delivering powerful anticancer drugs directly to target sites. Using specific polymers as nanocarriers allows for targeted drug delivery and controlled release development. Xia et al. developed redox/pH dual-responsive nanoparticles with reversible surface charge which were prepared using HA-SH and CS for the controlled release of the anticancer drug DOX [77]. Zhou et al. developed a pH-responsive charge-reversal polyelectrolyte, and an integrin $\alpha\text{V}\beta\text{3}$ antibody-functionalized GO complex was developed for targeted, controlled release of DOX, enabling selective drug release in acidic intracellular organelles for enhanced cancer

treatment [78]. Wang et al. developed a pH-responsive, charge-reversible, and photo-cross-linkable polymer nanoparticle composed of [poly(VBMC-*co*-AA)] and a block of [poly(DMAEMA-*co*-St)] for controlled DOX release. This nanocarrier enabled pH and light-triggered release adjustments, showed effective tumour cell inhibition in vitro, and potential for precision-controlled drug delivery [79]. Zhang et al. synthesised a pH-responsive, charge-reversal nanocarrier, PAH-cit/APTES-MSNs, which was developed for controlled drug release, effectively delivering doxorubicin to the nucleus of HeLa cells, showing a promising result for targeted cancer therapy [80].

3.3 Combination therapy (or) co-delivery

Single-drug treatments often fall short therapeutically and risk tumour cell resistance, whereas combination therapy uses multiple agents to enhance effects and reduce resistance. CR-NDDSs-based co-delivery systems, including dual-drug, dual-gene, and co-loading systems of drug-and-gene, are also expected to be used in the combined treatment of tumours [88]. Jia et al. reported a dual-responsive shape-transformable charge-reversible nanoparticle (DHP@BPP) combined with chemo-photodynamic immunotherapy for treating breast cancer and lung metastasis [81]. Hu et al. developed a hybrid nanocarrier, UPOE, using stimuli-responsive, charge-reversal metal–organic-framework-based polymer-coated nanoparticles to improve co-delivery of doxorubicin and cisplatin, enhancing combination therapy for multidrug-resistant cancer [31]. The pH-responsive, charge-reversal sericin-based nanocarrier MR-SNC was developed by Aghaz et al. for the co-delivery of resveratrol and melatonin to MCF-7 breast cancer cells, achieved efficient cellular uptake and significant cytotoxicity, which led to cell apoptosis in acidic conditions [82]. Guo et al. designed dual-pH-responsive, CRNs DMMA-P-DOX/LAP for co-delivering doxorubicin and lapatinib to breast cancer cells, enabling effective tumour penetration and notable reduction in MCF-7 tumours, with excellent biosafety in vivo [83].

3.4 Improved cellular uptake

Upon exposure to mildly acidic conditions of the tumour microenvironment (around pH 6.5–6.8), ionizable groups such as amines, imidazoles, or carboxyl-based moieties, CRNs become protonated or lose their protective shells, leading to a shift in surface charge from negative to positive. This transformation enhances electrostatic attraction toward negatively charged tumour cell membranes, thereby facilitating more efficient endocytosis and intracellular delivery of therapeutic agents. [87]. Zhou et al. developed a dual pH-responsive nanocarrier, CRN (PMLA-PEI-DOX-TAT@PEG-DMA), designed for tumour-targeted drug delivery with improved specificity and efficacy. This system leverages distinct pH-triggered mechanisms to enhance drug release within the acidic tumour microenvironment while maintaining stability in physiological conditions, resulting in significantly enhanced anti-tumour activity and reduced systemic toxicity. The dual pH-responsiveness enables precise control over therapeutic delivery, optimizing treatment outcomes [84]. Another straightforward approach to enhance the uptake of nanocarriers (NCs) by tumour cells is by increasing their positive surface charge. However, as previously mentioned, highly positive NCs tend to be cytotoxic. To address this issue, Feng et al. developed a pH-sensitive nanocarrier based on a cisplatin (IV) prodrug-loaded charge-reversal system (CDs-Pt (IV)@PEG-PAH/DMA) for imaging-guided drug delivery, which enhanced cancer therapeutic effects [85].

4 Preclinical and clinical insights of charge-reversible nanocarriers

Preclinical studies have revealed that CRNs significantly improve antitumour performance by enhancing tumour accumulation, cellular uptake, and controlled drug release in response to tumour microenvironmental cues. Different CRN architectures, including pH-responsive polymeric micelles, lipid-based nanoparticles, and dendrimer-based systems, have demonstrated improved tumour penetration and minimised systemic toxicity in murine and xenograft models. Additionally, CRNs have shown the ability to overcome multidrug resistance through effective endosomal escape and cytoplasmic delivery of therapeutic agents. While clinical evaluation is still in its preliminary stages, several CRN formulations are being assessed in phase I/II clinical trials for their safety, pharmacokinetic behaviour, and therapeutic potential. Collectively, these findings underscore the promise of CRNs as next-generation, stimulus-responsive drug delivery platforms capable of achieving precise tumour targeting with reduced off-target effects. Li et al. developed a dual immune checkpoint-inhibiting nanocarrier, aLS@VpNPs, which is cloaked with triple-negative breast cancer (TNBC) cell membranes and incorporates anti-LAG3 and Siglec10 proteins. This biomimetic design enhances tumour targeting and biocompatibility. Moreover, the nanocarrier is

combined with photodynamic therapy (PDT), where light-triggered ROS generation induces immunogenic cell death, effectively transforming immunologically “cold” tumours into “hot” ones. Consequently, this combination synergistically potentiates the efficacy of dual checkpoint blockade by activating both T cells and macrophages, offering a promising therapeutic strategy for TNBC [89]. In a similar approach, Yang et al. designed biomimetic nanovaccines targeting the CXCR4 receptor, incorporating ROS-responsive cores to simultaneously deliver STING agonists and tumour-associated antigens to dendritic cells through macropinocytosis. This strategy effectively activated the STING pathway within the cytosol, leading to a strong adaptive immune response [90].

Charge-reversible nanocarriers are also advancing the field of gene-based immunotherapy. In a 2024 study, Wang et al. developed MSN@MT nanocarriers composed of dendritic mesoporous silica coated with manganese ions and tannic acid, specifically designed to activate the cGAS-STING pathway in dendritic cells. This approach significantly improved antigen cross-presentation and stimulated T-cell activation in murine models, resulting in strong anti-tumour responses [91]. In addition to vaccines, CRNs are now being applied to deliver gene-editing systems such as CRISPR-Cas9. Nie et al. emphasised the advancement of stimuli-responsive nanoplateforms such as pH-sensitive structures and redox-responsive polymers that enable protected and precise intracellular transport of CRISPR components [92]. Ben-Akiva et al. engineered biodegradable, lipophilic polymer-based nanocarriers capable of systemically delivering mRNA along with TLR agonists to dendritic cells in the spleen, leading to strong activation of CD8⁺ T cells and effective tumour suppression in mouse models [93]. Most CRNs are still at the preclinical level; however, notable strides have been made toward their clinical implementation. While CRN-specific platforms have yet to appear in phase I/II clinical trials, early stage studies involving pH-sensitive and ionizable lipid-based nanoparticles for mRNA and gene-editing delivery are underway. Liang et al. highlight that these emerging technologies lay the groundwork for CRNs to become key components in future personalized cancer therapy approaches [32].

5 Challenges and limitations

CRNs offer a significant advantage over traditional nanocarriers by promoting higher cellular uptake and minimizing non-specific interactions, thereby enhancing therapeutic accuracy. However, despite their potential, several challenges limit their clinical translation. Regulatory authorities, including the FDA and EMA, require extensive safety assessments due to the complex stimuli-responsive nature of CRNs, which can affect immunogenicity, cytotoxicity, and long-term biocompatibility [94]. Research showing low toxicity at high concentrations for

specific nanocarriers emphasizes their advantages over inorganic substitutes, such as silica and gold nanoparticles, which are often associated with safety concerns [95]. Despite these encouraging findings, comprehensive evaluation and mitigation of safety issues remain essential to facilitate the successful translation of nanocarrier technologies from experimental research to clinical application. Addressing challenges such as long-term biocompatibility, accumulation, and dose-dependent toxicity will be critical for advancing these promising systems towards safe and effective patient use [96].

Their intricate structural design, composed of multiple functional elements, complicates standardization and reproducibility among various formulations [97]. In addition, the synthesis of CRNs often involves elaborate multistep processes to achieve accurate charge-switching properties, which can lead to inconsistencies between production batches and create scalability challenges [98]. The inclusion of diverse functional groups and the need for precise control over physicochemical characteristics further increase manufacturing costs and delay clinical development. Maintaining stability during storage is another critical concern, as environmental factors such as temperature fluctuations and light exposure may induce premature charge reversal, thereby altering drug release profiles and reducing therapeutic efficacy [99].

The clinical translation of CRNs remains challenging due to interpatient variability, tumour microenvironment heterogeneity, and differential immune responses, all of which significantly impact their pharmacokinetics, biodistribution, and therapeutic efficacy [100]. These factors collectively influence the biological behaviour and therapeutic efficacy of CRNs, complicating their predictability and consistency in patients. In addition, the intricate composition of these systems often extends regulatory approval and clinical evaluation processes. Ethical and environmental considerations further complicate their translation, as the degradation of by-products and long-term accumulation of synthetic nanomaterials in ecosystems necessitate thorough investigation [101]. To address these limitations, current research focuses on multiple strategies, including standardizing large-scale production to ensure consistency, developing formulations with superior physicochemical stability, and adopting personalized medicine approaches to optimize CRN efficacy based on individual patient profiles [102]. Furthermore, comprehensive environmental impact assessments are vital to promote safe, ethical, and sustainable applications of CRNs in clinical practice.

6 Future perspectives

Future development of charge-reversible nanocarriers must prioritize translating proof-of-concept systems into clinically

viable drug delivery platforms by emphasizing biodegradability, biocompatibility, and high positive surface potentials to optimize cellular uptake and endosomal escape. Addressing safety and regulatory challenges, especially for inorganic materials such as carbon nanotubes and mesoporous silica nanoparticles and optimizing polymeric nanocarriers such as PAMAM dendrimers are critical for minimising toxicity and enhancing clinical applicability. Advancing FDA-approved excipients with enzymatically cleavable coatings, innovating adaptable charge-reversal mechanisms responsive to heterogeneous tumour microenvironments, and exploring alternative activation modalities beyond photoresponsive systems will accelerate clinical translation and broaden applications beyond oncology to include retinal therapy, inflammatory diseases, and mRNA vaccine delivery, heralding a new era of personalized, multimodal, and highly effective therapies driven by the next generation of charge-reversible nanocarriers.

Conclusion

CRNs enable targeted cancer therapy by maintaining neutral or negative charge in circulation and switching to positive charge in the acidic tumour microenvironment, enhancing cellular uptake and therapeutic efficacy. This switchable charge feature boosts therapeutic effectiveness and minimises harm to healthy tissues, positioning these systems as promising candidates for clinical application. The adaptability of CRNs is characterised by their ability to respond to a broad spectrum of stimuli, including changes in pH, enzymatic activity, redox environments, temperature, light, ultrasound, X-rays, and magnetic fields. These stimulus-responsive mechanisms enable precise, site-specific drug release, significantly improving the accuracy of cancer therapies. For example, pH-sensitive nanocarriers utilise the acidic conditions of the tumour microenvironment to trigger charge switching, enzyme-responsive systems to activate in the presence of tumour-associated enzymes, and redox-sensitive carriers to release drugs in response to elevated intracellular glutathione levels.

Furthermore, advanced platforms employing external stimuli such as light, ultrasound, or magnetic fields offer the advantage of precise spatiotemporal control over therapeutic delivery. These approaches have shown promising outcomes in preclinical studies, supporting the development of combination treatments and co-delivery systems applications that integrate therapeutic and diagnostic functions. While challenges such as stability, large-scale production, and regulatory approval remain, ongoing progress in nanocarrier engineering and materials innovation continues to drive this field forward. Ultimately, CRNs can potentially transform cancer therapy by offering safer, more efficient, and highly individualised treatment options.

Acknowledgements

The authors thank GITAM (Deemed to be University), India, and its School of Pharmacy for administrative assistance, and the necessary support and infrastructure to facilitate this study. The graphical abstract for this study was created in BioRender. Yeduvaka, M. (2025) <https://BioRender.com/9fqwgm>. This content is not subject to CC BY 4.0.

Funding

The authors thank GITAM (Deemed to be University), India, and its School of Pharmacy for providing financial support through the GITAM New-Faculty Seed Grant (Proposal Ref. No. 2025/006).

Conflict of Interest

The authors declare that they have no known competing financial interests or personal relationships that could have appeared to influence the work reported in this paper.

Author Contributions

Madhuri Yeduvaka: conceptualization; investigation; methodology; writing – original draft; writing – review & editing. Pooja Mittal: investigation; writing – original draft; writing – review & editing. Ameer Boyalakuntla: investigation; methodology; writing – original draft. Usman Bee Shaik: investigation; methodology; writing – original draft. Himanshu Sharma: investigation; methodology; writing – original draft. Thakur Gurjeet Singh: investigation; methodology; writing – original draft. Siva Nageswara Rao Gajula: conceptualization; writing – review & editing. Lakshmi Vineela Nalla: conceptualization; writing – review & editing.

ORCID® iDs

Siva Nageswara Rao Gajula - <https://orcid.org/0000-0003-0449-4282>

Lakshmi Vineela Nalla - <https://orcid.org/0000-0002-6077-1099>

Data Availability Statement

Data sharing is not applicable as no new data was generated or analyzed in this study.

References

- Cong, B.; Cao, X.; Jiang, W. G.; Ye, L. *OncoTargets Ther.* **2025**, 199–209. doi:10.2147/ott.s503272
- Pérez-Herrero, E.; Fernández-Medarde, A. *Eur. J. Pharm. Biopharm.* **2015**, 93, 52–79. doi:10.1016/j.ejpb.2015.03.018
- Bray, F.; Laversanne, M.; Sung, H.; Ferlay, J.; Siegel, R. L.; Soerjomataram, I.; Jemal, A. *Ca-Cancer J. Clin.* **2024**, 74, 229–263. doi:10.3322/caac.21834
- Yildizhan, H.; Barkan, N. P.; Turan, S. K.; Demiralp, Ö.; Demiralp, F. D. Ö.; Uslu, B.; Özkan, S. A. Treatment strategies in cancer from past to present. *Drug targeting and stimuli sensitive drug delivery systems*; William Andrew: Oxford, UK, 2018; pp 1–37. doi:10.1016/b978-0-12-813689-8.00001-x
- Baskar, R.; Lee, K. A.; Yeo, R.; Yeoh, K.-W. *Int. J. Med. Sci.* **2012**, 9, 193–199. doi:10.7150/ijms.3635
- Suveltha, S.; Kumar, A. Y. N.; Ghosh, M.; Prasad, R.; Yadav, P. K. Cancer Nanotherapeutics. *Nanotechnology Theranostics in Livestock Diseases and Management*; Springer: Singapore, 2024; pp 563–585. doi:10.1007/978-981-16-1610-5_24
- Debela, D. T.; Muzazu, S. G.; Heraro, K. D.; Ndalama, M. T.; Mesele, B. W.; Haile, D. C.; Kitui, S. K.; Manyazewal, T. *SAGE Open Med.* **2021**, 9, 20503121211034366. doi:10.1177/20503121211034366
- Sharma, N.; Shankar Singh, H.; Khanna, R.; Kaur, A.; Agarwal, M. *Biomed. Signal Process. Control* **2025**, 99, 106826. doi:10.1016/j.bspc.2024.106826
- Altun, I.; Sonkaya, A. *Iran. J. Public Health* **2018**, 47, 1218.
- Alshawwa, S. Z.; Kassem, A. A.; Farid, R. M.; Mostafa, S. K.; Labib, G. S. *Pharmaceutics* **2022**, 14, 883. doi:10.3390/pharmaceutics14040883
- Qiao, W.; Wang, B.; Wang, Y.; Yang, L.; Zhang, Y.; Shao, P. *J. Nanomater.* **2010**, 796303. doi:10.1155/2010/796303
- Vieira, D. B.; Gamarra, L. F. *Einstein (São Paulo)* **2016**, 14, 99–103. doi:10.1590/s1679-45082016rb3475
- Chamundeeswari, M.; Jeslin, J.; Verma, M. L. *Environ. Chem. Lett.* **2019**, 17, 849–865. doi:10.1007/s10311-018-00841-1
- Joudeh, N.; Linke, D. *J. Nanobiotechnol.* **2022**, 20, 262. doi:10.1186/s12951-022-01477-8
- Zhang, P.; Chen, D.; Li, L.; Sun, K. *J. Nanobiotechnol.* **2022**, 20, 31. doi:10.1186/s12951-021-01221-8
- Hu, Y.; Gong, X.; Zhang, J.; Chen, F.; Fu, C.; Li, P.; Zou, L.; Zhao, G. *Polymers (Basel, Switz.)* **2016**, 8, 99. doi:10.3390/polym8040099
- Shah, S.; Rangaraj, N.; Singh, S. B.; Srivastava, S. *Colloid Interface Sci. Commun.* **2021**, 42, 100406. doi:10.1016/j.colcom.2021.100406
- Vincent, M. P.; Bobbala, S.; Karabin, N. B.; Frey, M.; Liu, Y.; Navidzadeh, J. O.; Stack, T.; Scott, E. A. *Nat. Commun.* **2021**, 12, 648. doi:10.1038/s41467-020-20886-7
- Deiss-Yehiely, E.; Cárcamo-Oyarce, G.; Berger, A. G.; Ribbeck, K.; Hammond, P. T. *ACS Biomater. Sci. Eng.* **2023**, 9, 4794–4804. doi:10.1021/acsbomaterials.3c00481
- Liu, J.; Huang, Y.; Kumar, A.; Tan, A.; Jin, S.; Mozhi, A.; Liang, X.-J. *Biotechnol. Adv.* **2014**, 32, 693–710. doi:10.1016/j.biotechadv.2013.11.009
- Zhang, J.; Wu, G.; Bobrin, V. A. *RSC Appl. Polym.* **2025**, 3, 1403–1427. doi:10.1039/d5lp00154d
- Shi, Y.; Yu, Q.; Tan, L.; Wang, Q.; Zhu, W.-H. *Angew. Chem., Int. Ed.* **2025**, 64, e202503776. doi:10.1002/anie.202503776
- Yuan, F.; Li, Z.-D.; Li, Q.; Zeng, Y.; Zhang, G.; Li, Y. *Nanomedicine (London, U. K.)* **2025**, 20, 1213–1217. doi:10.1080/17435889.2025.2476377
- Singh, R.; Long, F. R.; Saini, A.; Joma, N.; Basu, A.; Mahmoudi, M.; Vali, H.; Kakkar, A. *RSC Pharm.* **2025**, 2, 44–58. doi:10.1039/d4pm00170b
- Bai, Y.; Liu, C.-P.; Chen, D.; Liu, C.-F.; Zhuo, L.-H.; Li, H.; Wang, C.; Bu, H.-T.; Tian, W. *Carbohydr. Polym.* **2020**, 246, 116654. doi:10.1016/j.carbpol.2020.116654

26. Sun, H.; Li, X.; Liu, Q.; Sheng, H.; Zhu, L. *J. Drug Targeting* **2024**, *32*, 672–706. doi:10.1080/1061186x.2024.2349124
27. Abri Aghdam, M.; Bagheri, R.; Mosafer, J.; Baradaran, B.; Hashemzaei, M.; Baghbanzadeh, A.; de la Guardia, M.; Mokhtarzadeh, A. *J. Controlled Release* **2019**, *315*, 1–22. doi:10.1016/j.jconrel.2019.09.018
28. Zhang, T.; Huang, S.; Lin, H.; An, N.; Tong, R.; Chen, Y.; Wang, Y.; Qu, F. *New J. Chem.* **2017**, *41*, 2468–2478. doi:10.1039/c6nj02357f
29. Li, Y.; Du, L.; Wu, C.; Yu, B.; Zhang, H.; An, F. *Curr. Top. Med. Chem.* **2019**, *19*, 74–97. doi:10.2174/1568026619666190125144621
30. Wu, H.; Guo, S.; Yang, T. H. *Enzyme-Responsive Nanomedicine. Stimuli-Responsive Nanomedicine*; Jenny Stanford Publishing: New York, NY, USA, 2021; pp 69–98. doi:10.1201/9780429295294-3
31. Hu, L.; Xiong, C.; Wei, G.; Yu, Y.; Li, S.; Xiong, X.; Zou, J.-J.; Tian, J. *J. Colloid Interface Sci.* **2022**, *608*, 1882–1893. doi:10.1016/j.jcis.2021.10.070
32. Liang, Y.; Wu, J.; Yan, Y.; Wang, Y.; Zhao, H.; Wang, X.; Chang, S.; Li, S. *Int. J. Mol. Sci.* **2024**, *25*, 9779. doi:10.3390/ijms25189779
33. Ghassami, E.; Varshosaz, J.; Taymouri, S. *Curr. Pharm. Des.* **2018**, *24*, 3303–3319. doi:10.2174/1381612824666180813114841
34. Fadel, T. R.; Sharp, F. A.; Vudattu, N.; Ragheb, R.; Garyu, J.; Kim, D.; Hong, E.; Li, N.; Haller, G. L.; Pfeifferle, L. D.; Justesen, S.; Herold, K. C.; Fahmy, T. M. *Nat. Nanotechnol.* **2014**, *9*, 639–647. doi:10.1038/nnano.2014.154
35. Sahoo, P. R. *Light responsive materials: properties, design, and applications. Stimuli-Responsive Materials for Biomedical Applications*; ACS Publications: Washington, DC, USA, 2023; pp 101–127. doi:10.1021/bk-2023-1436.ch005
36. Ai, X.; Mu, J.; Xing, B. *Theranostics* **2016**, *6*, 2439–2457. doi:10.7150/thno.16088
37. Wei, P.; Cornel, E. J.; Du, J. *Drug Delivery Transl. Res.* **2021**, *11*, 1323–1339. doi:10.1007/s13346-021-00963-0
38. Yazdan, M.; Naghib, S. M. *Curr. Drug Delivery* **2025**, *22*, 283–309. doi:10.2174/0115672018283792240115053302
39. Hua, Y.; Huang, J.-H.; Shao, Z.-H.; Luo, X.-M.; Wang, Z.-Y.; Liu, J.-Q.; Zhao, X.; Chen, X.; Zang, S.-Q. *Adv. Mater. (Weinheim, Ger.)* **2022**, *34*, 2203734. doi:10.1002/adma.202203734
40. Song, X.; Sun, Z.; Li, L.; Zhou, L.; Yuan, S. *Front. Oncol.* **2023**, *13*, 1088878. doi:10.3389/fonc.2023.1088878
41. Manoharan, D.; Chang, L.-C.; Wang, L.-C.; Shan, Y.-S.; Lin, F.-C.; Wu, L.-C.; Sheu, H.-S.; Su, W.-P.; Yeh, C.-S. *ACS Nano* **2021**, *15*, 9084–9100. doi:10.1021/acsnano.1c02283
42. Abed, Z.; Beik, J.; Laurent, S.; Eslahi, N.; Khani, T.; Davani, E. S.; Ghaznavi, H.; Shakeri-Zadeh, A. *J. Cancer Res. Clin. Oncol.* **2019**, *145*, 1213–1219. doi:10.1007/s00432-019-02870-x
43. Shivanna, A. T.; Dash, B. S.; Chen, J.-P. *Micromachines* **2022**, *13*, 1279. doi:10.3390/mi13081279
44. Kola, P.; Nagesh, P. K. B.; Roy, P. K.; Deepak, K.; Reis, R. L.; Kundu, S. C.; Mandal, M. *Wiley Interdiscip. Rev.: Nanomed. Nanobiotechnol.* **2023**, *15*, e1876. doi:10.1002/wnan.1876
45. Ding, H.; Tan, P.; Fu, S.; Tian, X.; Zhang, H.; Ma, X.; Gu, Z.; Luo, K. *J. Controlled Release* **2022**, *348*, 206–238. doi:10.1016/j.jconrel.2022.05.056
46. Liu, Y.; Si, L.; Jiang, Y.; Jiang, S.; Zhang, X.; Li, S.; Chen, J.; Hu, J. *Int. J. Nanomed.* **2025**, 705–721. doi:10.2147/ijn.s504629
47. He, Y.; Lei, L.; Cao, J.; Yang, X.; Cai, S.; Tong, F.; Huang, D.; Mei, H.; Luo, K.; Gao, H.; He, B.; Peppas, N. A. *Sci. Adv.* **2021**, *7*, eaba0776. doi:10.1126/sciadv.aba0776
48. Fu, J.; Lu, L.; Li, M.; Guo, Y.; Han, M.; Guo, Y.; Wang, X. *Pharmaceutics* **2023**, *15*, 1335. doi:10.3390/pharmaceutics15051335
49. Sun, R.; Zhang, Y.; Lin, X.; Piao, Y.; Xie, T.; He, Y.; Xiang, J.; Shao, S.; Zhou, Q.; Zhou, Z.; Tang, J.; Shen, Y. *Angew. Chem., Int. Ed.* **2023**, *62*, e202217408. doi:10.1002/anie.202217408
50. Liu, Y.; Liu, Y.; Wang, C.; Zhang, J.; Yang, J.; Wan, D.; Pan, J. *ACS Appl. Nano Mater.* **2025**, *8*, 16082–16092. doi:10.1021/acsnm.5c02824
51. Lin, Q.; Jia, M.; Fu, Y.; Li, B.; Dong, Z.; Niu, X.; You, Z. *Front. Pharmacol.* **2021**, *12*, 738630. doi:10.3389/fphar.2021.738630
52. Zou, L.; Liu, X.; Li, J.; Li, W.; Zhang, L.; Fu, C.; Zhang, J.; Gu, Z. *Theranostics* **2021**, *11*, 4171–4186. doi:10.7150/thno.42260
53. Xu, C.; Song, R.-j.; Lu, P.; Chen, J.-c.; Zhou, Y.-q.; Shen, G.; Jiang, M.-j.; Zhang, W. *Int. J. Nanomed.* **2018**, 7229–7249. doi:10.2147/ijn.s182197
54. Tang, Y.; Wang, G. *J. Photochem. Photobiol., C* **2021**, *47*, 100420. doi:10.1016/j.jphotochemrev.2021.100420
55. Hu, D.; Li, Y.; Niu, Y.; Li, L.; He, J.; Liu, X.; Xia, X.; Lu, Y.; Xiong, Y.; Xu, W. *RSC Adv.* **2014**, *4*, 47929–47936. doi:10.1039/c4ra07345b
56. Choi, H. W.; Lim, J. H.; Kim, C. W.; Lee, E.; Kim, J.-M.; Chang, K.; Chung, B. G. *Antioxidants* **2022**, *11*, 174. doi:10.3390/antiox11010174
57. Xing, W.; Li, T.; Yang, G.; Wu, S.; Pang, B.; Xu, Y.; Qian, X.; Zhu, W. *Acta Biomater.* **2025**, *192*, 353–365. doi:10.1016/j.actbio.2024.11.035
58. Li, X.; Wang, Z.; Xia, H. *Front. Chem. (Lausanne, Switz.)* **2019**, *7*, 59. doi:10.3389/fchem.2019.00059
59. Cai, P.; Leow, W. R.; Wang, X.; Wu, Y.-L.; Chen, X. *Adv. Mater. (Weinheim, Ger.)* **2017**, *29*, 1605529. doi:10.1002/adma.201605529
60. Liu, F.; Lou, J.; Hristov, D. *Nanoscale* **2017**, *9*, 14627–14634. doi:10.1039/c7nr04684g
61. Parhi, R.; Kaishap, P. P.; Jena, G. K. *ADMET DMPK* **2024**, *12*, 107–150. doi:10.5599/admet.2088
62. Liu, N.; Zhu, J.; Zhu, W.; Chen, L.; Li, M.; Shen, J.; Chen, M.; Wu, Y.; Pan, F.; Deng, Z.; Liu, Y.; Yang, G.; Liu, Z.; Chen, Q.; Yang, Y. *Adv. Mater. (Weinheim, Ger.)* **2023**, *35*, 2302220. doi:10.1002/adma.202302220
63. Liu, J. F.; Jang, B.; Issadore, D.; Tsourkas, A. *Wiley Interdiscip. Rev.: Nanomed. Nanobiotechnol.* **2019**, *11*, e1571. doi:10.1002/wnan.1571
64. Vangijzegem, T.; Lecomte, V.; Ternad, I.; Van Leuven, L.; Muller, R. N.; Stanicki, D.; Laurent, S. *Pharmaceutics* **2023**, *15*, 236. doi:10.3390/pharmaceutics15010236
65. Ghazi, R.; Ibrahim, T. K.; Nasir, J. A.; Gai, S.; Ali, G.; Boukhris, I.; Rehman, Z. *RSC Adv.* **2025**, *15*, 11587–11616. doi:10.1039/d5ra00728c
66. Ferjaoui, Z.; Jamal Al Dine, E.; Kulmukhamedova, A.; Bezdetsnaya, L.; Soon Chang, C.; Schneider, R.; Mutelet, F.; Mertz, D.; Begin-Colin, S.; Quilès, F.; Gaffet, E.; Alem, H. *ACS Appl. Mater. Interfaces* **2019**, *11*, 30610–30620. doi:10.1021/acsnami.9b10444
67. Fernandes, S.; Fernandez, T.; Metzke, S.; Balakrishnan, P. B.; Mai, B. T.; Conteh, J.; De Mei, C.; Turdo, A.; Di Franco, S.; Stassi, G.; Todaro, M.; Pellegrino, T. *ACS Appl. Mater. Interfaces* **2021**, *13*, 15959–15972. doi:10.1021/acsnami.0c21349
68. Li, Y.; Yang, H. Y.; Thambi, T.; Park, J.-H.; Lee, D. S. *Biomaterials* **2019**, *217*, 119299. doi:10.1016/j.biomaterials.2019.119299
69. Chen, S.; Zhu, F.; Nie, Z.; Yang, C.; Yang, J.; He, J.; Tan, X.; Liu, X.; Zhang, J.; Zhao, Y. *Langmuir* **2023**, *39*, 13588–13598. doi:10.1021/acs.langmuir.3c01604

70. Wang, Z.; Cheng, Q.; Jiang, X.; Chu, X.; Li, B.; Zhang, L.; Wu, W.; Li, J.; Narain, R. *Colloids Surf., A* **2024**, *703*, 135277. doi:10.1016/j.colsurfa.2024.135277
71. Miao, Y.; Qiu, Y.; Yang, W.; Guo, Y.; Hou, H.; Liu, Z.; Zhao, X. *Colloids Surf., B* **2018**, *169*, 313–320. doi:10.1016/j.colsurfb.2018.05.026
72. Cui, L.; Feng, X.; Liu, W.; Liu, H.; Qin, Q.; Wu, S.; He, S.; Pang, X.; Men, D.; Zhu, C. *Mol. Pharmaceutics* **2020**, *17*, 1910–1921. doi:10.1021/acs.molpharmaceut.0c00004
73. Cheah, E.; Bansal, M.; Nguyen, L.; Chalard, A.; Malmström, J.; O'Carroll, S. J.; Connor, B.; Wu, Z.; Svirskis, D. *Acta Biomater.* **2023**, *158*, 87–100. doi:10.1016/j.actbio.2023.01.013
74. Esmaili, Y.; Dabiri, A.; Mashayekhi, F.; Rahimmanesh, I.; Bidram, E.; Karbasi, S.; Rafienia, M.; Javanmard, S. H.; Ertas, Y. N.; Zarrabi, A.; Shariati, L. *Biomed. Pharmacother.* **2024**, *173*, 116465. doi:10.1016/j.biopha.2024.116465
75. Yu, L.; Zhang, M.; He, J.; Sun, X.; Ni, P. *Acta Biomater.* **2024**, *179*, 272–283. doi:10.1016/j.actbio.2024.02.048
76. Chen, C.; Ma, T.; Tang, W.; Wang, X.; Wang, Y.; Zhuang, J.; Zhu, Y.; Wang, P. *Nanoscale Horiz.* **2020**, *5*, 986–998. doi:10.1039/d0nh00032a
77. Xia, D.; Wang, F.; Pan, S.; Yuan, S.; Liu, Y.; Xu, Y. *Polymers (Basel, Switz.)* **2021**, *13*, 3785. doi:10.3390/polym13213785
78. Zhou, T.; Zhou, X.; Xing, D. *Biomaterials* **2014**, *35*, 4185–4194. doi:10.1016/j.biomaterials.2014.01.044
79. Wang, M.; He, K.; Li, J.; Shen, T.; Li, Y.; Xu, Y.; Yuan, C.; Dai, L. *J. Biomater. Sci., Polym. Ed.* **2020**, *31*, 849–868. doi:10.1080/09205063.2020.1725279
80. Zhang, P.; Wu, T.; Kong, J.-L. *ACS Appl. Mater. Interfaces* **2014**, *6*, 17446–17453. doi:10.1021/am5059519
81. Jia, W.; Gong, B.; Chen, J.; Yan, J.; Shi, Y.; Wang, H.; Qin, M.; Gao, H. *Adv. Funct. Mater.* **2024**, *34*, 2408581. doi:10.1002/adfm.202408581
82. Aghaz, F.; Asadi, Z.; Sajadimajd, S.; Kashfi, K.; Arkan, E.; Rahimi, Z. *Sci. Rep.* **2023**, *13*, 11090. doi:10.1038/s41598-023-37668-y
83. Guo, Z.; Sui, J.; Ma, M.; Hu, J.; Sun, Y.; Yang, L.; Fan, Y.; Zhang, X. *J. Controlled Release* **2020**, *326*, 350–364. doi:10.1016/j.jconrel.2020.07.030
84. Zhou, Q.; Hou, Y.; Zhang, L.; Wang, J.; Qiao, Y.; Guo, S.; Fan, L.; Yang, T.; Zhu, L.; Wu, H. *Theranostics* **2017**, *7*, 1806–1819. doi:10.7150/thno.18607
85. Feng, T.; Ai, X.; An, G.; Yang, P.; Zhao, Y. *ACS Nano* **2016**, *10*, 4410–4420. doi:10.1021/acsnano.6b00043
86. Han, Q.-J.; Lan, X.-T.; Wen, Y.; Zhang, C.-Z.; Cleary, M.; Sayyed, Y.; Huang, G.; Tuo, X.; Yi, L.; Xi, Z.; Li, L.-Y.; Zhang, Q.-Z. *Adv. Healthcare Mater.* **2021**, *10*, 2002143. doi:10.1002/adhm.202002143
87. Sun, Q.; Zhu, Y.; Du, J. *Biomed. Mater.* **2021**, *16*, 042010. doi:10.1088/1748-605x/abffb5
88. Fang, Z.; Pan, S.; Gao, P.; Sheng, H.; Li, L.; Shi, L.; Zhang, Y.; Cai, X. *Int. J. Pharm.* **2020**, *575*, 118841. doi:10.1016/j.ijpharm.2019.118841
89. Li, J.; Gu, Y.; Sun, W.; Wen, B.; Li, B.; Liu, J.; Sun, Z.; Zhao, Q.; Sun, C. *ACS Appl. Nano Mater.* **2024**, *7*, 27476–27488. doi:10.1021/acsnanm.4c05465
90. Yang, C.; Zhang, F.; Chen, F.; Chang, Z.; Zhao, Y.; Shao, D.; Sun, W.; Dong, W.-f.; Wang, Z. *Adv. Healthcare Mater.* **2023**, *12*, 2202064. doi:10.1002/adhm.202202064
91. Wang, Q.; Gao, Y.; Li, Q.; He, A.; Xu, Q.; Mou, Y. *Int. J. Nanomed.* **2024**, 263–280. doi:10.2147/ijn.s438359
92. Nie, J.-J.; Liu, Y.; Qi, Y.; Zhang, N.; Yu, B.; Chen, D.-F.; Yang, M.; Xu, F.-J. *J. Controlled Release* **2021**, *333*, 362–373. doi:10.1016/j.jconrel.2021.03.030
93. Ben-Akiva, E.; Karlsson, J.; Hemmati, S.; Yu, H.; Tzeng, S. Y.; Pardoll, D. M.; Green, J. J. *Proc. Natl. Acad. Sci. U. S. A.* **2023**, *120*, e2301606120. doi:10.1073/pnas.2301606120
94. Lim, S. B.; Banerjee, A.; Önyüksel, H. J. *Controlled Release* **2012**, *163*, 34–45. doi:10.1016/j.jconrel.2012.06.002
95. Yu, S. S.; Lau, C. M.; Thomas, S. N.; Jerome, W. G.; Maron, D. J.; Dickerson, J. H.; Hubbell, J. A.; Giorgio, T. D. *Int. J. Nanomed.* **2012**, 799–813. doi:10.2147/ijn.s28531
96. Buya, A. B.; Mahlangu, P.; Witika, B. A. *Int. J. Pharm.: X* **2024**, *8*, 100266. doi:10.1016/j.ijpx.2024.100266
97. Nijhara, R.; Balakrishnan, K. *Nanomedicine (N. Y., NY, U. S.)* **2006**, *2*, 127–136. doi:10.1016/j.nano.2006.04.005
98. Zhao, Z.; Ukidve, A.; Krishnan, V.; Mitragotri, S. *Adv. Drug Delivery Rev.* **2019**, *143*, 3–21. doi:10.1016/j.addr.2019.01.002
99. Đorđević, S.; Gonzalez, M. M.; Conejos-Sánchez, I.; Carreira, B.; Pozzi, S.; Acúrcio, R. C.; Satchi-Fainaro, R.; Florindo, H. F.; Vicent, M. J. *Drug Delivery Transl. Res.* **2022**, *12*, 500–525. doi:10.1007/s13346-021-01024-2
100. Shi, J.; Kantoff, P. W.; Wooster, R.; Farokhzad, O. C. *Nat. Rev. Cancer* **2017**, *17*, 20–37. doi:10.1038/nrc.2016.108
101. Leong, H. S.; Butler, K. S.; Brinker, C. J.; Azzawi, M.; Conlan, S.; Dufès, C.; Owen, A.; Rannard, S.; Scott, C.; Chen, C.; Dobrovolskaia, M. A.; Kozlov, S. V.; Prina-Mello, A.; Schmid, R.; Wick, P.; Caputo, F.; Boisseau, P.; Crist, R. M.; McNeil, S. E.; Fadeel, B.; Tran, L.; Hansen, S. F.; Hartmann, N. B.; Clausen, L. P. W.; Skjolding, L. M.; Baun, A.; Ågerstrand, M.; Gu, Z.; Lamprou, D. A.; Hoskins, C.; Huang, L.; Song, W.; Cao, H.; Liu, X.; Jandt, K. D.; Jiang, W.; Kim, B. Y. S.; Wheeler, K. E.; Chetwynd, A. J.; Lynch, I.; Moghimi, S. M.; Nel, A.; Xia, T.; Weiss, P. S.; Sarmiento, B.; das Neves, J.; Santos, H. A.; Santos, L.; Mitragotri, S.; Little, S.; Peer, D.; Amiji, M. M.; Alonso, M. J.; Petri-Fink, A.; Balog, S.; Lee, A.; Drasler, B.; Rothen-Rutishauser, B.; Wilhelm, S.; Acar, H.; Harrison, R. G.; Mao, C.; Mukherjee, P.; Ramesh, R.; McNally, L. R.; Busatto, S.; Wolfram, J.; Bergese, P.; Ferrari, M.; Fang, R. H.; Zhang, L.; Zheng, J.; Peng, C.; Du, B.; Yu, M.; Charron, D. M.; Zheng, G.; Pastore, C. *Nat. Nanotechnol.* **2019**, *14*, 629–635. doi:10.1038/s41565-019-0496-9
102. Dai, Q.; Du, Z.; Jing, L.; Zhang, R.; Tang, W. *ACS Appl. Mater. Interfaces* **2024**, *16*, 6208–6220. doi:10.1021/acsnami.3c11500

License and Terms

This is an open access article licensed under the terms of the Beilstein-Institut Open Access License Agreement (<https://www.beilstein-journals.org/bjnano/terms>), which is identical to the Creative Commons Attribution 4.0 International License

(<https://creativecommons.org/licenses/by/4.0>). The reuse of material under this license requires that the author(s), source and license are credited. Third-party material in this article could be subject to other licenses (typically indicated in the credit line), and in this case, users are required to obtain permission from the license holder to reuse the material.

The definitive version of this article is the electronic one which can be found at:

<https://doi.org/10.3762/bjnano.17.10>



Biomimetic nanoparticles in cancer photodynamic therapy: a review of targeted delivery systems and therapeutic outcomes

Valentina I. Gorbacheva[‡], Alexey S. Grabovoy[‡], Polina S. Marukhina, Anastasiia O. Syrocheva and Ekaterina P. Kolesova^{*}

Review

Open Access

Address:
Sirius University of Science and Technology, 1 Olympic Avenue,
Sirius, Krasnodar Region, 354340, Russia

Email:
Ekaterina P. Kolesova^{*} - e.p.kolesova@gmail.com

^{*} Corresponding author [‡] Equal contributors

Keywords:
biomimetic nanoparticles; immunogenic cell death; nanocarriers;
photodynamic therapy; targeted drug delivery; tumor hypoxia
modulation

Beilstein J. Nanotechnol. **2026**, *17*, 396–422.
<https://doi.org/10.3762/bjnano.17.27>

Received: 13 November 2025
Accepted: 18 February 2026
Published: 05 March 2026

This article is part of the thematic issue "Advanced nanomedicine for drug delivery and biotherapy".

Guest Editor: K. Andrieux



© 2026 Gorbacheva et al.; licensee Beilstein-Institut.
License and terms: see end of document.

Abstract

Photodynamic therapy (PDT) is a minimally invasive cancer treatment that uses photosensitizers (PSs) activated by light to produce cytotoxic reactive oxygen species (ROS). Although PDT shows clinical promise, its effectiveness is limited by factors such as insufficient tumor targeting, tumor hypoxia, PS instability, and weak immune responses. Biomimetic nanoparticles (BNPs), which combine natural biological materials like cell membranes with synthetic nanocarriers, have emerged as versatile platforms to overcome these challenges. BNPs improve PDT by enhancing tumor-specific delivery of PSs, relieving hypoxia through oxygen delivery or catalytic oxygen generation, and boosting antitumor immunity by promoting immunogenic cell death and working synergistically with immune checkpoint inhibitors. This review details recent progress in BNP-based strategies for targeted PS delivery, ROS production enhancement, hypoxia modulation, and immune system activation. Additionally, it explores multifunctional and theranostic nanoplatfoms, their applications in various cancers, and advances toward clinical use. By integrating targeted delivery, tumor microenvironment modulation, and immunotherapy, BNP-facilitated PDT holds great potential for advancing precise cancer treatments.

Review

Introduction

Cancer remains a formidable global health challenge, demanding innovative therapeutic strategies that balance efficacy with reduced systemic toxicity [1]. Among emerging treat-

ments, photodynamic therapy (PDT) has garnered considerable attention due to its minimally invasive nature, spatiotemporal control, and ability to selectively destroy tumor tissues while

sparing healthy cells [2]. PDT operates through a unique mechanism involving three key components: a photosensitizer (PS), light of a specific wavelength, and molecular oxygen [3]. Upon light activation, the PS transitions to an excited state and transfers energy to surrounding oxygen molecules, generating reactive oxygen species (ROS) that can eradicate tumor cells. While PDT offers advantages like precision targeting and minimal invasiveness, its clinical translation faces significant hurdles, namely, poor tumor accumulation of hydrophobic PSs [4], hypoxia-induced treatment resistance [5], and limited immune activation [6].

To overcome these limitations, nanoencapsulation strategies for PSs are being actively developed [7,8]. Encapsulation of hydrophobic PSs in nanocarriers such as liposomes, polymeric nanoparticles, or micelles addresses solubility and stability, preventing aggregation [9]. Nanoparticles with sizes of 10–200 nm passively accumulate in tumor tissue via the enhanced permeability and retention (EPR) effect, driven by tumor vasculature characteristics [10]. This enhances delivery selectivity, reducing therapeutic doses and impact on healthy tissues. The nanoparticle shell isolates the PS, reducing dark toxicity and systemic phototoxicity [11,12].

Biomimetic nanoparticles (BNPs) represent a transformative novel approach for PS delivery [13]. By mimicking biological structures, such as cell membranes, proteins, or endogenous carriers, BNPs enhance PS delivery through improved biocompatibility, immune evasion, and active tumor targeting. Beyond delivery, BNPs address hypoxia [5], a critical barrier to PDT efficacy, through oxygen-carrying systems like hemoglobin-based nanostructures, which retain the oxygen-binding capacity of hemoglobin and can effectively transport and release oxygen within the hypoxic tumor microenvironment (TME). Furthermore, biomimetic platforms can synergize PDT with immunomodulation by promoting immunogenic cell death (ICD) and checkpoint inhibitor co-delivery [14–16]. By leveraging biomimicry, these systems seek to overcome biological barriers, increase treatment efficacy, and reduce side effects.

This review examines recent progress in the development of BNPs for cancer photodynamic therapy, with particular attention to their ability to target tumors, counteract hypoxia, and stimulate the immune system. We also explore their use in treating different types of cancer, the emergence of multifunctional platforms that combine imaging and therapy, and the challenges that remain for translating these technologies into clinical practice. By merging principles of biomimicry with nanotechnology, BNPs offer a promising new approach to more precise and effective cancer treatments tailored to individual patients.

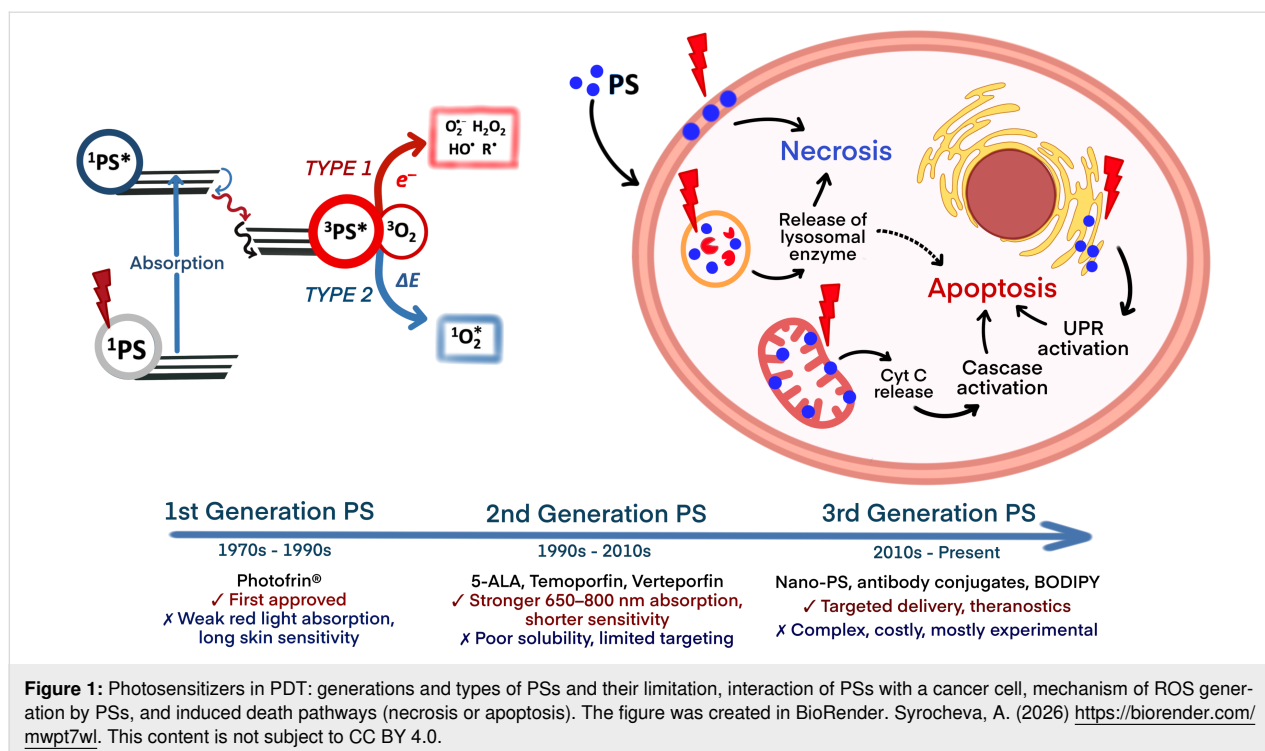
Overview of photodynamic therapy

PDT is a clinically established and continuously evolving treatment modality for various cancers and non-oncological conditions. Its therapeutic efficacy hinges on PSs, that is, specialized agents capable of absorbing light at specific wavelengths and transferring this energy to molecular oxygen or other substrates, generating cytotoxic ROS [17]. Historically, PDT relied on organic molecules, either naturally derived or synthetically produced, but since the early 21st century, advancements in nanotechnology have revealed the photosensitizing capabilities of nanostructured materials, significantly expanding the range of agents available for PDT applications [18].

The photochemical pathway for ROS generation involves non-radiative relaxation of the excited PS, typically occurring through two primary mechanisms [19]. Type-I reactions involve electron transfer, producing radical species such as superoxide anions, while type-II reactions involve energy transfer, generating singlet oxygen, the primary cytotoxic agent in PDT (Figure 1). Although nanostructured PSs are often associated with type-I reactions and molecular PSs with type-II reactions, the generation of one ROS type frequently triggers cascades leading to others, making the distinction primarily about the predominant mechanism rather than exclusivity.

Efficacy and safety of PDT are largely determined by the PS's properties [20]. An ideal PS must exhibit a high absorption coefficient in the near-infrared (NIR) range to enable deep tissue penetration, addressing a key PDT limitation. However, the use of longer wavelengths (>800 nm) is not practical due to their inefficiency in exciting an oxygen molecule from the triplet ground state to the excited singlet state [21]. A high quantum yield for ROS generation requires efficient excitation and minimal competing non-ROS-producing relaxation pathways. Low dark toxicity minimizes harm in the absence of light. High stability and low aggregation under physiological conditions are essential for maintaining photochemical activity [22]. A balanced hydrophilicity/lipophilicity ensures selective accumulation in target tissues, such as tumors via the EPR effect, and efficient cellular internalization. Low photobleaching sustains activity during treatment, while biocompatibility and biodegradability reduce adverse effects and enhance the therapeutic index. PSs are classified into generations, each reflecting progressive improvement (Figure 1).

The first generation of PSs included hematoporphyrin derivatives (e.g., Photofrin) [23]. The second generation of PSs encompasses purified compounds, including porphyrins [24], chlorins (e.g., chlorin e6 (Ce6) [25], mTHPC [26], bacteriochlorins [27], and phthalocyanines [28]), as well as non-porphyrinic structures like BODIPY dyes modified for enhanced ROS gen-



eration [29] and natural compounds such as hypericin and curcumin, primarily used in antimicrobial PDT [30]. Third-generation PSs focus on targeted delivery, achieved by conjugating second-generation PSs with carriers like antibodies, peptides, or nanoparticles to enhance specificity and reduce off-target effects [31,32].

The third generation of PSs should demonstrate minimal accumulation in healthy tissues and high selectivity toward pathological sites, thereby reducing side effects and increasing the therapeutic index. In this context, the use of nanocarriers for PS delivery gains particular importance, offering new opportunities to enhance both the selectivity and safety of PDT [33]. Currently, nanoparticles serve as versatile delivery system for a broad range of molecular therapeutics, including small molecules [34], RNA [35], plasmids [36], CRISPR/Cas systems [37], and other bioactive agents.

Several key advantages of nanocarriers in PDT can be highlighted: (i) improved solubility and stability of PSs, (ii) enhanced delivery through both passive and active targeting mechanisms, (iii) controlled and stimuli-responsive release profiles, (iv) overcoming of tumor hypoxia, (v) efficient light conversion, and (vi) the development of multifunctional platforms by combining PDT with other therapeutic modalities [38]. Additionally, nanoparticles enable theranostic applications [39] by facilitating tumor visualization through various imaging techniques [40], including fluorescence imaging [41],

computed tomography [42], and magnetic resonance imaging (MRI) [43].

The development of nanobiotechnology in PDT opens new horizons for creating more effective and safer cancer treatments. Further research in this field is expected to drive the design of personalized PDT approaches tailored to the unique characteristics of individual patients and tumors, as well as to broaden the clinical application of PDT across a wide range of oncological diseases.

Biomimetic nanoparticles: principles and platforms

The BNP concept: nature-inspired delivery

Advances in synthetic methods have enabled the fabrication of nanoparticles with a wide range of compositions, sizes, shapes, and surface properties [44,45]. These tunable characteristics make nanoparticles highly versatile for applications in disease diagnosis and sensing technologies. Despite the promising potential of nanomedicine, significant progress has been limited. This can be attributed to the low targeted accumulation of the nanocarriers at the desired site of action. For instance, in cancer therapy, the accumulation of nanoparticles within solid tumors typically does not exceed 1% of the administered dose [46]. The limited progress in achieving higher carrier targeted accumulation can be attributed to two main factors: (i) rapid clearance of the nanoparticles from the body, that is, nanoparticles are cleared from the systemic circulation by the organs and

the cells of the mononuclear phagocyte system (MPS), primarily the liver and spleen, and (ii) ineffective overcoming of biological barriers, that is, nanoparticles have to overcome numerous biological barriers to reach the target tissue, including extravasation from the vasculature, penetration through the interstitial space, and cellular internalization at the target site [47]. Conferring the carriers with a biomimetic shell that mimics the functions of biological cells potentially increases their circulation time and targeting properties, while significantly reducing the body's immune response [48]. BNPs utilizing a cell membrane to coat a synthetic core were reported in 2011. These nanoparticles consisted of a poly(lactic-co-glycolic) acid (PLGA) core coated with an outer layer derived from red blood cell (RBC) membranes [49]. It was demonstrated that the presence of this biomimetic shell increased more than two times the circulation time of the carriers in the bloodstream compared to uncoated PEGylated (polyethylene glycol-coated) nanoparticles, representing the gold standard approach to nanoparticle circulation time. Since then, a wide variety of cell phenotypes have been explored as sources for biomimetic membranes to coat nanoparticles such that inherent biological functions and properties of specific cells could be exploited to enhance the performance and versatility of BNPs. According to some authors, biomimetic systems comprising proteins from cells to mimic their functions belong to the third generation of nanodelivery systems [50]. The first generation of particles was based on surface modifications to reduce the interactions with immune cells and to increase biocompatibility. Among them, biocompatible polymers like PEG and PPE have been widely used [51]. The second generation of nanocarriers harnessed surface functionalization with antibodies, peptides, and aptamers to increase the targeting of pathogenic tissues and cells by interacting with the receptors expressed on the surface of the target cells [52]. In contrast, BNPs are designed to imitate the biological identity of cells through the corresponding surface proteins and clusters of biological molecules; these modifications enable the actions of aforementioned technologies and provide the particles with new functions.

Limitations of biomimetic nanoparticles

The clinical translation of BNPs is primarily hindered by challenges related to large-scale production, reproducibility, and quality control. The multistep fabrication process, including extraction of cellular membranes and coating of nanoparticle cores, requires careful optimization to ensure stability and consistency [53].

Cell lysis is essential for the extraction of biomimetic membranes; the membrane composition is directly influenced by the severity of the lysis method. Common techniques include (i) ultrasound, that is, membrane rupture via pressure waves

(20–50 kHz), requiring precise control to prevent heat damage [54]; (ii) freeze–thaw cycles, that is, cell disruption via narrow pores (enhanced at low temperatures) [55]; (iii) mechanical shearing, that is, cell disruption via narrow pores (enhanced at low temperatures) [56]; and (iv) osmotic pressure, that is, hypotonic solutions are used to induce swelling and rupture [53].

Lysis buffer selection (containing membrane disruptors and protease inhibitors) depends on cell type and target protein localization. For example, cancer cells and macrophages respond better to hypotonic protocols [57], and harsh homogenization suits cytomembrane protein extraction (above 30% cell composition).

Various methods exist for coating synthetic nanoparticle cores with biomimetic shells, each with unique advantages and limitations. A crucial factor is ensuring the correct “right-side-out” orientation of membrane proteins, which preserves system stability and enables proper interaction with target cells [58]. Common techniques include (i) physical co-extrusion, where nanoparticles and membranes are forced through porous membranes to form uniform coatings; (ii) sonication, which uses ultrasonic energy to induce membrane fusion and often favors correct protein orientation; and (iii) electroporation, which creates temporary pores in membranes to facilitate coating while preserving protein integrity. Electroporation is simpler, more versatile, and scalable, especially when combined with microfluidic devices that allow for precise control over coating conditions, improving uniformity and reproducibility [59]. Tailoring and combining these approaches enables the design of BNPs with desired functionalities, though challenges remain in standardizing protocols and scaling up production.

Other significant limitations include nonuniform coating, difficulties in purification, and maintaining sterility, especially for BNPs derived from bacterial membranes [60]. Heterogeneous coverage can affect nanoparticle stability and drug delivery efficiency, while purification processes must effectively separate fully coated particles from impurities. For bacterial membrane-based BNPs, thorough detoxification is essential to eliminate toxic components without compromising immunogenic properties [61].

Finally, the biomimetic coating can influence drug release profiles, potentially hindering the controlled release of therapeutic agents [62]. Optimizing these systems requires careful consideration of coating thickness, core material, and release mechanisms. Addressing these challenges through standardized production protocols, improved characterization, and enhanced biocompatibility will be critical to advancing BNPs toward clinical application.

Biomimetic nanocarriers, designed to replicate structure and functions of biological cells, present promising advantages for drug delivery and therapeutic applications. Nonetheless, they face notable challenges that require thorough investigation. Key areas of focus include developing standardized, scalable manufacturing techniques, elucidating their interactions with cells and mechanisms for crossing physiological barriers, enhancing stability for controlled drug release, and improving biocompatibility to ensure clinical safety. Tackling these challenges is essential to optimize biomimetic nanocarriers for better efficacy and successful translation into clinical practice.

Crossing of biological barriers

BNPs face a series of biological barriers upon administration, which significantly influence their therapeutic and diagnostic effectiveness [63]. One of the first challenges is opsonization, where plasma proteins form a “protein corona” [64] on the nanoparticle surface, often reducing targeting specificity and biocompatibility. Coating nanoparticles with cell membranes, such as those from RBCs or leukocytes, can minimize protein corona formation, preserve targeting ligands, and extend circulation time by evading immune clearance. This strategy leverages natural “self-markers” like CD47 to inhibit phagocytosis and enhance passive tumor accumulation via the EPR effect [65].

Immune clearance by the MPS, primarily in liver and spleen, is another major hurdle. Biomimetic coatings help nanoparticles avoid rapid removal from the bloodstream, as demonstrated by prolonged circulation and increased tumor targeting in systems coated with erythrocyte or stem cell membranes [66]. Such coatings can also facilitate homotypic targeting, where nanoparticles preferentially bind to and are internalized by cancer cells of the same origin, further improving specificity and reducing off-target effects.

The behavior of BNPs in the bloodstream is also shaped by hemodynamics and vessel wall interactions. Platelet-mimicking nanoparticles, for example, can adhere to vascular injury sites and inflamed tissues, enhancing accumulation at target areas and even supporting hemostasis. These properties are particularly valuable for treating inflammatory diseases and targeting tumors.

Crossing the blood–brain barrier (BBB) remains a significant challenge for nanomedicine. BNPs coated with membranes from cells capable of BBB penetration, such as neutrophils or cancer cells, show improved brain delivery [67]. Additional modifications with targeting peptides can further enhance BBB crossing, opening new possibilities for treating neurological diseases.

Finally, successful therapy depends on efficient cellular uptake and drug release. Biomimetic shells can increase nanoparticle internalization through receptor-mediated endocytosis and homotypic binding, as well as improve colloidal stability. Strategies such as incorporating pH-sensitive components or lysosomal escape mechanisms further enable controlled drug release within target cells. Despite these advances, optimizing BNP design to overcome all biological barriers remains an active area of research essential for clinical translation.

BNP functionalization

The development of biomimetic drug delivery systems has advanced rapidly, with multifunctional platforms emerging as a key focus [68,69]. By leveraging the natural properties of cell membranes, such as immune evasion, prolonged circulation, and specific targeting, BNPs can be further enhanced through surface modifications to improve their therapeutic performance. These modifications enable BNPs to address complex challenges in drug delivery, including targeted transport, controlled release, and overcoming biological barriers.

One promising strategy is the creation of hybrid biomimetic coatings, where membranes from multiple cell types are fused to combine their unique functionalities. For example, NPs coated with a mix of RBC, cancer cell, and immune cell membranes can simultaneously evade the immune system, target tumors, and deliver drugs to metastatic sites. This approach has demonstrated improved blood circulation, enhanced tumor targeting, and increased therapeutic efficacy in preclinical models. However, the process of membrane fusion and the need for additional purification steps add complexity to manufacturing [70].

Genetic modification of source cells offers another avenue for BNP functionalization. By engineering cells to express specific targeting proteins or receptors before membrane extraction, it is possible to produce BNPs with highly selective targeting capabilities. For instance, membranes from CAR-T cells or stem cells engineered to overexpress homing receptors can be used to create BNPs that efficiently recognize and bind to tumor cells or inflamed tissues, minimizing off-target effects and systemic toxicity [71,72].

Post-synthesis surface modification is also widely used to enhance BNP functionality [73–75]. Non-covalent methods, such as lipid insertion, allow for the integration of targeting ligands, peptides, or imaging agents into the membrane without disrupting protein activity. Covalent modifications, including the attachment of antibodies or peptides via amide or thiol–maleimide linkages, provide stable and specific functionalization but may risk altering membrane protein function if

not carefully controlled. Enzymatic approaches can offer greater specificity but require additional steps and conditions.

These advanced BNPs can be engineered to respond to specific stimuli, such as pH, enzymes, or external triggers like light, enabling controlled drug release at the target site [76]. For example, pH-sensitive lipids or peptides can be incorporated to accelerate drug release in the acidic tumor microenvironment. Additionally, BNPs can be loaded with imaging agents or therapeutic enzymes to facilitate tumor visualization and penetration, further expanding their utility in cancer therapy. Targeting strategies can be further refined by integrating ligands such as arginylglycylaspartic acid (RGD) peptides, antibodies, or aptamers onto the BNP surface, enhancing their ability to recognize and bind to specific cell markers [77]. Incorporating imaging dyes or contrast agents into the BNP membrane also enables real-time tracking and monitoring of drug delivery in vivo. The main stages of biomimetic nanoparticle fabrication and subsequent surface modification are summarized in Figure 2.

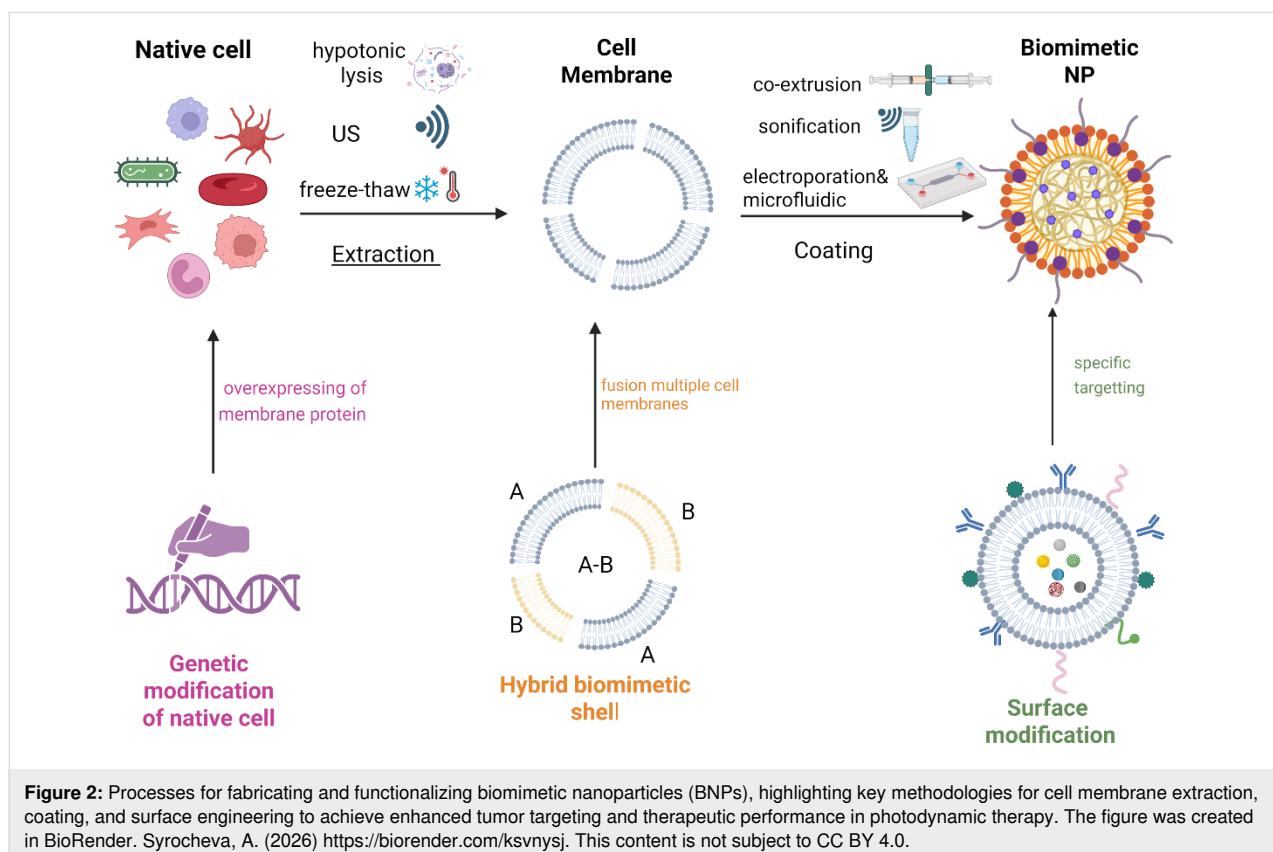
BNPs for enhanced delivery and specificity in PDT

BNPs achieve spatial specificity within the TME through a hierarchical targeting strategy, combining passive accumulation

mechanisms with innate or engineered active targeting capabilities. This multilevel approach significantly enhances the delivery efficiency of PSs compared to conventional nanocarriers [78].

Passive targeting primarily exploits EPR effect, a pathophysiological feature of many solid tumors characterized by leaky vasculature and impaired lymphatic drainage [79,80]. BNPs amplify passive accumulation through their extended circulation time, a direct consequence of immune evasion conferred by their biomimetic coatings [81]. Prolonged systemic exposure increases opportunities for extravasation through tumor vasculature. For instance, erythrocyte membrane-coated BNPs consistently demonstrate 1.5- to 2.0-fold higher tumor accumulation than their uncoated counterparts with identical cores, attributable solely to superior circulation half-life and EPR potentiation [82–84]. While EPR is a universal mechanism for nanocarriers, the significant enhancement provided by biomimetic coatings, particularly erythrocyte and mesenchymal stem cell membranes, represents a critical advantage over synthetic platforms, enabling greater passive PS deposition within tumors [85].

Active targeting utilizes specific molecular interactions to enhance tumor cell binding and internalization. BNPs employ both innate (source cell-derived) and engineered strategies to



achieve this. Innate active targeting exploits the inherent biological tropism preserved on the source cell membrane, requiring no additional modification [86]. As exemplified by mesenchymal stem cell (MSC) membrane-coated BNPs, this system can utilize the natural homing capability of the source cells (e.g., MSCs migrating towards TME chemokine gradients like SDF-1 α and CCL2) [87]. This conserved tropism results in significantly higher tumor accumulation compared to untargeted controls [88].

The biological specificity of different cell types is determined by proteins present on their plasma membranes, which not only serve structural roles but also mediate cell–cell adhesion, either homotypic or heterotypic, depending on molecular affinity. The primary mechanisms underlying homotypic binding involve various classes of adhesion proteins, such as integrins, selectins, cadherins, and members of the immunoglobulin superfamily (IgSF). Integrins typically interact with the extracellular matrix, whereas selectins, cadherins, and IgSF proteins are primarily responsible for cell–cell adhesion [89]. The cytoplasmic and extracellular domains of these proteins confer distinct physicochemical properties that influence cellular interactions and tissue organization. Given the crucial role of integrins in tumor progression, there is significant interest in their use not only as markers of malignant potential but also as targets for precision therapies.

One of the most extensively studied integrins, α V β 3, is a transmembrane receptor for extracellular matrix proteins that binds cyclic RGD peptides with high affinity and interacts with SRC oncogene to promote lymph node metastasis. For example, RGD-coated BNPs enhanced doxorubicin (DOX) uptake by 1.4 times in α V β 3-positive U-87 MG glioblastoma cells compared to α V β 3-negative HeLa cells [90]. In urological cancers, integrin α 5 β 1 is upregulated, facilitating cell adhesion to fibronectin; PHSCN peptide-targeted BNPs have shown efficacy in inhibiting prostate cancer metastasis in preclinical and clinical settings [91]. High malignancy cancer cells display reduced homotypic adhesion but increased heterotypic adhesion to endothelial cells, mediated by molecules such as IL6R [92], CXCR4 [93], and EPCAM [94], which are targeted via peptide-functionalized BNPs to inhibit metastasis. Additionally, NGR peptides targeting aminopeptidase N have improved photoinduced activity of chlorin e6 in fibrosarcoma cells [95]; dual peptide modification of PLGA nanoparticles enhanced brain targeting in glioma models [96]. Integrin expression varies across tumor types, influencing homotypic targeting strategies [89,97]. A membrane coverage of 50% and more enables cellular uptake of individual nanoparticles, while lower coverage requires aggregation for internalization [60]. Using cancer cell membranes (CCMs) with high coverage on BNPs ensures selec-

tive targeting through integrin-mediated homotypic binding, promoting efficient therapeutic delivery (Figure 3). Relevant proteins enabling homotypic targeting via BNPs are listed in Table 1.

Early studies on BNPs often employed simple coatings derived from CCMs. This approach effectively camouflaged the nanoparticles by conferring the properties of “self” cells, thereby enhancing biocompatibility and reducing neutrophil-mediated immune clearance. For instance, BNPs loaded with DOX and coated with glioblastoma cell membranes were employed as a targeted therapy for malignant tumors. The presence of surface adhesion molecules, including N-cadherin, galectin-3, and epithelial cell adhesion molecules, facilitated enhanced uptake of the drug in the human glioblastoma U87 MG cell line. This resulted in an 8.5-fold increase in cellular internalization compared to uncoated nanoparticles [105]. However, over time, it became evident that such simple membrane coatings have limited functional capabilities. This realization has driven the development of additional surface modifications aimed at improving targeting specificity to particular cells or tissues, enhancing stability in the bloodstream, controlling drug release kinetics, and tailoring nanoparticle systems to meet diverse clinical requirements. Recent advances in this field have demonstrated the remarkable efficacy of homophilic targeting. Specifically, the involvement of CD47 from lung CCM has been shown to facilitate evasion of phagocytosis, while N-cadherin, galectin-3, CD44, and CD326 mediate homotypic binding to cancer cells; this resulted in a threefold increase in the accumulation of PLGA nanoparticles within the tumor [106]. A notable study aimed to evaluate the translational potential of biomimetic delivery systems for precise tumor therapy. Gold@carbon nanoparticles were coated with proteins derived from different cell types, including a squamous cell carcinoma cell line and patient-derived cells. To address tumor heterogeneity, these systems were tested across various xenograft models, namely, cell line-derived subcutaneous xenografts, orthotopic tongue xenografts, immunocompetent primary and distant tumor models, and patient-derived xenografts. In all models, the biomimetic coating enhanced nanoparticle accumulation within tumors and improved therapeutic efficacy. The authors emphasize the importance of such comprehensive evaluations to facilitate the translation of these findings into clinical practice [107].

A prominent trend in drug delivery is the creation of multifunctional, stable, and biocompatible platforms with tunable biological activity, often achieved by using hybrid membrane coatings that combine proteins from multiple cell phenotypes, thereby enhancing their therapeutic and diagnostic versatility. The concept of hybrid membrane coating was first introduced in 2017 [108], where PLGA nanoparticles were coated with

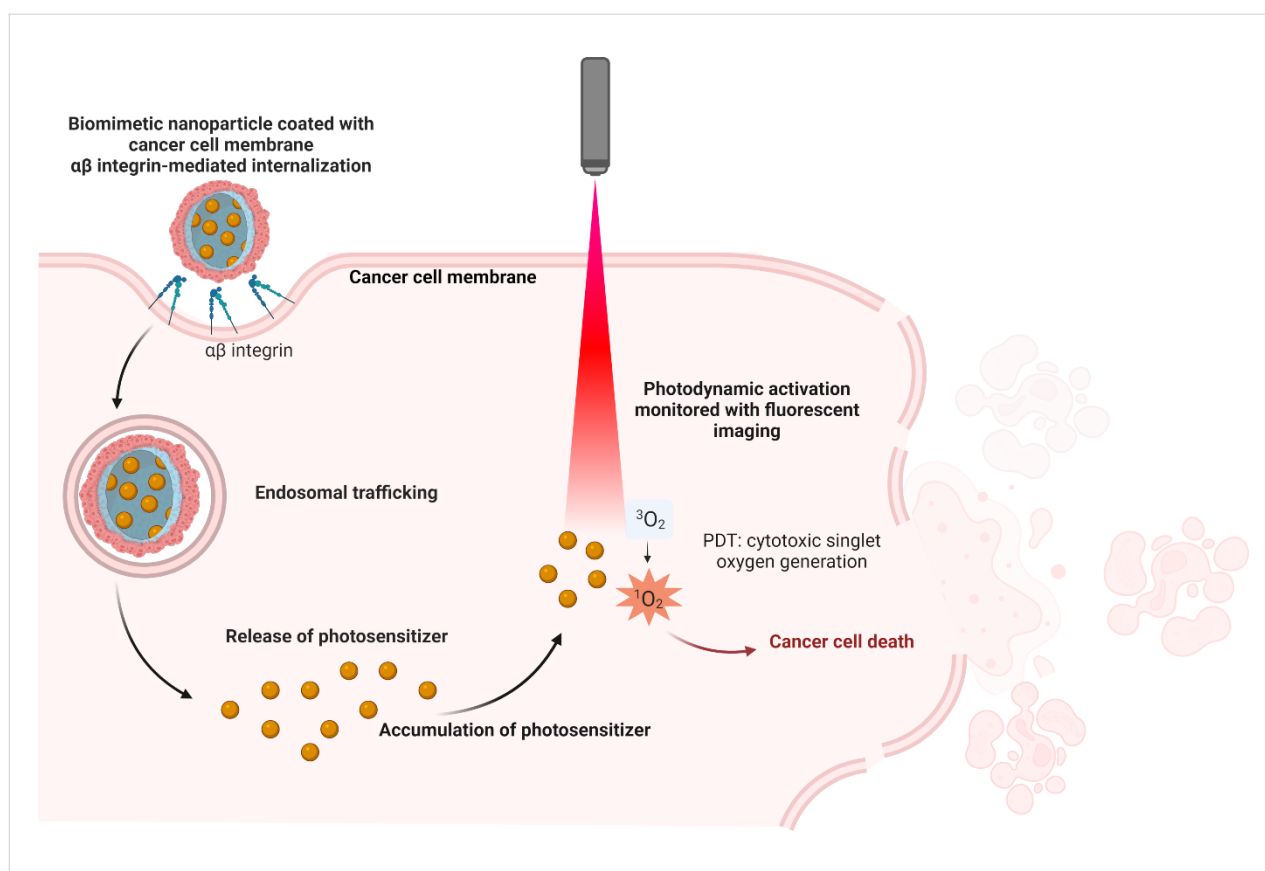


Figure 3: Selective targeting and internalization via homotypic binding and receptor-mediated endocytosis of biomimetic nanoparticles coated with cancer cell membranes, enabling enhanced photosensitizer accumulation and reactive oxygen species generation for improved photodynamic therapy. The figure was created in BioRender. Syrocheva, A. (2026) <https://biorender.com/jjvlem9>. This content is not subject to CC BY 4.0.

Table 1: A list of proteins that can be incorporated into biomimetic nanoparticles to facilitate targeted delivery via homotypic binding.

Protein	Cell lines	Cancer type	Application in drug delivery	Ref
α- and β-integrins	4T1, BT-20, B16, C4-2B	breast cancer, breast carcinoma, melanoma, prostate cancer, bone metastases	In biomimetic nanoparticles, proteins and peptides containing the RGD (arginine-glycine-aspartate) motif are most often used for targeted binding to α- and β-integrins. The main proteins used in such systems are fibronectin, vitronectin, and laminin, as well as synthetic RGD-based peptides (for example, cyclic RGD peptides). The use of fibronectin in the coating of nanoparticles loaded with doxorubicin, tannic acid, and iron contributed to the targeted therapy of the B16 tumor with high expression of integrin α5β3. Intracellular absorption of nanoparticles was confirmed by confocal laser scanning microscopy. For the treatment of prostate cancer C4-2B, poly(lactic-co-glycolic acid) nanoparticles coated with cancer cell membranes containing integrin β3, a subunit of integrin α5β3, were used. The resulting nanoparticles demonstrated a fourfold increase in absorption in C4-2B cells compared to uncoated nanoparticles, which was measured using flow cytometry.	[98-100]
E-cadherin and N-cadherin	4T1 cells	breast cancer, lung metastases	4T1 cancer cell membrane-coated paclitaxel nanoparticles showed 3.3 times and 2.5 times higher accumulation in primary breast tumors and lung metastases versus uncoated NPs. Negative controls (RBC-coated and liposome-coated NPs) had lower uptake. E- and N-cadherins mediated binding.	[101]

Table 1: A list of proteins that can be incorporated into biomimetic nanoparticles to facilitate targeted delivery via homotypic binding. (continued)

P-selectin	H22 cells	hepatoma	Platelet membrane-coated biomimetic nanoparticles loaded with bufalin targeted hepatoma via P-selectin–CD44 interaction, enhancing uptake and inhibiting tumor growth.	[102]
E-selectin	A549, Hs 578T	circulating tumor cells (various)	Surfactant–nanotube biomimetic complexes with E-selectin facilitated capture of circulating A549 and Hs 578T carcinoma cells, confirmed by flow cytometry.	[103]
galectin-1 and galectin-3	4T1 cells	breast cancer	biomimetic nanoparticles containing calcium phosphate and STING Mn ²⁺ agonist, Cypate photosensitizer, and indolamine 2,3-dioxygenase 1 (IDO1); the inhibitor was coated with galactose to act on galectin-1 and galectin-3 receptors; after intravenous administration to mice, this system demonstrated high accumulation in 4T1 tumors, which ensured accurate diagnosis and effective elimination.	[104]

combined erythrocyte and platelet membranes, leveraging their unique functions to evade immune clearance and target inflammatory sites. Since then, an increasing variety of differentiated cell membranes have been combined to modify biomimetic nanoparticle surfaces, such as cancer cell–erythrocyte [108] and macrophage–cancer cell [109] hybrids (Figure 4). For combinational therapy of triple-negative breast cancer, BNPs based on tumor cell membranes and PLGA loaded with the cytolytic peptide melittin and the photosensitizer mTHPC have been developed. In vitro and in vivo studies demonstrated that these nanoparticles mitigated the acute toxicity of melittin and enhanced tumor accumulation of mTHPC in 4T1 tumor-bearing mice, while facilitating accelerated melittin release due to disruption of the membrane integrity [110].

Similar to other nanodelivery systems, a wide variety of surface functionalization strategies have emerged to enhance targeting efficiency in BNPs. In a 2022 study, a sophisticated biomimetic system was developed comprising paclitaxel nanocrystals coated with SKBR-3 cell membranes. The membrane coating was further functionalized with Herceptin, a monoclonal antibody that selectively binds to HER2 receptors, rendering the platform a promising candidate for the treatment of HER2-positive breast cancer [111]. In vivo experiments demonstrated homotypic targeting, significantly enhanced cellular uptake compared to uncoated nanocrystals, and confirmed the system’s ability to induce apoptosis in HER2-positive breast cancer cells. Another study reported the development of a multifunctional biomimetic system coated with erythrocyte

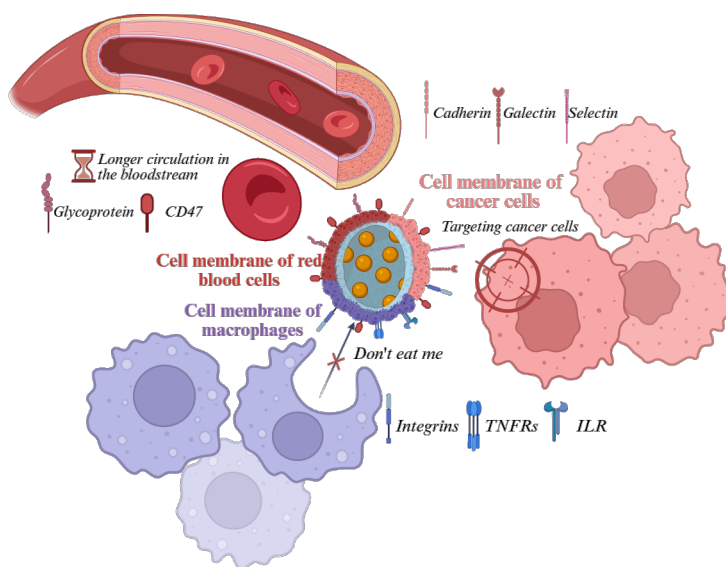


Figure 4: Modifications of biomimetic nanoparticle coatings using erythrocyte, macrophage, and cancer cell membranes, conferring unique functional properties including prolonged systemic circulation, immune response evasion, and homotypic tumor targeting for enhanced photodynamic therapy. The figure was created in BioRender. Syrocheva, A. (2026) <https://biorender.com/ffuwj1>. This content is not subject to CC BY 4.0.

membranes for the co-delivery of chlorin e6 and DOX to enhance synergistic targeted tumor therapy. This system exhibited high targeting efficiency toward HepG2 cells via folic acid receptor-mediated endocytosis, followed by effective tumor eradication through singlet oxygen generation. Modification with erythrocyte membranes also conferred prolonged circulation time to the nanoparticles, attributed to the presence of the CD47 molecule [112].

An alternative approach to the functionalization of biomimetic coatings is based on genetic engineering. In a recent study employing this strategy, the cell membrane from a genetically engineered HEK-293 cell line expressing synthetic SpyCatcher proteins was used to coat NPs, enabling targeted binding to both tumor cells and viral particles. Treatment with these nanoparticles in a mouse model of ovarian cancer suppressed tumor growth and improved survival outcomes [113]. For the therapy of uveal melanoma, BNPs coated with recombinant low-density lipoproteins were developed to deliver the PS verteporfin and the vascular-normalizing agent dexamethasone. Following intravenous administration, these nanoparticles selectively accumulated in tumor tissue; verteporfin generates ROS, resulting in tumor cell death, while the ROS also facilitated rapid release of dexamethasone, which inhibited neovascularization in the tumor microenvironment. Thus, the ability to program specific protein sequences allows for their precise display on the nanoparticle surface in physiologically relevant conformations and orientations, thereby enhancing their functional activity in binding to cellular receptors.

A key emerging trend in such delivery systems is the development of smart platforms that respond to external stimuli, enabling remote-controlled release of therapeutic payloads. A significant advancement came from Wang's group in 2023 [114], who developed "adaptive" CCM-coated nanoparticles that could dynamically alter their surface properties in response to the TME. By incorporating pH-sensitive linkers between the membrane coating and targeting ligands, these nanoparticles maintained their stealth properties during circulation but exposed their homophilic binding sites specifically within the acidic tumor environment, resulting in a 2.5-fold increase in tumor-specific uptake compared to conventional membrane-coated systems.

Main classes of biomimetic nanoplatforms for photosensitizer delivery

Exosome-based platforms utilize naturally secreted extracellular vesicles (40–100 nm) possessing a lipid bilayer and a unique surface protein profile derived from various cell types (e.g., dendritic cells, T cells, and macrophages) [86,115,116]. Their endogenous role in intercellular communication confers

low immunogenicity and high biocompatibility, facilitating evasion of immune clearance [117]. A key advantage is their ability to penetrate biological barriers, including the BBB [118], enabling access to challenging tumor sites like glioblastoma [119]. The surface-exposed proteins support inherent cell-specific interactions, which can be augmented by engineering targeting ligands for improved tumor specificity [120]. In PDT, exosomes effectively deliver PSs like Ce6, demonstrating enhanced tumor accumulation and photodynamic efficacy compared to free PSs [121]. Challenges include complex isolation procedures, heterogeneity, scalability limitations, and potential loss of membrane protein activity during processing [122].

CCM-coated platforms involve cloaking synthetic nanoparticle cores (e.g., PLGA, silica, and metal-organic frameworks (MOFs)) with membranes derived from tumor cells [123]. This biomimetic strategy primarily exploits homotypic targeting; the CCM retains adhesion molecules (e.g., galectin-3 or T-antigen binding proteins) enabling preferential binding and deep penetration into homologous tumor tissues. CCM-coated NPs have successfully delivered diverse PSs (e.g., Ce6 [124,125], PCN-224 [126], and IR-780 [127,128]), often in combination therapies (e.g., chemo-PDT and immune checkpoint blockade [129]), achieving high tumor accumulation and potent PDT responses in preclinical models. Critical limitations include the inherent specificity of homotypic targeting to the parent cancer cell type, restricting broad applicability, and scalability challenges in membrane production and fusion.

RBC membrane-coated platforms employ the readily available membranes of RBCs to encapsulate nanoparticle cores [130]. Their primary advantages are their exceptional ability to evade the immune system and their long circulation half-life, which exceeds 100 days *in vivo* for native RBCs [84]. These properties have popularized two major strategies, that is, using RBC membranes as a biomimetic shell for nanoparticles [131] and directly targeting circulating RBCs *in vivo* for drug delivery [132]. This is largely mediated by CD47 expression on the RBC membrane, which delivers a potent "do not eat me" signal by binding to SIRP- α on phagocytes [133]. This inherent property ensures high biocompatibility and minimal toxicity. While lacking innate tumor targeting, RBC-coated NPs can be effectively functionalized with ligands (e.g., folate [83,134] or peptides like RGD [135,136]) to achieve active targeting, enhancing accumulation at tumor or infection sites. These platforms efficiently deliver PSs (e.g., Ce6 [137], TPC [138], MC540 [83], indocyanine green (ICG) [139], or IR-780 [140]), leveraging the EPR effect, long circulation times, and potential ligand-mediated targeting to improve tumor PS levels, thereby enhancing PDT efficacy and enabling combination strategies (e.g., with anti-PD-1 immunotherapy [141]). The need for addi-

tional functionalization for specific targeting and potential batch variability in membrane extraction represent key considerations.

MSC membrane-coated platforms utilize membranes derived from stem cells to cloak nanoparticle cores [142]. A defining characteristic is their ability to mimic the tumor tropism of native MSCs. This is achieved through the retention of chemokine receptors (e.g., CXCR4) on the MSC membrane, which mediate specific adhesion to ligands (e.g., SDF-1 α) prevalent on the endothelium within TME [143]. This property facilitates active migration towards tumor and metastatic sites. Additionally, MSC membranes confer low immunogenicity and reduced MPS clearance, enhancing overall biocompatibility and tumor penetration. MSC-coated NPs have been employed to deliver PSs such as Ce6 [144], ZnPc, and MC540 [145], demonstrating improved tumor accumulation and cellular uptake compared to non-biomimetic counterparts. While the tropism is advantageous, the precise molecular mechanisms governing MSC homing require further elucidation, and scalability/reproducibility of MSC culture and membrane isolation remain practical challenges.

Immune cell membrane-based platforms incorporate membranes from various immune cells (e.g., macrophages, neutrophils, dendritic cells (DCs), T cells, and natural killer (NK) cells) onto nanoparticle cores or utilize derived extracellular vesicles [53]. Immune cell membrane-based BNPs represent a breakthrough platform that seamlessly integrates PDT with immunotherapy. The membranes retain source cell-specific functionalities: (i) Macrophage membranes exhibit tropism towards inflammatory sites and tumors via chemokine receptors (e.g., CCR2) and adhesion molecules. Pre-polarization to an M1 phenotype *ex vivo* can further equip these nanoparticles to reprogram the immunosuppressive TME [146,147]. (ii) Neutrophil membranes inherently target inflamed endothelium and tumor sites; facilitate crossing vascular barriers [148]. (iii) DC membranes possess inherent homing to lymph nodes and carry tumor-associated antigens, promoting antigen presentation and T-cell activation when combined with PDT-induced ICD [149]. (iv) T-cell membranes (including CAR-T) enable specific antigen recognition via TCR or CAR [150-152]. (v) NK cell membranes inherit natural cytotoxicity receptors (e.g., NKG2D and NKp30) for innate tumor recognition and killing activation [153]. (vi) Platelet-derived membranes exhibit natural adhesion to damaged vasculature (common in tumors) and circulating tumor cells (CTCs); they also express CD47 for extended circulation and modulate immune cell interactions and inflammation [154].

These properties allow for deep tumor penetration and direct interaction with immune components within the TME. Conse-

quently, immune cell BNPs can deliver PSs while simultaneously modulating the immune landscape; for instance, they promote ICD via PDT and concurrently deliver checkpoint inhibitors (e.g., anti-PD-1/PD-L1) or immunomodulators (e.g., R848). This potent combination therapy approach is explored further in the context of immune modulation. Challenges include the complexity and variability of immune cell membrane isolation, potential for immune rejection depending on allogenicity, reproducibility, and scalability. Hybrid platforms represent an advanced strategy where membranes from two or more distinct cell types (e.g., RBC + cancer cell, RBC + immune cell, and cancer cell + macrophage) are fused to create a single biomimetic coating [155]. This approach combines the unique advantages of each parental membrane.

PS loading into biomimetic nanocarriers

Efficient encapsulation of PSs into BNPs is a pivotal step that directly influences the overall therapeutic outcome of PDT. The success of PDT hinges not only on the intrinsic photochemical properties of the PS but also on its effective delivery to the tumor site, stability during circulation, bioavailability within the TME, and ability to be activated by light to generate ROS. BNPs, by virtue of their biological surface functionalities and synthetic nanoscale architecture, offer sophisticated platforms that maximize these criteria. However, the process of loading PS into such carriers must be carefully optimized to maintain the delicate balance between high loading capacity, preserved photophysical activity, controlled release, and targeting specificity. Several advanced strategies have been developed and tailored to integrate PSs into BNPs. These approaches take into consideration the hydrophobic nature of the PS, the chemical functionalities available for conjugation, and the physicochemical characteristics of the carrier. For instance, encapsulation techniques must ensure that PS molecules remain stably entrapped within the nanoparticle core to prevent premature leakage during blood circulation while enabling efficient release or activation within the tumor site.

A widely adopted approach is to first encapsulate hydrophobic PS molecules into synthetic nanoparticle cores. These stable PS-loaded cores are subsequently cloaked with natural cell membranes, imparting immune evasion, prolonged circulation, and targeting. Ce6 was loaded to methoxy PEG-PLGA NPs via microfluidic flow, covered with RBC membrane and modified with folic acid. The loading efficiency was 20%, and coating with the biomimetic membrane reduced the initial burst release during the first 4 h while sustaining gradual release over 48 h. The biomimetic coating increased the rate of cancer cell apoptosis induced by the photodynamic effect by 50% and prolonged the circulation time of the nanoparticles in the bloodstream [112].

BNPs composed of materials such as melanin or polydopamine exploit strong π - π stacking interactions with aromatic PSs like Ce6 to achieve high loading capacity. For instance, melanin-based nanoparticles loaded with Ce6 (loading efficiency \approx 30%) showed enhanced biocompatibility and water solubility, with synergistic photodynamic and photothermal effects under imaging guidance [156].

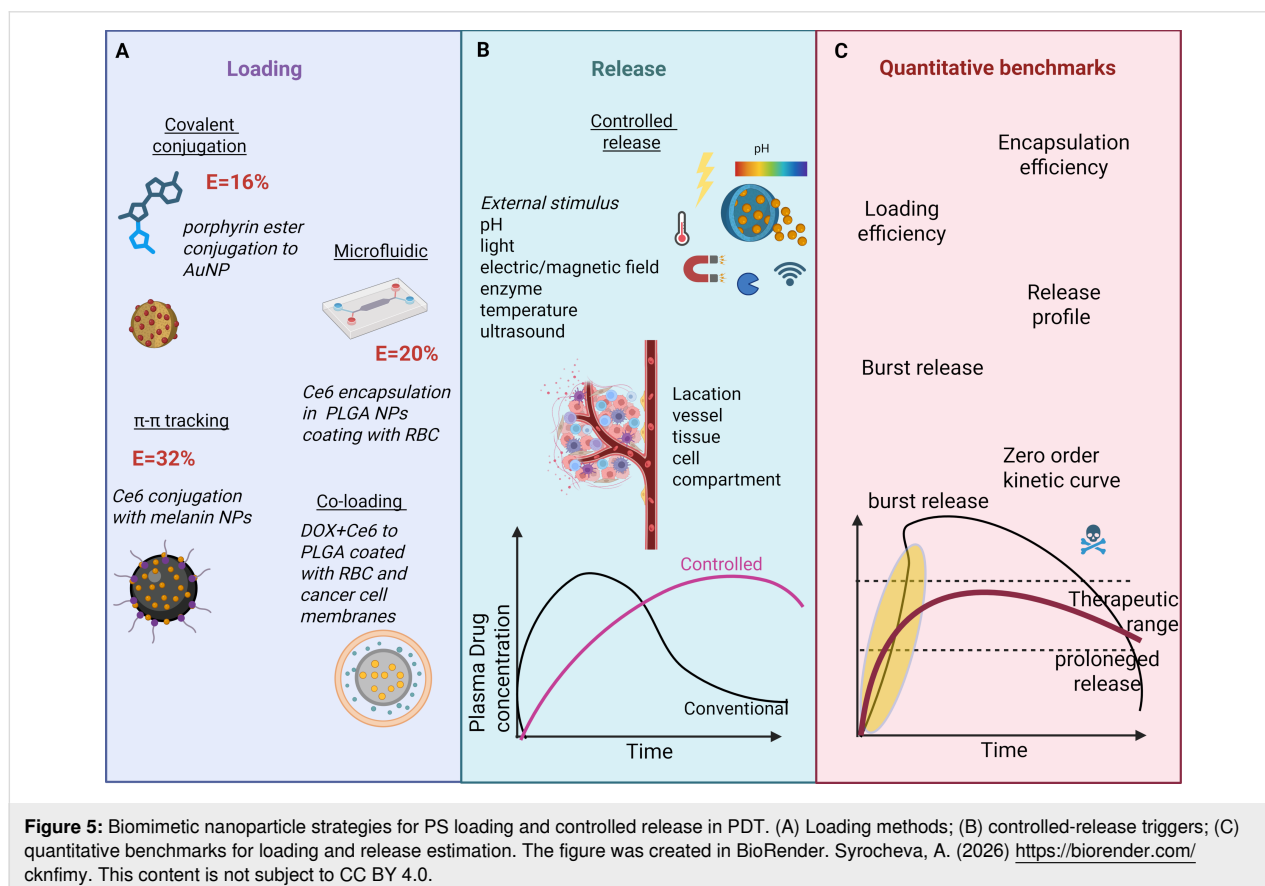
Another strategy involves chemically attaching porphyrin-based PSs bearing conjugatable functional groups (e.g., carboxyl) onto the surface of bioinspired nanoparticles such as noble metal nanoparticles (Ag and Au). Stable ester bond formation secures the PS to the nanocarrier surface, offering hydrophilicity, biocompatibility, and enhanced biological delivery. Loading efficiencies of \approx 16% have been reported for synthesized porphyrin PS and bioinspired metal nanoparticles (rich in -OH groups), suitable for dual PDT and photothermal therapy (PTT) [157].

Some biomimetic platforms enable co-loading of the PS with other agents to boost therapeutic outcomes. For example, DOX was preloaded into RBC nanovesicles while Ce6 was encapsulated in polymeric cores coated with RBC membranes [112]. Doxorubicin and ICG were loaded to BNPs with CCMs and in vivo demonstrated high tumor ablation with low systemic toxic-

ity. This multifunctional system combines chemotherapy and PDT, together with a number of diagnosis tools [158].

Beyond efficient loading, controlled PS release from BNPs represents a complementary critical factor governing PDT efficacy within the TME. Biomimetic coatings not only facilitate high payload delivery but also enable stimuli-responsive release mechanisms tailored to TME conditions, including light-triggered bursts (e.g., $>$ 70% PS liberation within 5 min via azobenzene linker cleavage under 660 nm irradiation [159]), enzyme-sensitive untethering (MMP-2 hydrolysis of peptide linkers overexpressed in tumor ECM [160]), and biomimetic pH gradients (sustained zero-order release over 24–72 h during endosomal acidification [161]). These strategies ensure spatiotemporal ROS generation while minimizing off-target phototoxicity, as exemplified by membrane-cloaked systems exhibiting reduced initial burst ($<$ 20% at 4 h) and prolonged therapeutic windows. These integrated loading/release optimizations are illustrated in Figure 5.

In summary, biomimetic platforms coated with cell membranes or molecules offer a highly promising strategy for the targeted delivery in cancer theranostics, particularly in PDT. By leveraging homotypic recognition and binding to tumor cells, these



coatings enhance selective accumulation within tumors while minimizing adverse effects on healthy tissues. Moreover, the integration of diverse therapeutic agents within these BNPs can yield synergistic antitumor effects, thereby improving the overall efficacy of PDT. This approach represents a significant advancement in the development of precise and effective cancer treatments. The precise loading and controlled release of PS into BNPs represent equally pivotal determinants of PDT efficacy, warranting comprehensive analysis alongside encapsulation strategies. While high loading capacities ensure adequate PS payloads for sufficient ROS generation at tumor sites, release kinetics govern bioavailability within the tumor microenvironment, spatiotemporal control of photoactivation, and minimization of off-target phototoxicity during systemic circulation.

Addressing tumor hypoxia: BNP innovations

The intrinsic hypoxic nature of solid tumors poses a major challenge to PDT efficacy, as limited oxygen availability restricts ROS production. Furthermore, the oxygen consumption during PDT can exacerbate tumor hypoxia, which not only diminishes therapeutic outcomes but also promotes tumor progression, metastasis, and resistance to treatment. Consequently, overcoming tumor hypoxia has become a critical focus in enhancing PDT effectiveness, with numerous strategies being developed to improve oxygen supply, reduce oxygen consumption, or employ oxygen-independent mechanisms to circumvent this limitation. Addressing hypoxia is essential for advancing PDT toward more reliable and potent cancer therapies.

The primary strategies for alleviating tumor hypoxia can be categorized into four main approaches: (i) direct oxygen delivery to the tumor [162-165], (ii) in situ oxygen generation [166-169] within the hypoxic microenvironment, (iii) reduction of oxygen consumption by tumor cells [170-172], and (iv) suppression of hypoxia-inducible factor 1 (HIF-1) activity in the tumor [173,174]. Typically, these nanoparticles consist of a functional core, perfluorocarbons (PFCs) [175-177] or MOFs [165,178,179], and a stabilizing matrix often composed of polymers, lipids, or proteins like human serum albumin (HSA) [177]. Figure 6 schematically illustrates examples of these key strategies for mitigating hypoxia in tumor tissues using BNPs. Table 2 presents the main strategies for using BNPs to mitigate hypoxia in tumors.

Oxygen delivery

To overcome tumor hypoxia and enhance the efficacy of PDT in triple-negative breast cancer, a multifunctional BNP system was developed. The photosensitizer ICG was encapsulated within a HSA matrix to prevent aggregation and supplemented with perfluorotributylamine (PFTBA) as an oxygen carrier. The

nanoparticles were further coated with a 4T1 CCM to enable targeting. Direct oxygen delivery to the tumor via PFTBA resulted in a significant reduction of hypoxia, and immunofluorescence staining revealed a tenfold decrease in hypoxic regions within the tumors. In 4T1 cells exposed to NIR laser irradiation, membrane-coated nanoparticles generated singlet oxygen with threefold greater efficiency compared to non-coated nanoparticles. In BALB/c mouse models bearing 4T1 tumors, the membrane-coated nanoparticles preferentially accumulated in tumor tissue, whereas non-coated particles also distributed to the liver and kidneys. Fourteen days post-treatment, a threefold reduction in tumor volume was observed [177].

An alternative strategy has also been described, wherein the photosensitizer ICG is encapsulated within a zirconium-based MOF that functions both as an oxygen reservoir and carrier. The particles were coated with an erythrocyte membrane, which confers immune evasion and enables passive tumor targeting via the EPR effect. Oxygen delivery was mediated directly by the MOF. Studies using murine macrophages (RAW264.7) demonstrated that membrane-coated nanoparticles effectively evade phagocytosis. In three-dimensional MCF-7 cell spheroids, oxygen-saturated nanoparticles increased system cytotoxicity fourfold. In animal models (Balb/c-nu mice bearing MCF-7 tumors), combination treatment resulted in a significant reduction of tumor hypoxia, as demonstrated by photoacoustic imaging showing increased oxygenated hemoglobin levels; also, immunofluorescence staining revealed decreased HIF-1 α expression compared to the control group. By day 27 after treatment initiation, the relative tumor volume was 100 times smaller compared to the control group [178].

Another system consisted of ICG and PFTBA loaded into a HSA core, which was subsequently coated with an erythrocyte membrane containing the CD47 protein to enable prolonged circulation (up to 24 h) and immune evasion. In vitro studies using HeLa cells and RAW264.7 macrophages demonstrated that the biomimetic membrane coating reduced macrophage-mediated clearance of the nanoparticles to a half, while maintaining efficient uptake by HeLa cells and preserving phototoxicity upon NIR irradiation. In vivo experiments in a CT-26 tumor mouse model showed that membrane-coated nanoparticles accumulated in tumors at twice the level of their non-coated counterparts. Fourteen days after treatment, tumor size was reduced to a half with PDT alone and 22-fold with combined PDT and PTT [183].

In situ oxygen generation

To therapeutically target hypoxic tumors, nanoparticles comprising the PS protoporphyrin IX conjugated with nitrogen-doped graphene quantum dots, catalase for the decomposition

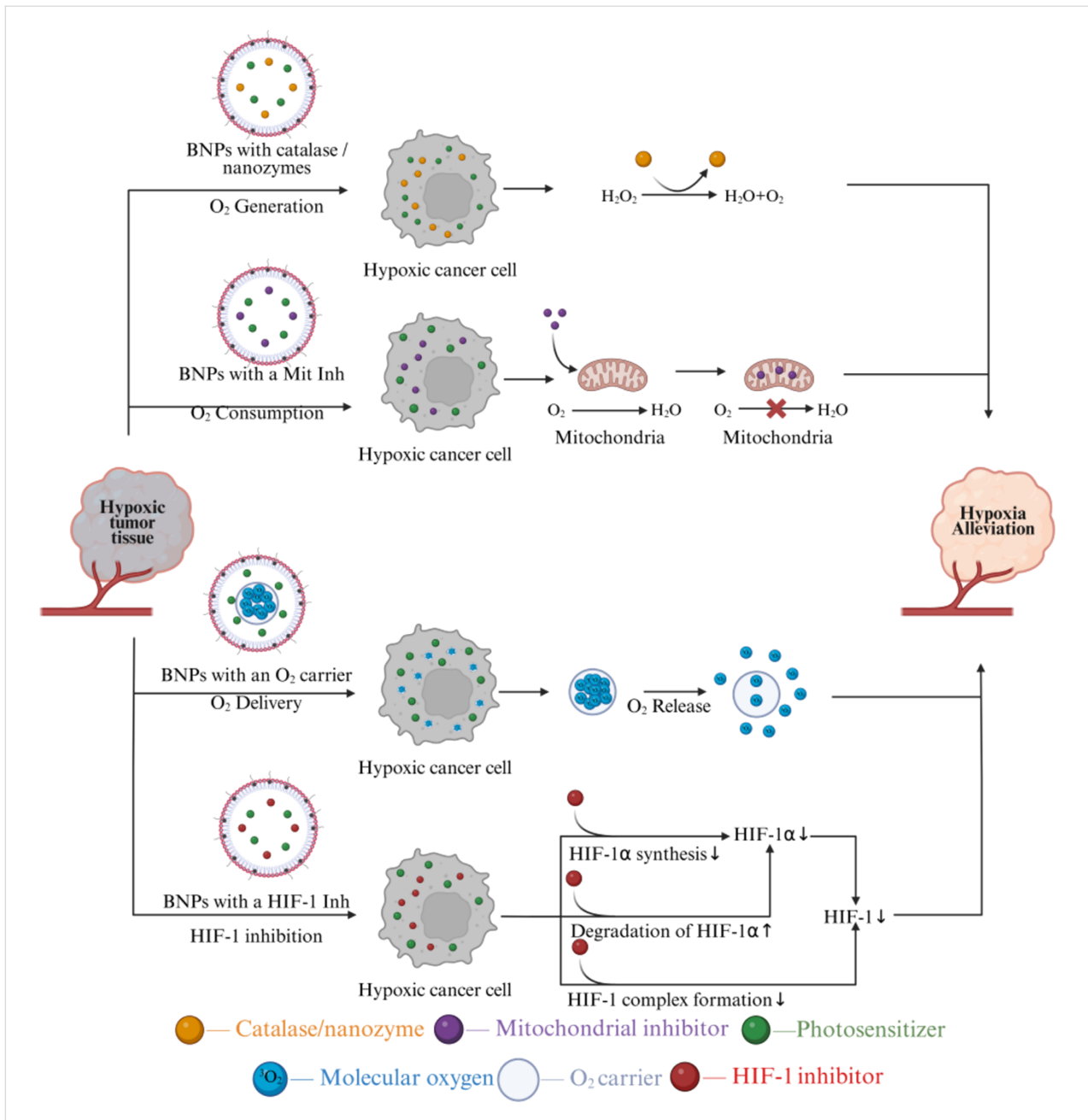


Table 2: Various strategies for tumor hypoxia alleviation.

System	PS	Source of biomimetic shell	Strategy	Ref
CCm–HSA–ICG–PFTBA	ICG	CCM of 4T1	oxygen delivery via high solubility in perfluorotributylamine (PFTBA), enabling passive release within the tumor to alleviate hypoxia and enhance photodynamic therapy efficacy	[177]

Table 2: Various strategies for tumor hypoxia alleviation. (continued)

O ₂ @UiO-66@ICG@RBC	ICG	RBC	Under 808 nm NIR laser irradiation, the photosensitizer ICG coordinated with UiO-66 generates singlet oxygen that disrupts erythrocyte membranes, while the photothermal effect of ICG induces localized heating to facilitate rapid oxygen release from UiO-66 pores.	[178]
N/P@MCC	PpIX	CCM of 4T1	Catalase immobilized in hollow mesoporous nanospheres decomposes endogenous H ₂ O ₂ within the tumor to generate O ₂ .	[180]
PM-W ₁₈ O ₄₉ -Met	W ₁₈ O ₄₉	PM (platelet membrane)	Metformin reduces tumor cell oxygen consumption by inhibiting complex I of the mitochondrial respiratory chain.	[181]
RBCm@Ato-IR780-PFC	IR780	RBC	A perfluorocarbon core within liposomes dissolves high levels of O ₂ , releasing it into the hypoxic TME; concurrently, atovaquone inhibits complex III of the mitochondrial respiratory chain, reducing cellular oxygen consumption.	[182]
ARISP	ICG	RBC	Delivery of salidroside, which inhibits HIF-1 α , reduces hypoxia in the cell.	[174]

of H₂O₂ to generate molecular oxygen, and a biomimetic coating derived from 4T1 cell membranes were developed. Oxygen generation occurred directly within the TME. Under hypoxic conditions, BNPs exhibited high ROS production, reduced macrophage uptake, and a twofold decrease in 4T1 cell viability as a result of PDT and PTT. In BALB/c mice bearing 4T1 tumors, nanoparticle accumulation in tumors was fivefold higher compared to the liver, and tumor growth was reduced 15-fold by day 21 relative to the control group. The BNPs demonstrated biodegradability with clearance occurring within 48 h [180].

An effective strategy for suppressing hypoxia in triple-negative breast cancer and lung metastases was achieved using nanoparticles composed of Ce6 combined with catalase for oxygen generation, monophosphoryl lipid A for TLR4 activation, and a 4T1 cell membrane coating to provide homotypic targeting and immune evasion, resulting in circulation times of up to 12 h. The toxicity of the system on 4T1 cells was increased sevenfold compared to free Ce6. In murine tumor models, membrane-coated nanoparticles exhibited a twofold increase in tumor accumulation and reduced tumor hypoxia from 60% to 11%. By day 24 post-treatment, tumor volume was decreased 12-fold. Median survival was extended to 40 days, and the average number of lung metastases was reduced from eleven to two [184].

Currently, nanoparticle platforms for sonodynamic therapy, which utilizes ultrasound rather than light as the external stimulus, are under development for tumor treatment. Systems based on Ag₂S quantum dots embedded in a Pluronic F-127 matrix, combined with catalase and coated with erythrocyte membranes, have been fabricated. These nanoparticles enabled effec-

tive NIR-II imaging. In vitro studies on C26 cells demonstrated that membrane-coated nanoparticles induced 60% cytotoxicity while maintaining active ROS generation under hypoxic conditions. In vivo experiments using C26 tumor-bearing mice showed a twofold increase in preferential tumor accumulation of the coated nanoparticles, with tumor volume reduced threefold by day 21 post-treatment. When combined with phenethyl isothiocyanate, complete tumor eradication was achieved, and survival reached 60% at 40 days [185].

As another example distinct from PDT, chemotherapy under hypoxic conditions was achieved using BNPs: A PLGA-based platform was developed encapsulating DOX and catalase; it was coated with membranes derived from activated M1 macrophages expressing integrins α 4 and β 1, which mediate targeting via VCAM-1. After 48 h of treatment, biomimetic systems reduced the migration rate of 4T1 cells threefold compared to the control and 1.5-fold compared to free DOX. Furthermore, 4 h after exposure, membrane-coated nanoparticles exhibited a tenfold increase in cellular uptake relative to the control and 1.5-fold higher accumulation compared to free DOX. In vivo, the system resulted in a fivefold reduction in tumor volume by day 21 and a twofold decrease in the number of lung metastases [186].

Reduction of oxygen consumption

Nanoparticles based on W₁₈O₄₉ loaded with metformin were designed to synergistically combine PDT and PTT. These particles were coated with platelet membranes expressing P-selectin for active targeting via PCLP1. Metformin inhibited mitochondrial complex I, thereby decreasing oxygen consumption. In vitro studies on Raji cells demonstrated 80% cytotoxicity. In

BALB/c-nude mice bearing Raji lymphoma, the proportion of tumor tissue overexpressing HIF-1 α decreased to 7% (compared to 100% in controls), and tumor volume was reduced 5.5-fold by day 12 post-treatment [181].

As an example of a platform addressing hypoxia via dual mechanisms, nanoparticles containing the PS IR780, PFTBA for oxygen delivery, and atovaquone for mitochondrial complex III inhibition were developed and coated with erythrocyte membranes and modified for mitochondrial targeting. This dual approach combined oxygen delivery with reduced oxygen consumption. Under *in vitro* conditions, these nanoparticles nearly completely inhibited HIF-1 α expression and increased ROS generation 1.5-fold compared to free PS. In AGS tumor-bearing mice, tumor volume decreased threefold by day 16, with HIF-1 α levels reduced to baseline and pronounced signs of cell death observed [182].

Suppression of hypoxia-inducible factor 1

In the context of PDT, HIF-1 plays a dual and critical role. The hypoxic state stabilizes and activates HIF-1, a master regulator of cellular responses to low oxygen levels [187]. HIF-1 induces the expression of genes involved in angiogenesis, metabolism, and survival pathways, promoting tumor adaptation and resistance to PDT-induced stress [188]. Notably, PDT can also directly activate HIF-1 signaling, even under normoxic conditions, through prostaglandin pathways and oxidative stress. While HIF-1-driven responses may initially alleviate tumor hypoxia by stimulating angiogenesis, its activation ultimately contributes to therapeutic resistance by enhancing tumor cell survival, metabolic reprogramming, and immunosuppression. Therefore, targeting HIF-1 or its downstream effectors alongside PDT is a strategic approach to mitigate hypoxia-associated limitations.

To suppress HIF-1 α and reduce chemoresistance, siRNA targeting HIF-1 α was loaded into magnetic nanoparticles coated with a biomimetic membrane derived from macrophages (J774A.1) and cancer cells (4T1). This biomimetic coating enhanced tumor accumulation of the nanoparticles and resulted in a fourfold reduction in HIF-1 α expression [173]. ARISP are BNPs developed for targeted PDT under tumor hypoxia conditions. They comprise a core of PLGA loaded with the photosensitizer ICG and salidroside, an inhibitor of HIF-1 α synthesis, surrounded by a shell of erythrocyte membranes modified with anti-LDLR antibodies to enable delivery specifically to hypoxic tumor regions. *In vitro* experiments using the 4T1 cell line under hypoxic conditions demonstrated that ARISP generated ROS at levels 2.6-fold higher than nanoparticles lacking the biomimetic coating and fourfold higher than free ICG, resulting in over a 40-fold increase in cytotoxicity. *In vivo* studies in 4T1

and MDA-MB-231 mouse models showed that these nanoparticles significantly shortened tumor elimination time. Furthermore, ARISP exhibited prolonged blood circulation for up to 72 h and effectively inhibited both tumor growth and metastasis [174].

ROS generation enhancing

Enhancing ROS production upon light activation of PSs is crucial for maximizing the therapeutic efficacy of PDT. Conventional PSs often face intrinsic limitations, including inefficient ROS generation, aggregation, photobleaching, and susceptibility to the hypoxic TME, which severely restrict their clinical performance. BNPs offer a highly promising and versatile platform to overcome these challenges. BNPs not only improve PS delivery but also enable innovative strategies to actively enhance ROS production.

Classical PSs often follow a type-II photosensitization pathway, transferring energy to molecular oxygen to generate singlet oxygen, which is limited in hypoxic tumors. Biomimetic assemblies facilitate a switch to or enhancement of the type-I pathway, which proceeds via electron transfer (superoxide O₂⁻, hydroxyl radicals) that can form even under low-oxygen conditions. Recent studies demonstrated that biomimetic phosphate-templated supramolecular assemblies of PS promote efficient nanoscale aggregation that blocks energy transfer-type quenching and instead promotes photoinduced charge separation [189]. This favors electron transfer reactions producing superoxide radicals at high efficiency. By converting type-II PSs into type-I supramolecular PSs, biomimetic nanocarriers enhance overall ROS yield, enable ROS generation in hypoxia, and significantly boost PDT efficacy.

The association between PSs and the nanocarrier's biomimetic components can modulate photophysical and photochemical behavior, thereby controlling ROS generation pathways and efficacy, which depends on the relative probabilities of various excited-state relaxation pathways. The probability of singlet oxygen generation by type-II PSs can be increased by enhancing the transition probability of the PS to the triplet state, with biomimetic nanocarriers influencing this transition and thereby modulating energy transfer to surrounding molecular oxygen [190]. Immobilization or constrained orientation of the PSs within BNPs restrict vibrational and rotational relaxation and shield the PS from quenching by external molecules (e.g., water or biomolecules). Photobleaching and aggregation can also introduce new relaxation pathways that decrease the efficiency of ROS generation. For example, cell membrane coating creates a natural lipid environment that maintains monomeric state and photosensitivity of the PS [112]. Incorporation of plasmonic materials such as gold or silver nanoparticles into

biomimetic nanocarriers can enhance local electromagnetic fields near the PS through localized surface plasmon resonance, amplifying light absorption and promoting singlet oxygen generation. Hybrid systems embedding plasmonic silver nanoparticles coated with mesoporous silica and loaded with a PS (e.g., hematoporphyrin IX) exhibit resonance coupling that dramatically increases singlet oxygen production under broad spectral excitation, including NIR wavelengths [191].

Immune modulation: BNPs empowering PDT-induced tumor immunity

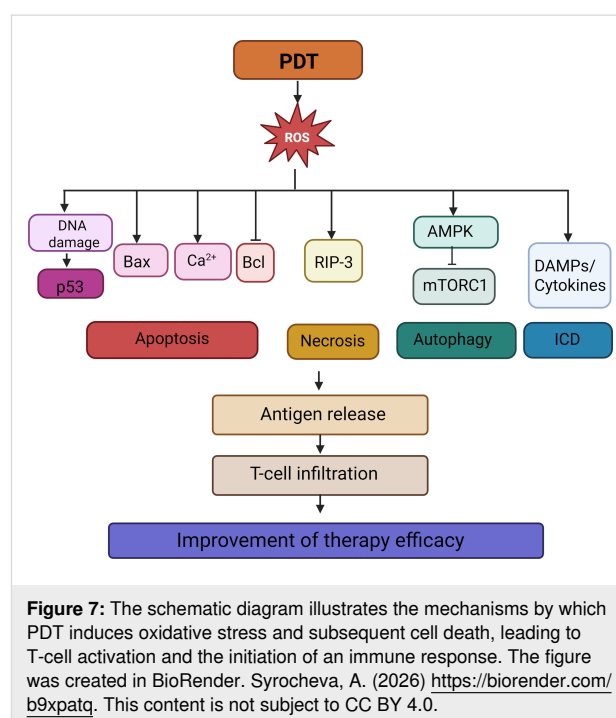
PDT-induced immune activation

The immunological potential of PDT was largely unlocked with the discovery of its ability to induce ICD, a regulated form of cell death that activates the adaptive immune system rather than merely eliminating tumor cells [192]. This represents a paradigm shift from early research in the 1990s focused on tumor ablation. The efficacy of immune activation hinges on the presence of tumor-associated antigens (TAAs) and tumor neoantigens (TNAs), which confer antigenicity to cancer cells. However, these antigens alone are typically insufficient to drive robust antitumor immunity without additional signals that recruit and activate antigen-presenting cells. ICD provides precisely this adjuvant-like function through the release of damage-associated molecular patterns (DAMPs); these are molecules normally sequestered within healthy cells and integral to their homeostasis, which, upon extracellular release, act as potent danger signals [193–195]. Key DAMPs include surface-exposed calreticulin (CRT), which promotes phagocytosis [196,197], extracellular ATP, a chemoattractant for motile phagocytes [198,199], released HMGB1, which binds Toll-like receptors (TLRs) to enhance immune activation [200], and heat shock proteins (HSP70/90), which facilitate antigen presentation [201–203]. Collectively, these signals promote tumor antigen uptake, DC maturation, and the cross-priming of cytotoxic T lymphocytes, initiating a systemic antitumor response [204].

The efficacy of PDT in inducing robust ICD is not universal; it critically depends on two main factors, namely, the intracellular localization of the PS and the magnitude and nature of ROS generation [205]. Importantly, ROS should not be regarded as a homogeneous entity; different species, such as singlet oxygen ($^1\text{O}_2$), superoxide anions ($\text{O}_2^{\cdot-}$), hydroxyl radicals ($\cdot\text{OH}$), and hydrogen peroxide (H_2O_2), exhibit distinct reactivities, diffusion capacities, and half-lives, which collectively determine the spatial extent and biochemical consequences of oxidative damage. The majority of clinically used PSs operate primarily via type-II photochemical reactions, generating singlet oxygen as the dominant reactive species [206]. $^1\text{O}_2$ is highly reactive but extremely short-lived ($<0.04 \mu\text{s}$ in cells [207]), confining its effects to the immediate vicinity

of the PS. In contrast, $\text{O}_2^{\cdot-}$ and $\cdot\text{OH}$ can initiate chain reactions and propagate oxidative damage more broadly [208], while H_2O_2 , though less reactive, is relatively long-lived and can diffuse across membranes to modulate redox-sensitive signaling pathways, often in an iron- or copper-dependent manner [209,210]. This chemical heterogeneity implies that the subcellular site of ROS generation is as critical as the ROS itself since oxidative stress in one compartment (e.g., endoplasmic reticulum (ER)) can trigger immunogenic signaling, whereas the same species in another (e.g., cytosol) may lead to non-immunogenic collapse or even immunosuppression. Notably, the intensity of oxidative stress directly scales with ICD efficacy; antioxidant interventions consistently reduce DAMP emission and impair adaptive immunity, confirming ROS as non-redundant mediators of immunogenicity.

The selection of the PS and its subcellular target dictates the cell death pathway and the ensuing immunogenic profile through distinct stress-signaling cascades (Figure 7) [211]. For instance, endoplasmic reticulum-targeting PSs (e.g., hypericin) trigger intense ER stress, leading to the activation of the unfolded protein response and the PERK–eIF2 α pathway. This cascade promotes the pre-apoptotic translocation of CRT to the plasma membrane, an essential “eat me” signal for dendritic cell recognition, making ER-localized PSs particularly potent inducers of ICD [212,213]. Lysosomal PSs (e.g., Photosens) cause lysosomal membrane permeabilization upon irradiation, releasing cathepsins into the cytosol. This proteolytic burst can activate both caspase-dependent apoptosis and, under conditions of iron



accumulation and lipid peroxidation, contribute to ferroptotic cell death, though the resulting DAMP profile is often less coordinated than that induced by ER stress [214–216]. Mitochondrial PSs (e.g., Photofrin) primarily induce rapid mitochondrial outer membrane permeabilization, cytochrome-c release, and swift caspase activation [217]. While this efficiently kills tumor cells, the speed and caspase dominance of this apoptotic pathway often suppress key ICD hallmarks, such as CRT exposure and ATP secretion, resulting in limited dendritic cell activation and weaker adaptive immunity. While caspase-dominated or rapid apoptotic death often fails to elicit robust immunity, lytic forms such as necroptosis typically provoke stronger DAMP release and a more pronounced pro-inflammatory response [218,219]. Additionally, the temporal kinetics of DAMP release alongside the immunological milieu of TME critically influence both the magnitude and quality of the immune response. Sublethal PDT doses can induce a pre-immunogenic cell death phenotype characterized by partial DAMP exposure and modulated cytokine secretion, potentially resulting in either immune enhancement or suppression contingent upon the TME composition.

The effect of PDT on immune cells

PDT exerts both direct and context-dependent effects on immune cells, with macrophages playing a central role in modulating of TME and inflammatory responses. Macrophages display polarized phenotypes, including pro-inflammatory, anti-tumor (M1) and anti-inflammatory, often pro-tumor (M2) states, with tumor-supportive macrophages predominantly exhibiting M2 polarization. PDT-induced ROS can reprogram macrophage polarization from M2 to M1, thereby enhancing antitumor immunity [220]. For example, low-dose PDT using temoporfin-loaded nanoparticles drives repolarization of M2-polarized THP-1 macrophages toward an M1-like phenotype, evidenced by upregulated expression of iNOS, CD86, and TNF- α [221]. Similarly, 5-aminolevulinic acid (5-ALA)-based PDT exhibits selective cytotoxicity toward M2 macrophages, attributable to their higher intracellular accumulation of protoporphyrin IX, while sparing or promoting differentiation of monocyte precursors toward an M1-like state [222]. In vivo, PDT-mediated depletion of M2 tumor-associated macrophages (TAMs) and subsequent infiltration of M1 macrophages have been demonstrated in murine breast cancer models, correlating with improved tumor control [223]. Mechanistically, ROS activate signaling cascades such as COX-2/TREM-1 under inflammatory conditions and ERK/MAPK–NLRP3 inflammasome pathways, which may operate similarly in oncological settings to sustain pro-inflammatory reprogramming [224].

Beyond macrophages, PDT recruits and activates neutrophils, which contribute to early tumor destruction via ROS and NETs

[225], and enhances NK cell cytotoxicity through IL-12 and type-I interferons released by activated myeloid cells [226]. DCs are primarily activated indirectly, that is, DAMPs (CRT, ATP, and HMGB1) from PDT-killed tumor cells drive DC maturation and cross-priming of T cells [227–229]. Although high-dose PDT can impair DCs upon direct irradiation, therapeutic regimens predominantly elicit DC activation.

BNP-enhanced PDT-immunotherapy synergy

The antitumor immune response in PDT can be potentiated through two primary, non-mutually exclusive mechanisms, that is, first, by intensifying the direct photodynamic effect on cancer cells to robustly induce ICD, and second, by engineering nanocarriers to actively engage and modulate immune cells within the TME via inherent cellular tropism [230]. Nanoparticles cloaked in immune cell membranes, such as those derived from TAMs, exploit the natural homing ability of these cells to the tumor site. For instance, TAM membrane-coated upconversion nanoparticles loaded with Ce6 (NPR@TAMM) have been shown to not only elicit ICD but also to reprogram immunosuppressive M2-like TAMs toward an M1-like, pro-inflammatory phenotype, thereby enhancing CD8⁺ T-cell activation in breast cancer models [231,232]. Another study confirmed that TAM-mimetic nanoparticles significantly increase intratumoral infiltration of CD8⁺ T cells while concomitantly reducing regulatory T-cell populations [233]. An alternative strategy leverages CCM-coated nanoparticles, which achieve homotypic tumor targeting through the preservation of native surface antigens. Yang et al. demonstrated that Ce6-loaded silica nanoparticles coated with gastric CCMs enable precise tumor accumulation, leading to effective PDT and potent ICD induction [125].

Dehaini et al. pioneered the use of erythrocyte-platelet hybrid membranes to confer both prolonged systemic circulation (via CD47) and vascular targeting capabilities (from platelet membranes) [234]. When loaded with the PS verteporfin, these constructs demonstrated superior PDT efficacy in lung cancer models [235]. Collectively, these approaches, spanning immune cells, cancer cells, hybrids, and microbe-inspired biomimetic coatings, represent a versatile toolkit for immuno-photodynamic therapy, as summarized in Table 3.

Emerging trends and challenges

In recent years, significant progress has been made in the development and application of biomimetic nanoparticle-engineered PDT for cancer treatment. Innovative approaches are advancing the field, including the creation of multifunctional and theranostic nanoparticles, improved methods to counteract tumor hypoxia, and more precise targeting strategies based on tumor characteristics. However, the translation of these technologies

Table 3: BNPs in PDT-induced immune activation.

Membrane source	Immune mechanisms	System	PS	Ref
cancer cell membrane (autologous)	endogenous tumor-associated antigens (TAAs) displayed on membrane serve as in situ vaccine; PDT-induced ICD releases DAMPs → DC uptake of TAAs, maturation, and cross-presentation → potent CD8 ⁺ T-cell responses and immunological memory	HLP@SiTGF-β1	IR-780	[236]
		Cur/Ce6-MCNPs	curcumin and Ce6	[237]
		CM/SLN/Ce6	Ce6	[238]
		IRCB@M	IR-780	[239]
microbe-inspired platforms	cancer–bacterial hybrids co-display tumor-associated antigens and PAMPs, functioning as self-adjuvanting nanovaccines.	HPDA@OMV-CC	HPDA	[240]
		bacteria-plant hybrid vesicles	thylakoid membranes	[241]
myeloid-derived suppressor cell membrane	homotypic targeting to MDSC-rich TME; PDT/PTT induces ICD while reprogramming immunosuppressive MDSCs → shifts TME toward pro-inflammatory state (↑ TNF-α, IL-12; ↓ TGF-β, IL-10), enhances CD8 ⁺ T-cell infiltration and M1 macrophage polarization	BP@ Decitabine @MDSCs	black phosphorus	[242]
NK cell membrane	NK cell membrane enables tumor targeting via NKG2D/DNAM-1 and drives pro-inflammatory M1 macrophage polarization; PDT-induced ICD amplifies DAMP release → DC maturation, CD8 ⁺ /CD4 ⁺ T-cell infiltration, and systemic abscopal immunity	NK-NPs	TCPP	[196]
hybrid membrane (e.g., cancer + dendritic cell)	hybrid cytomembrane from fused cancer and dendritic cells enables homotypic tumor targeting and intrinsic antigen presentation; PDT-driven ICD synergizes with membrane-displayed tumor antigens and co-stimulatory signals → direct DC-like activation, robust CD8 ⁺ T-cell priming, and durable systemic antitumor immunity (including abscopal effect)	PCN@FM	MOFs	[243]
macrophage membrane (TAM)	TAM membrane coating enables tumor homing and immune compatibility; acts as a CSF1 decoy → blocks CSF1–CSF1R signaling → repolarizes TAMs from M2 to M1 → suppresses IL-10/TGF-β/Arg-1 → enhances antigen presentation, CD8 ⁺ /CD4 ⁺ T-cell infiltration, IFN-γ production, and abscopal response	NPR@TAMM	UCNP and Rose Bengal	[231]
neutrophil membrane	neutrophil membrane enables ROS-guided homing to inflamed tumors, vascular barrier penetration, and pro-inflammatory immune activation	CR-NML	Ce6	[244]

into clinical practice faces several challenges, such as production scalability, safety concerns, regulatory requirements, tumor heterogeneity, and cost. This part reviews key emerging trends in biomimetic nanoparticle-mediated PDT and discusses the main obstacles that need to be overcome to enable broader clinical use (Figure 8).

Recent developments in BNP design focus on combining diagnostic and therapeutic functions within a single platform. These theranostic BNPs can carry both imaging agents, such as MRI contrast compounds or photoacoustic dyes, and PSs, allowing for real-time tracking of nanoparticle distribution, tumor oxygen levels, and treatment effectiveness. Additionally, stimuli-responsive systems are being created to release their therapeutic agents in response to specific tumor microenvironment cues like pH changes, redox conditions, or enzyme presence. This improves precise control over drug release, minimizes side

effects, and enhances overall efficacy. Moreover, hybrid BNPs are being explored to deliver multiple therapies simultaneously, such as PDT, PTT, chemotherapy, and immunotherapy; this can leverage synergistic effects and address resistance mechanisms.

A notable development in BNP design involves expanding the variety of cell membranes used for nanoparticle coating, such as those derived from platelets, stem cells, and immune cells, alongside RBC and cancer cell membranes. This strategy aims to improve targeting accuracy and tailor BNPs to the specific characteristics of both primary and metastatic tumors. In addition, modifying the nanoparticle surface with tumor-specific ligands, patient-derived antigens, or aptamers helps advance personalized nanomedicine approaches. Alongside these biological advancements, computational methods are increasingly applied to guide BNP design, including predicting physical

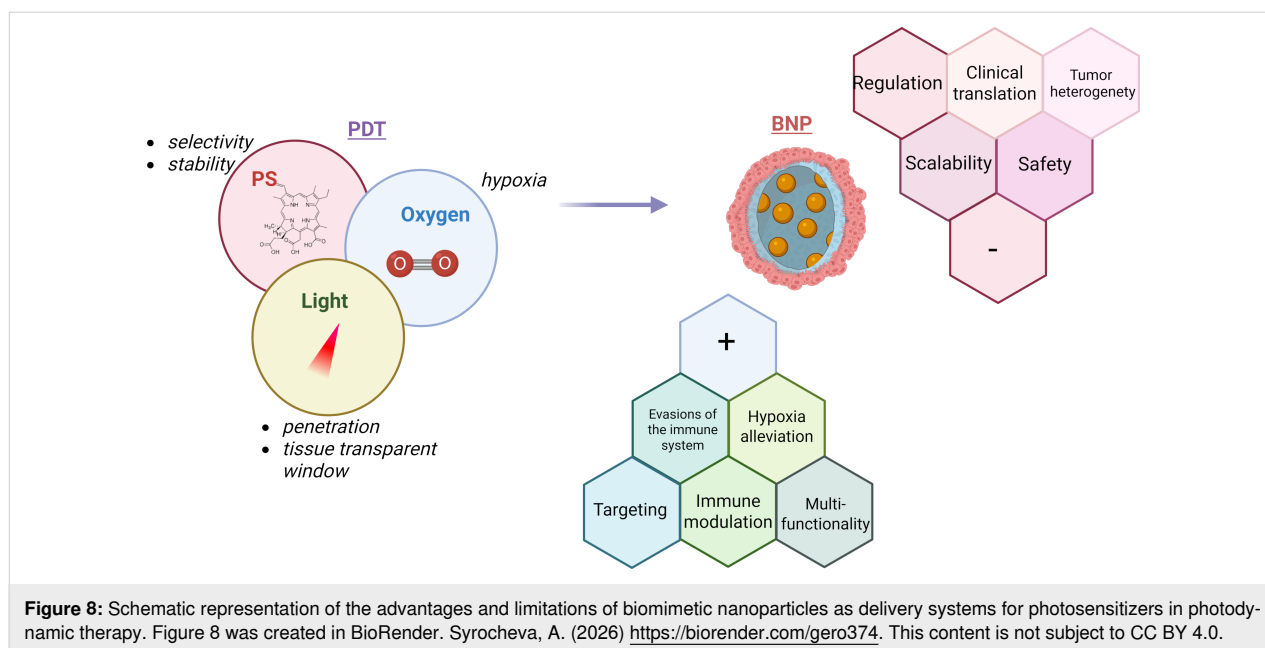


Figure 8: Schematic representation of the advantages and limitations of biomimetic nanoparticles as delivery systems for photosensitizers in photodynamic therapy. Figure 8 was created in BioRender. Syrocheva, A. (2026) <https://biorender.com/gero374>. This content is not subject to CC BY 4.0.

properties, selecting appropriate surface markers, modeling in vivo distribution, and anticipating treatment responses, which together support more efficient development and clinical translation of BNP-based PDT platforms.

Addressing the challenges posed by the TME is a major focus in current research. To overcome hypoxia, a critical factor limiting PDT effectiveness, BNPs are being developed to include oxygen carriers, such as hemoglobin or perfluorocarbons, or catalytic materials like manganese dioxide and catalase-mimetic nanoparticles that generate oxygen directly within the tumor. At the same time, advances in immune-targeted BNPs enable the combined delivery of immunotherapeutic agents or adjuvants alongside PSs, enhancing antitumor immune responses by promoting ICD and supporting strong activation of T cells.

To overcome the limited tissue penetration of conventional PDT, there is growing interest in NIR-responsive BNPs. Approaches involving upconversion nanoparticles and two-photon excitation are being explored to enhance PS activation at increased depths, thereby expanding the applicability of minimally invasive PDT to a wider variety of tumors.

Clinical translation of BNPs faces challenges including complex large-scale production, ensuring batch consistency, and maintaining surface functionality. Immunogenic risks, especially from non-autologous materials, require thorough in vivo evaluation of biodistribution, clearance, and long-term toxicity. Tumor and patient heterogeneity affect targeting and treatment response, making personalized BNPs promising but difficult to

implement broadly. Regulatory guidelines for BNPs are still emerging, and few PDT platforms have reached clinical trials. Additionally, manufacturing costs and the need for advanced imaging and light delivery systems may limit widespread adoption and patient access. Successful resolution of these challenges will be critical for the realization of the full potential of BNP-engineered PDT as a foundational strategy for precision oncology.

While BNPs have shown promising three- to fourfold enhancements in PS delivery and ROS production, often translating to complete tumor regression in preclinical models, the extent to which these improvements represent a qualitative leap over conventional PDT remains an open question. Achieving clinical superiority, particularly for aggressive or deep tumors, may necessitate not merely incremental gains but orders-of-magnitude increases in tumor accumulation (e.g., more than tenfold) and localized ROS generation (e.g., exceeding 10^{15} ROS molecules per cancer cell for apoptosis [245]) to fully compensate for light penetration constraints and hypoxic resistance. For context, conventional Photofrin[®] PDT achieves 25–86% local control rate at concentrations of 0.78–7.1 μM and fluences of 300–700 J/cm^2 with ROS yields of 0.70–1.15 mM [246], whereas BNPs often match or exceed this (e.g., fourfold ROS increase, >90% cell killing at 15 $\mu\text{g}/\text{mL}$ ICG equivalents) with two- to fivefold reduced doses. Establishing objective quantitative benchmarks, such as standardized metrics for ROS yield per PS dose and comparative survival endpoints against FDA-approved agents, is essential for rigorous evaluation. Emerging preclinical data await phase-I clinical validation to bridge this translational gap.

Conclusion

BNPs have shown great potential as flexible and effective platforms to improve PDT for cancer treatment. By combining natural cell membrane functions with the adaptable design of nanocarriers, these nanoparticles overcome some limitations of traditional delivery methods. They enhance photosensitizer solubility and stability, reducing common problems like aggregation and poor bioavailability. The biomimetic coating also improves tumor targeting through mechanisms such as homotypic binding and recognition of tumor markers, increasing photosensitizer uptake in cancer cells while protecting healthy tissue and lowering toxicity. Additionally, BNPs can carry oxygen or other features to counteract tumor hypoxia and boost reactive oxygen species production, further improving treatment effectiveness. Altogether, these capabilities work together to increase the selectivity and safety of PDT, enabling more efficient tumor destruction with fewer side effects. However, challenges remain, including the complex and costly process of large-scale production, risks of immune reactions, variability in tumor targeting, limited light penetration into tissue, and regulatory obstacles that need resolution before widespread clinical use. Future work should aim to refine nanoparticle designs for personalized treatment, enhance safety, and combine PDT with immune-based approaches to strengthen anticancer effects. With ongoing research and collaboration, biomimetic nanoparticle-based PDT could become a key tool in personalized cancer therapy, providing safer and more effective treatment options across many tumor types.

Acknowledgements

The graphical abstract for this study was created in BioRender. Syrocheva, A. (2026) <https://biorender.com/ytbwton>. This content is not subject to CC BY 4.0.

Funding

This research was funded by the Russian Science Foundation (grant # 24-24-20102).

Author Contributions

Valentina I. Gorbacheva: writing – original draft. Alexey S. Grabovoy: writing – original draft. Polina S. Marukhina: writing – original draft. Anastasiia O. Syrocheva: visualization. Ekaterina P. Kolesova: conceptualization; funding acquisition; project administration; supervision.

ORCID® iDs

Valentina I. Gorbacheva - <https://orcid.org/0009-0005-1073-5339>

Alexey S. Grabovoy - <https://orcid.org/0009-0008-5254-9624>

Polina S. Marukhina - <https://orcid.org/0009-0004-9495-5816>

Anastasiia O. Syrocheva - <https://orcid.org/0009-0008-5035-8445>

Ekaterina P. Kolesova - <https://orcid.org/0000-0002-6730-1858>

Data Availability Statement

Data sharing is not applicable as no new data was generated or analyzed in this study.

References

- Li, G.; Wang, C.; Jin, B.; Sun, T.; Sun, K.; Wang, S.; Fan, Z. *Cell Death Discovery* **2024**, *10*, 466. doi:10.1038/s41420-024-02236-4
- Ozog, D. M.; Rkein, A. M.; Fabi, S. G.; Gold, M. H.; Goldman, M. P.; Lowe, N. J.; Martin, G. M.; Munavalli, G. S. *Dermatol. Surg.* **2016**, *42*, 804–827. doi:10.1097/dss.0000000000000800
- Allison, R. R.; Moghissi, K. *Clin. Endosc.* **2013**, *46*, 24–29. doi:10.5946/ce.2013.46.1.24
- Li, Y.; Wang, J.; Zhang, X.; Guo, W.; Li, F.; Yu, M.; Kong, X.; Wu, W.; Hong, Z. *Org. Biomol. Chem.* **2015**, *13*, 7681–7694. doi:10.1039/c5ob01035g
- Du, Y.; Han, J.; Jin, F.; Du, Y. *Pharmaceutics* **2022**, *14*, 1763. doi:10.3390/pharmaceutics14091763
- Huis in 't Veld, R. V.; Heuts, J.; Ma, S.; Cruz, L. J.; Ossendorp, F. A.; Jager, M. J. *Pharmaceutics* **2023**, *15*, 330. doi:10.3390/pharmaceutics15020330
- Lucky, S. S.; Soo, K. C.; Zhang, Y. *Chem. Rev.* **2015**, *115*, 1990–2042. doi:10.1021/cr5004198
- Gorbacheva, V. I.; Syrocheva, A. O.; Kolesova, E. P. *Int. J. Mol. Sci.* **2025**, *26*, 11559. doi:10.3390/ijms262311559
- Liu, Y.; Liang, Y.; Yuhong, J.; Xin, P.; Han, J. L.; Du, Y.; Yu, X.; Zhu, R.; Zhang, M.; Chen, W.; Ma, Y. *Drug Des., Dev. Ther.* **2024**, *18*, 1469–1495. doi:10.2147/dddt.s447496
- Subhan, M. A.; Yalamarty, S. S. K.; Filipczak, N.; Parveen, F.; Torchilin, V. P. *J. Pers. Med.* **2021**, *11*, 571. doi:10.3390/jpm11060571
- da Silva, D. B.; da Silva, C. L.; Davanzo, N. N.; da Silva Souza, R.; Correa, R. J.; Tedesco, A. C.; Riemma Pierre, M. B. *Photodiagn. Photodyn. Ther.* **2021**, *35*, 102317. doi:10.1016/j.pdpdt.2021.102317
- Darwish, W. M.; Bayoumi, N. A.; El-Shershaby, H. M.; Allahloubi, N. M. *J. Photochem. Photobiol., B* **2020**, *203*, 111777. doi:10.1016/j.jphotobiol.2020.111777
- Carmona-Ribeiro, A. M. *Int. J. Nanomed.* **2010**, 249–259. doi:10.2147/ijn.s9035
- Hao, Y.; Chung, C. K.; Gu, Z.; Schomann, T.; Dong, X.; Huis in 't Veld, R. V.; Camps, M. G.; ten Dijke, P.; Ossendorp, F. A.; Cruz, L. J. *Mol. Biomed.* **2022**, *3*, 26. doi:10.1186/s43556-022-00086-z
- Chen, S.-X.; Ma, M.; Xue, F.; Shen, S.; Chen, Q.; Kuang, Y.; Liang, K.; Wang, X.; Chen, H. *J. Controlled Release* **2020**, *324*, 218–227. doi:10.1016/j.jconrel.2020.05.006
- Zhao, Y.; Liu, X.; Liu, X.; Yu, J.; Bai, X.; Wu, X.; Guo, X.; Liu, Z.; Liu, X. *Front. Immunol.* **2022**, *13*, 955920. doi:10.3389/fimmu.2022.955920
- Allison, R. R.; Downie, G. H.; Cuenca, R.; Hu, X.-H.; Childs, C. J.; Sibata, C. H. *Photodiagn. Photodyn. Ther.* **2004**, *1*, 27–42. doi:10.1016/s1572-1000(04)00007-9
- Escudero, A.; Carrillo-Carrión, C.; Castillejos, M. C.; Romero-Ben, E.; Rosales-Barrios, C.; Khair, N. *Mater. Chem. Front.* **2021**, *5*, 3788–3812. doi:10.1039/d0qm00922a
- Castano, A. P.; Demidova, T. N.; Hamblin, M. R. *Photodiagn. Photodyn. Ther.* **2004**, *1*, 279–293. doi:10.1016/s1572-1000(05)00007-4

20. MacRobert, A. J.; Bown, S. G.; Phillips, D. What are the Ideal Photoproperties for a Sensitizer?. In *Photosensitizing Compounds: Their Chemistry, Biology and Clinical Use: Ciba Foundation Symposium 146*; Bock, G.; Harnett, S., Eds.; Wiley Online Library, 2007; pp 4–16. doi:10.1002/9780470513842.ch2
21. Kim, M. M.; Darafsheh, A. *Photochem. Photobiol.* **2020**, *96*, 280–294. doi:10.1111/php.13219
22. Tanielian, C.; Schweitzer, C.; Mechin, R.; Wolff, C. *Free Radical Biol. Med.* **2001**, *30*, 208–212. doi:10.1016/s0891-5849(00)00460-3
23. Dougherty, T. J.; Kaufman, J. E.; Goldfarb, A.; Weishaupt, K. R.; Boyle, D.; Mittleman, A. *Cancer Res.* **1978**, *38*, 2628–2635.
24. Kou, J.; Dou, D.; Yang, L. *Oncotarget* **2017**, *8*, 81591–81603. doi:10.18632/oncotarget.20189
25. Sheleg, S. V.; Zhavrid, E. A.; Khodina, T. V.; Kochubeev, G. A.; Istomin, Y. P.; Chalov, V. N.; Zhuravkin, I. N. *Photodermatol., Photoimmunol. Photomed.* **2004**, *20*, 21–26. doi:10.1111/j.1600-0781.2004.00078.x
26. Moore, C. M.; Nathan, T. R.; Lees, W. R.; Mosse, C. A.; Freeman, A.; Emberton, M.; Bown, S. G. *Lasers Surg. Med.* **2006**, *38*, 356–363. doi:10.1002/lsm.20275
27. Chen, Y.; Li, G.; Pandey, R. K. *Curr. Org. Chem.* **2004**, *8*, 1105–1134. doi:10.2174/1385272043370131
28. Lo, P.-C.; Rodríguez-Morgade, M. S.; Pandey, R. K.; Ng, D. K. P.; Torres, T.; Dumoulin, F. *Chem. Soc. Rev.* **2020**, *49*, 1041–1056. doi:10.1039/c9cs00129h
29. Ortiz, M. J.; Agarrabeitia, A. R.; Duran-Sampedro, G.; Bañuelos Prieto, J.; Lopez, T. A.; Massad, W. A.; Montejano, H. A.; García, N. A.; Lopez Arbeloa, I. *Tetrahedron* **2012**, *68*, 1153–1162. doi:10.1016/j.tet.2011.11.070
30. Polat, E.; Kang, K. *Biomedicines* **2021**, *9*, 584. doi:10.3390/biomedicines9060584
31. Mfouo-Tynga, I. S.; Dias, L. D.; Inada, N. M.; Kurachi, C. *Photodiagn. Photodyn. Ther.* **2021**, *34*, 102091. doi:10.1016/j.pdpdt.2020.102091
32. Kutumova, E. O.; Akberdin, I. R.; Egorova, V. S.; Kolesova, E. P.; Parodi, A.; Pokrovsky, V. S.; Zamyatnin, A. A., Jr.; Kolpakov, F. A. *Heliyon* **2024**, *10*, e30962. doi:10.1016/j.heliyon.2024.e30962
33. Garapati, C.; Boddu, S. H.; Jacob, S.; Ranch, K. M.; Patel, C.; Babu, R. J.; Tiwari, A. K.; Yasin, H. *Arabian J. Chem.* **2023**, *16*, 104583. doi:10.1016/j.arabjc.2023.104583
34. Tang, L.; Li, J.; Zhao, Q.; Pan, T.; Zhong, H.; Wang, W. *Pharmaceutics* **2021**, *13*, 1151. doi:10.3390/pharmaceutics13081151
35. Moazzam, M.; Zhang, M.; Hussain, A.; Yu, X.; Huang, J.; Huang, Y. *Mol. Ther.* **2024**, *32*, 284–312. doi:10.1016/j.ymthe.2024.01.005
36. Piperno, A.; Sciortino, M. T.; Giusto, E.; Montesi, M.; Panseri, S.; Scala, A. *Int. J. Nanomed.* **2021**, *16*, 5981–6002. doi:10.2147/ijn.s321329
37. Kolesova, E.; Pulone, S.; Kostyushev, D.; Tasciotti, E. *Adv. Drug Delivery Rev.* **2025**, *224*, 115619. doi:10.1016/j.addr.2025.115619
38. Chen, L.; Huang, J.; Li, X.; Huang, M.; Zeng, S.; Zheng, J.; Peng, S.; Li, S. *Front. Bioeng. Biotechnol.* **2022**, *10*, 920162. doi:10.3389/fbioe.2022.920162
39. Wu, Y.; Vazquez-Prada, K. X.; Liu, Y.; Whittaker, A. K.; Zhang, R.; Ta, H. T. *Nanotheranostics* **2021**, *5*, 499–514. doi:10.7150/ntno.62730
40. Najdian, A.; Beiki, D.; Abbasi, M.; Gholamrezanezhad, A.; Ahmadzadehfahr, H.; Amani, A. M.; Ardestani, M. S.; Assadi, M. *Cancer Imaging* **2024**, *24*, 127. doi:10.1186/s40644-024-00762-z
41. Liu, K.; Liu, X.; Zeng, Q.; Zhang, Y.; Tu, L.; Liu, T.; Kong, X.; Wang, Y.; Cao, F.; Lambrechts, S. A. G.; Aalders, M. C. G.; Zhang, H. *ACS Nano* **2012**, *6*, 4054–4062. doi:10.1021/nn300436b
42. Zhang, L.; Li, M.; Zhou, Q.; Dang, M.; Tang, Y.; Wang, S.; Fu, J.; Teng, Z.; Lu, G. *Acta Pharm. Sin. B* **2020**, *10*, 1719–1729. doi:10.1016/j.apsb.2020.05.003
43. Zhang, H.; Liu, K.; Li, S.; Xin, X.; Yuan, S.; Ma, G.; Yan, X. *ACS Nano* **2018**, *12*, 8266–8276. doi:10.1021/acsnano.8b03529
44. Chang, M.; Dong, C.; Huang, H.; Ding, L.; Feng, W.; Chen, Y. *Adv. Funct. Mater.* **2022**, *32*, 2204791. doi:10.1002/adfm.202204791
45. Gong, Y.-k.; Winnik, F. M. *Nanoscale* **2012**, *4*, 360–368. doi:10.1039/c1nr11297j
46. Wilhelm, S.; Tavares, A. J.; Dai, Q.; Ohta, S.; Audet, J.; Dvorak, H. F.; Chan, W. C. W. *Nat. Rev. Mater.* **2016**, *1*, 16014. doi:10.1038/natrevmats.2016.14
47. Blanco, E.; Shen, H.; Ferrari, M. *Nat. Biotechnol.* **2015**, *33*, 941–951. doi:10.1038/nbt.3330
48. Issaka, E.; Wariboko, M. A.; Agyekum, E. A. *Biomed. Mater. Devices* **2024**, *2*, 1–33. doi:10.1007/s44174-023-00084-x
49. Hu, C.-M. J.; Zhang, L.; Aryal, S.; Cheung, C.; Fang, R. H.; Zhang, L. *Proc. Natl. Acad. Sci. U. S. A.* **2011**, *108*, 10980–10985. doi:10.1073/pnas.1106634108
50. Gareev, K. G.; Grouzdev, D. S.; Kozaieva, V. V.; Sitkov, N. O.; Gao, H.; Zimina, T. M.; Shevtsov, M. *Nanomaterials* **2022**, *12*, 2485. doi:10.3390/nano12142485
51. Schöttler, S.; Becker, G.; Winzen, S.; Steinbach, T.; Mohr, K.; Landfester, K.; Mailänder, V.; Wurm, F. R. *Nat. Nanotechnol.* **2016**, *11*, 372–377. doi:10.1038/nnano.2015.330
52. Agnello, L.; Camorani, S.; Fedele, M.; Cerchia, L. *Explor. Targeted Anti-Tumor Ther.* **2021**, *2*, 107–121. doi:10.37349/etat.2021.00035
53. Oroojalian, F.; Beygi, M.; Baradaran, B.; Mokhtarzadeh, A.; Shahbazi, M.-A. *Small* **2021**, *17*, 2006484. doi:10.1002/sml.202006484
54. Muthukumar, S.; Kentish, S. E.; Stevens, G. W.; Ashokkumar, M. *Rev. Chem. Eng.* **2006**, *22*, 155–194. doi:10.1515/revce.2006.22.3.155
55. Whitney, K. E.; Dornan, G. J.; King, J.; Chahla, J.; Evans, T. A.; Philippon, M. J.; LaPrade, R. F.; Huard, J. *Biomedicines* **2021**, *9*, 1403. doi:10.3390/biomedicines9101403
56. Pfeifer, C. R.; Vashisth, M.; Xia, Y.; Discher, D. E. *Essays Biochem.* **2019**, *63*, 569–577. doi:10.1042/ebc20190007
57. Savchenko, I. V.; Zlotnikov, I. D.; Kudryashova, E. V. *Biomimetics* **2023**, *8*, 543. doi:10.3390/biomimetics8070543
58. Qin, X.; Zhu, L.; Zhong, Y.; Wang, Y.; Luo, X.; Li, J.; Yan, F.; Wu, G.; Qiu, J.; Wang, G.; Qu, K.; Zhang, K.; Wu, W. *Chem. Sci.* **2024**, *15*, 7524–7544. doi:10.1039/d4sc00761a
59. Shi, M.; Shen, K.; Yang, B.; Zhang, P.; Lv, K.; Qi, H.; Wang, Y.; Li, M.; Yuan, Q.; Zhang, Y. *Theranostics* **2021**, *11*, 2349–2363. doi:10.7150/thno.48407
60. Liu, L.; Bai, X.; Martikainen, M.-V.; Kårlund, A.; Roponen, M.; Xu, W.; Hu, G.; Tasciotti, E.; Lehto, V.-P. *Nat. Commun.* **2021**, *12*, 5726. doi:10.1038/s41467-021-26052-x
61. Naskar, A.; Cho, H.; Lee, S.; Kim, K.-s. *Pharmaceutics* **2021**, *13*, 1887. doi:10.3390/pharmaceutics13111887
62. Aryal, S.; Hu, C.-M. J.; Fang, R. H.; Dehaini, D.; Carpenter, C.; Zhang, D.-E.; Zhang, L. *Nanomedicine (London, U. K.)* **2013**, *8*, 1271–1280. doi:10.2217/nnm.12.153
63. Fukuta, T.; Kogure, K. *Chem. Pharm. Bull.* **2022**, *70*, 334–340. doi:10.1248/cpb.c21-00961

64. Panico, S.; Capolla, S.; Bozzer, S.; Toffoli, G.; Dal Bo, M.; Macor, P. *Pharmaceutics* **2022**, *14*, 2605. doi:10.3390/pharmaceutics14122605
65. Xia, Q.; Zhang, Y.; Li, Z.; Hou, X.; Feng, N. *Acta Pharm. Sin. B* **2019**, *9*, 675–689. doi:10.1016/j.apsb.2019.01.011
66. Parodi, A.; Quattrocchi, N.; van de Ven, A. L.; Chiappini, C.; Evangelopoulos, M.; Martinez, J. O.; Brown, B. S.; Khaled, S. Z.; Yazdi, I. K.; Enzo, M. V.; Isenhardt, L.; Ferrari, M.; Tasciotti, E. *Nat. Nanotechnol.* **2013**, *8*, 61–68. doi:10.1038/nnano.2012.212
67. Liu, Y.; Yu, Y.; Wang, M.; Zhang, C.; Li, C. *Nanomedicine (London, U. K.)* **2023**, *18*, 485–500. doi:10.2217/nnm-2022-0211
68. Gao, D.; Guo, X.; Zhang, X.; Chen, S.; Wang, Y.; Chen, T.; Huang, G.; Gao, Y.; Tian, Z.; Yang, Z. *Mater. Today Bio* **2020**, *5*, 100035. doi:10.1016/j.mtbio.2019.100035
69. Majumder, J.; Minko, T. *Expert Opin. Drug Delivery* **2021**, *18*, 205–227. doi:10.1080/17425247.2021.1828339
70. Fang, R. H.; Gao, W.; Zhang, L. *Nat. Rev. Clin. Oncol.* **2023**, *20*, 33–48. doi:10.1038/s41571-022-00699-x
71. Jiang, Z.; Jiang, X.; Chen, S.; Lai, Y.; Wei, X.; Li, B.; Lin, S.; Wang, S.; Wu, Q.; Liang, Q.; Liu, Q.; Peng, M.; Yu, F.; Weng, J.; Du, X.; Pei, D.; Liu, P.; Yao, Y.; Xue, P.; Li, P. *Front. Immunol.* **2017**, *7*, 690. doi:10.3389/fimmu.2016.00690
72. Ma, W.; Zhu, D.; Li, J.; Chen, X.; Xie, W.; Jiang, X.; Wu, L.; Wang, G.; Xiao, Y.; Liu, Z.; Wang, F.; Li, A.; Shao, D.; Dong, W.; Liu, W.; Yuan, Y. *Theranostics* **2020**, *10*, 1281–1295. doi:10.7150/thno.40291
73. Abd Allah, N. H.; Abouelmagd, S. A. *Expert Opin. Drug Delivery* **2017**, *14*, 201–214. doi:10.1080/17425247.2016.1213238
74. Moku, G.; Gopalsamuthiram, V. R.; Hoye, T. R.; Panyam, J. Surface modification of nanoparticles: methods and applications. In *Surface Modification of Polymers: Methods and Applications*; Pinson, J.; Thiry, D., Eds.; Wiley-VCH: Weinheim, Germany, 2019; pp 317–346. doi:10.1002/9783527819249.ch11
75. Yüce, M.; Kurt, H. *RSC Adv.* **2017**, *7*, 49386–49403. doi:10.1039/c7ra10479k
76. Siafaka, P. I.; Üstündağ Okur, N.; Karavas, E.; Bikiaris, D. N. *Int. J. Mol. Sci.* **2016**, *17*, 1440. doi:10.3390/ijms17091440
77. Hafsi, M.; Preveral, S.; Hoog, C.; Héroult, J.; Perrier, G. A.; Lefèvre, C. T.; Michel, H.; Pignol, D.; Doyen, J.; Pourcher, T.; Humbert, O.; Thariat, J.; Cambien, B. *Nanomedicine (N. Y., NY, U. S.)* **2020**, *23*, 102084. doi:10.1016/j.nano.2019.102084
78. Chen, L.; Hong, W.; Ren, W.; Xu, T.; Qian, Z.; He, Z. *Signal Transduction Targeted Ther.* **2021**, *6*, 225. doi:10.1038/s41392-021-00631-2
79. Wu, J. *J. Pers. Med.* **2021**, *11*, 771. doi:10.3390/jpm11080771
80. Sindhvani, S.; Syed, A. M.; Ngai, J.; Kingston, B. R.; Maiorino, L.; Rothschild, J.; MacMillan, P.; Zhang, Y.; Rajesh, N. U.; Hoang, T.; Wu, J. L. Y.; Wilhelm, S.; Zilman, A.; Gadde, S.; Sulaiman, A.; Ouyang, B.; Lin, Z.; Wang, L.; Egeblad, M.; Chan, W. C. W. *Nat. Mater.* **2020**, *19*, 566–575. doi:10.1038/s41563-019-0566-2
81. Zhang, Y.; Yue, X.; Yang, S.; Li, X.; Cui, L.; Cui, X.; Shi, Y.; Liu, Z.; Guo, X.; Li, Y. *J. Mater. Chem. B* **2022**, *10*, 5035–5044. doi:10.1039/d2tb00748g
82. Zhang, L.; Wang, Z.; Zhang, Y.; Cao, F.; Dong, K.; Ren, J.; Qu, X. *ACS Nano* **2018**, *12*, 10201–10211. doi:10.1021/acsnano.8b05200
83. Ding, H.; Lv, Y.; Ni, D.; Wang, J.; Tian, Z.; Wei, W.; Ma, G. *Nanoscale* **2015**, *7*, 9806–9815. doi:10.1039/c5nr02470f
84. Rao, L.; Bu, L.-L.; Xu, J.-H.; Cai, B.; Yu, G.-T.; Yu, X.; He, Z.; Huang, Q.; Li, A.; Guo, S.-S.; Zhang, W.-F.; Liu, W.; Sun, Z.-J.; Wang, H.; Wang, T.-H.; Zhao, X.-Z. *Small* **2015**, *11*, 6225–6236. doi:10.1002/smll.201502388
85. Xu, L.; Xu, M.; Sun, X.; Feliu, N.; Feng, L.; Parak, W. J.; Liu, S. *ACS Nano* **2023**, *17*, 2039–2052. doi:10.1021/acsnano.2c07295
86. Prajapati, S.; Hinchliffe, T.; Roy, V.; Shah, N.; Jones, C. N.; Obaid, G. *Pharmaceutics* **2021**, *13*, 786. doi:10.3390/pharmaceutics13060786
87. Wu, H.-H.; Zhou, Y.; Tabata, Y.; Gao, J.-Q. *J. Controlled Release* **2019**, *294*, 102–113. doi:10.1016/j.jconrel.2018.12.019
88. Feng, J.; Wang, S.; Wang, Y.; Wang, L. *J. Nanopart. Res.* **2020**, *22*, 176. doi:10.1007/s11051-020-04915-6
89. Harjunpää, H.; Llort Asens, M.; Guenther, C.; Fagerholm, S. C. *Front. Immunol.* **2019**, *10*, 1078. doi:10.3389/fimmu.2019.01078
90. Zhou, X.; Zhu, H.; Luo, C.; Xiao, H.; Zou, X.; Zou, J.; Zhang, G. *Front. Oncol.* **2023**, *13*, 1165073. doi:10.3389/fonc.2023.1165073
91. Yao, H.; Veine, D. M.; Zeng, Z.-Z.; Fay, K. S.; Staszewski, E. D.; Livant, D. L. *Clin. Exp. Metastasis* **2010**, *27*, 173–184. doi:10.1007/s10585-010-9316-1
92. Sprouse, M. L.; Welte, T.; Boral, D.; Liu, H. N.; Yin, W.; Vishnoi, M.; Goswami-Sewell, D.; Li, L.; Pei, G.; Jia, P.; Glitza-Oliva, I. C.; Marchetti, D. *Int. J. Mol. Sci.* **2019**, *20*, 1916. doi:10.3390/ijms20081916
93. Matsumura, Y.; Ito, Y.; Mezawa, Y.; Sulidan, K.; Daigo, Y.; Hiraga, T.; Mogushi, K.; Wali, N.; Suzuki, H.; Itoh, T.; Miyagi, Y.; Yokose, T.; Shimizu, S.; Takano, A.; Terao, Y.; Saeki, H.; Ozawa, M.; Abe, M.; Takeda, S.; Okumura, K.; Habu, S.; Hino, O.; Takeda, K.; Hamada, M.; Orimo, A. *Life Sci. Alliance* **2019**, *2*, e201900425. doi:10.26508/lsa.201900425
94. Hu, C.-L.; Zhang, Y.-J.; Zhang, X.-F.; Fei, X.; Zhang, H.; Li, C.-G.; Sun, B. *OncoTargets Ther.* **2021**, *14*, 2673–2688. doi:10.2147/ott.s298427
95. Torkhovskaya, T. I.; Kostryukova, L. V.; Tereshkina, Y. A.; Tikhonova, E. G.; Morozevich, G. E.; Plutinskaya, A. D.; Lupatov, A. Y.; Pankratov, A. A. *Biomed. Pharmacother.* **2021**, *134*, 111154. doi:10.1016/j.biopha.2020.111154
96. Cui, Y.; Sun, J.; Hao, W.; Chen, M.; Wang, Y.; Xu, F.; Gao, C. *Front. Oncol.* **2020**, *10*, 563938. doi:10.3389/fonc.2020.563938
97. Wu, K.-L.; Huang, E.-Y.; Yeh, W.-L.; Hsiao, C.-C.; Kuo, C.-M. *Oncotarget* **2017**, *8*, 61935–61943. doi:10.18632/oncotarget.18721
98. Beh, C. Y.; Prajnamitra, R. P.; Chen, L.-L.; Hsieh, P. C.-H. *Molecules* **2021**, *26*, 5052. doi:10.3390/molecules26165052
99. Xu, Y.; Guo, Y.; Zhang, C.; Zhan, M.; Jia, L.; Song, S.; Jiang, C.; Shen, M.; Shi, X. *ACS Nano* **2022**, *16*, 984–996. doi:10.1021/acsnano.1c08585
100. Gdowski, A. S.; Lampe, J. B.; Lin, V. J. T.; Joshi, R.; Wang, Y.-C.; Mukerjee, A.; Vishwanatha, J. K.; Ranjan, A. P. *ACS Appl. Nano Mater.* **2019**, *2*, 6249–6257. doi:10.1021/acsanm.9b01226
101. Sun, H.; Su, J.; Meng, Q.; Yin, Q.; Chen, L.; Gu, W.; Zhang, P.; Zhang, Z.; Yu, H.; Wang, S.; Li, Y. *Adv. Mater. (Weinheim, Ger.)* **2016**, *28*, 9581–9588. doi:10.1002/adma.201602173
102. Wang, H.; Wu, J.; Williams, G. R.; Fan, Q.; Niu, S.; Wu, J.; Xie, X.; Zhu, L.-M. *J. Nanobiotechnol.* **2019**, *17*, 60. doi:10.1186/s12951-019-0494-y
103. Mitchell, M. J.; Castellanos, C. A.; King, M. R. *J. Biomed. Mater. Res., Part A* **2015**, *103*, 3407–3418. doi:10.1002/jbm.a.35445
104. Cui, Y.; Liu, J.; Cui, L.; Wei, C.; Xu, M.; Wu, Z.; Guo, Y.; Mi, P. *Nano Today* **2024**, *57*, 102380. doi:10.1016/j.nantod.2024.102380
105. Zhang, F.; Luo, W.; Min, Z.; Wu, L.; Wang, Z.; Wang, Y.; Liao, W.; Liu, Y.; Chen, W.; Wen, L. *BMC Cancer* **2025**, *25*, 1071. doi:10.1186/s12885-025-14433-0

106. Li, Y.; Ke, J.; Jia, H.; Ren, J.; Wang, L.; Zhang, Z.; Wang, C. *Colloids Surf., B* **2023**, *222*, 113131. doi:10.1016/j.colsurfb.2023.113131
107. Wu, Q.; Chen, L.; Huang, X.; Lin, J.; Gao, J.; Yang, G.; Wu, Y.; Wang, C.; Kang, X.; Yao, Y.; Wang, Y.; Xue, M.; Luan, X.; Chen, X.; Zhang, Z.; Sun, S. *Int. J. Oral Sci.* **2023**, *15*, 9. doi:10.1038/s41368-022-00211-2
108. Wang, D.; Dong, H.; Li, M.; Cao, Y.; Yang, F.; Zhang, K.; Dai, W.; Wang, C.; Zhang, X. *ACS Nano* **2018**, *12*, 5241–5252. doi:10.1021/acsnano.7b08355
109. He, H.; Guo, C.; Wang, J.; Korzun, W. J.; Wang, X.-Y.; Ghosh, S.; Yang, H. *Nano Lett.* **2018**, *18*, 6164–6174. doi:10.1021/acs.nanolett.8b01892
110. Zhang, T.; Bai, L.; You, R.; Yang, M.; Chen, Q.; Cheng, Y.; Qian, Z.; Wang, Y.; Liu, Y. *J. Mater. Chem. B* **2024**, *12*, 5465–5478. doi:10.1039/d3tb02919k
111. Wu, Q.; Tong, L.; Zou, Z.; Li, Y.; An, J.; Shen, W.; Gao, Y.; Liu, Y.; Wu, C. *Mater. Des.* **2022**, *219*, 110818. doi:10.1016/j.matdes.2022.110818
112. Zhang, Y.; Ma, N.; Luo, C.; Zhu, J.; Bao, C. *RSC Adv.* **2020**, *10*, 9378–9386. doi:10.1039/c9ra08926h
113. Krishnan, N.; Jiang, Y.; Zhou, J.; Mohapatra, A.; Peng, F.-X.; Duan, Y.; Holay, M.; Chekuri, S.; Guo, Z.; Gao, W.; Fang, R. H.; Zhang, L. *Nat. Nanotechnol.* **2024**, *19*, 345–353. doi:10.1038/s41565-023-01533-w
114. Wang, Y.; Wang, D.; Zhang, Y.; Xu, H.; Shen, L.; Cheng, J.; Xu, X.; Tan, H.; Chen, X.; Li, J. *Bioact. Mater.* **2023**, *22*, 239–253. doi:10.1016/j.bioactmat.2022.09.025
115. Kumar, M. A.; Baba, S. K.; Sadida, H. Q.; Marzooqi, S. A.; Jerobin, J.; Altemani, F. H.; Algehainy, N.; Alanazi, M. A.; Abou-Samra, A.-B.; Kumar, R.; Al-Shabeeb Akil, A. S.; Macha, M. A.; Mir, R.; Bhat, A. A. *Signal Transduction Targeted Ther.* **2024**, *9*, 27. doi:10.1038/s41392-024-01735-1
116. Vader, P.; Mol, E. A.; Pasterkamp, G.; Schiffelers, R. M. *Adv. Drug Delivery Rev.* **2016**, *106*, 148–156. doi:10.1016/j.addr.2016.02.006
117. Xia, Y.; Zhang, J.; Liu, G.; Wolfram, J. *Adv. Mater. (Weinheim, Ger.)* **2024**, *36*, 2403199. doi:10.1002/adma.202403199
118. Ramos-Zaldívar, H. M.; Polakovicova, I.; Salas-Huenuleo, E.; Corvalán, A. H.; Kogan, M. J.; Yefi, C. P.; Andía, M. E. *Fluids Barriers CNS* **2022**, *19*, 60. doi:10.1186/s12987-022-00359-3
119. Nguyen Cao, T. G.; Kang, J. H.; Kang, S. J.; Truong Hoang, Q.; Kang, H. C.; Rhee, W. J.; Zhang, Y. S.; Ko, Y. T.; Shim, M. S. *Acta Pharm. Sin. B* **2023**, *13*, 3834–3848. doi:10.1016/j.apsb.2023.03.023
120. Wang, J.; Xing, K.; Zhang, G.; Li, Z.; Ding, X.; Leong, D. T. *ACS Nano* **2025**, *19*, 8433–8461. doi:10.1021/acsnano.4c16854
121. Guo, R.; Jiang, D.; Gai, Y.; Qian, R.; Zhu, Z.; Gao, Y.; Jing, B.; Yang, B.; Lan, X.; An, R. *Eur. J. Nucl. Med. Mol. Imaging* **2023**, *50*, 508–524. doi:10.1007/s00259-022-05978-4
122. Claridge, B.; Lozano, J.; Poh, Q. H.; Greening, D. W. *Front. Cell Dev. Biol.* **2021**, *9*, 734720. doi:10.3389/fcell.2021.734720
123. Guo, Q.; Wang, S.; Xu, R.; Tang, Y.; Xia, X. *RSC Adv.* **2024**, *14*, 10608–10637. doi:10.1039/d4ra01026d
124. Li, J.; Wang, X.; Zheng, D.; Lin, X.; Wei, Z.; Zhang, D.; Li, Z.; Zhang, Y.; Wu, M.; Liu, X. *Biomater. Sci.* **2018**, *6*, 1834–1845. doi:10.1039/c8bm00343b
125. Yang, J.; Teng, Y.; Fu, Y.; Zhang, C. *Int. J. Nanomed.* **2019**, *14*, 5061–5071. doi:10.2147/ijn.s202910
126. Li, S.-Y.; Cheng, H.; Qiu, W.-X.; Zhang, L.; Wan, S.-S.; Zeng, J.-Y.; Zhang, X.-Z. *Biomaterials* **2017**, *142*, 149–161. doi:10.1016/j.biomaterials.2017.07.026
127. Li, Z.; Li, X.; Lu, Y.; Zhu, X.; Zheng, W.; Chen, K.; Liu, S.; Wu, J.; Guan, W. *Small* **2024**, *20*, 2305174. doi:10.1002/sml.202305174
128. Gao, G.; Che, J.; Xu, P.; Chen, B.; Zhao, Y. *Aggregate* **2024**, *5*, e631. doi:10.1002/agt.2.631
129. Chen, Y.; Zhi, S.; Ou, J.; Gao, J.; Zheng, L.; Huang, M.; Du, S.; Shi, L.; Tu, Y.; Cheng, K. *ACS Nano* **2023**, *17*, 16620–16632. doi:10.1021/acsnano.3c02724
130. Nguyen, P. H. D.; Jayasinghe, M. K.; Le, A. H.; Peng, B.; Le, M. T. N. *ACS Nano* **2023**, *17*, 5187–5210. doi:10.1021/acsnano.2c11965
131. Miao, Y.; Yang, Y.; Guo, L.; Chen, M.; Zhou, X.; Zhao, Y.; Nie, D.; Gan, Y.; Zhang, X. *ACS Nano* **2022**, *16*, 6527–6540. doi:10.1021/acsnano.2c00893
132. Glassman, P. M.; Villa, C. H.; Marcos-Contreras, O. A.; Hood, E. D.; Walsh, L. R.; Greineder, C. F.; Myerson, J. W.; Shuvaeva, T.; Puentes, L.; Brenner, J. S.; Siegel, D. L.; Muzykantov, V. R. *Bioconjugate Chem.* **2022**, *33*, 1286–1294. doi:10.1021/acs.bioconjchem.2c00196
133. Oronsky, B.; Carter, C.; Reid, T.; Brinkhaus, F.; Knox, S. J. *Semin. Oncol.* **2020**, *47*, 117–124. doi:10.1053/j.seminoncol.2020.05.009
134. Wang, X.; Li, P.; Jing, X.; Zhou, Y.; Shao, Y.; Zheng, M.; Wang, J.; Ran, H.; Tang, H. *Front. Oncol.* **2022**, *12*, 864444. doi:10.3389/fonc.2022.864444
135. Su, J.; Sun, H.; Meng, Q.; Yin, Q.; Tang, S.; Zhang, P.; Chen, Y.; Zhang, Z.; Yu, H.; Li, Y. *Adv. Funct. Mater.* **2016**, *26*, 1243–1252. doi:10.1002/adfm.201504780
136. Xie, H.; Li, W.; Liu, H.; Chen, Y.; Ma, M.; Wang, Y.; Luo, Y.; Song, D.; Hou, Q.; Lu, W.; Bai, Y.; Li, B.; Ma, J.; Huang, C.; Yang, T.; Liu, Z.; Zhao, X.; Ding, P. *Small* **2022**, *18*, 2201933. doi:10.1002/sml.202201933
137. Su, J.; Sun, H.; Meng, Q.; Zhang, P.; Yin, Q.; Li, Y. *Theranostics* **2017**, *7*, 523–537. doi:10.7150/thno.17259
138. Pei, Q.; Hu, X.; Zheng, X.; Liu, S.; Li, Y.; Jing, X.; Xie, Z. *ACS Nano* **2018**, *12*, 1630–1641. doi:10.1021/acsnano.7b08219
139. Wang, P.; Wang, X.; Luo, Q.; Li, Y.; Lin, X.; Fan, L.; Zhang, Y.; Liu, J.; Liu, X. *Theranostics* **2019**, *9*, 369–380. doi:10.7150/thno.29817
140. Yang, Q.; Xiao, Y.; Yin, Y.; Li, G.; Peng, J. *Mol. Pharmaceutics* **2019**, *16*, 3208–3220. doi:10.1021/acs.molpharmaceut.9b00413
141. Kong, C.; Xu, B.; Qiu, G.; Wei, M.; Zhang, M.; Bao, S.; Tang, J.; Li, L.; Liu, J. *Int. J. Nanomed.* **2022**, *17*, 5391–5411. doi:10.2147/ijn.s373282
142. Wang, M.; Xin, Y.; Cao, H.; Li, W.; Hua, Y.; Webster, T. J.; Zhang, C.; Tang, W.; Liu, Z. *Biomater. Sci.* **2021**, *9*, 1088–1103. doi:10.1039/d0bm01164a
143. Haque, N.; Fareez, I. M.; Fong, L. F.; Mandal, C.; Kasim, N. H. A.; Kacharaju, K. R.; Soesilawati, P. *World J. Stem Cells* **2020**, *12*, 938–951. doi:10.4252/wjsc.v12.i9.938
144. Ouyang, X.; Wang, X.; Kraatz, H.-B.; Ahmadi, S.; Gao, J.; Lv, Y.; Sun, X.; Huang, Y. *Biomater. Sci.* **2020**, *8*, 1160–1170. doi:10.1039/c9bm01401b
145. Gao, C.; Lin, Z.; Wu, Z.; Lin, X.; He, Q. *ACS Appl. Mater. Interfaces* **2016**, *8*, 34252–34260. doi:10.1021/acsnano.4c16854
146. Lopes, J.; Lopes, D.; Pereira-Silva, M.; Peixoto, D.; Veiga, F.; Hamblin, M. R.; Conde, J.; Corbo, C.; Zare, E. N.; Ashrafizadeh, M.; Tay, F. R.; Chen, C.; Donnelly, R. F.; Wang, X.; Makvandi, P.; Paiva-Santos, A. C. *Small Methods* **2022**, *6*, 2200289. doi:10.1002/smt.202200289

147. Yin, T.; Fan, Q.; Hu, F.; Ma, X.; Yin, Y.; Wang, B.; Kuang, L.; Hu, X.; Xu, B.; Wang, Y. *Nano Lett.* **2022**, *22*, 6606–6614. doi:10.1021/acs.nanolett.2c01863
148. Wang, J.; Gu, X.; Ouyang, Y.; Chu, L.; Xu, M.; Wang, K.; Tong, X. *Int. J. Nanomed.* **2021**, *16*, 1175–1187. doi:10.2147/ijn.s288636
149. Ma, X.; Kuang, L.; Yin, Y.; Tang, L.; Zhang, Y.; Fan, Q.; Wang, B.; Dong, Z.; Wang, W.; Yin, T.; Wang, Y. *ACS Nano* **2023**, *17*, 2341–2355. doi:10.1021/acsnano.2c09033
150. Li, X.; Zhu, T.; Wang, R.; Chen, J.; Tang, L.; Huo, W.; Huang, X.; Cao, Q. *Adv. Mater. (Weinheim, Ger.)* **2023**, *35*, 2211138. doi:10.1002/adma.202211138
151. Kang, M.; Hong, J.; Jung, M.; Kwon, S. P.; Song, S. Y.; Kim, H. Y.; Lee, J.-R.; Kang, S.; Han, J.; Koo, J.-H.; Ryu, J. H.; Lim, S.; Sohn, H. S.; Choi, J.-M.; Doh, J.; Kim, B.-S. *Adv. Mater. (Weinheim, Ger.)* **2020**, *32*, 2003368. doi:10.1002/adma.202003368
152. Raza, F.; Zafar, H.; Khan, A. U.; Hatami Kahkesh, K. *Mater. Chem. Horiz.* **2022**, *1*, 199–217. doi:10.22128/mch.2022.611.1028
153. Deng, G.; Sun, Z.; Li, S.; Peng, X.; Li, W.; Zhou, L.; Ma, Y.; Gong, P.; Cai, L. *ACS Nano* **2018**, *12*, 12096–12108. doi:10.1021/acsnano.8b05292
154. Wang, S.; Duan, Y.; Zhang, Q.; Komarla, A.; Gong, H.; Gao, W.; Zhang, L. *Small Struct.* **2020**, *1*, 2000018. doi:10.1002/sstr.202000018
155. Yu, Y.; Peng, Y.; Shen, W.-T.; Zhou, Z.; Kai, M.; Gao, W.; Zhang, L. *Small Struct.* **2024**, *5*, 2300473. doi:10.1002/sstr.202300473
156. Tian, Y.; Zhao, Y.; Liu, W.; Liu, Y.; Tang, Y.; Teng, Z.; Zhang, C.; Wang, S.; Lu, G. *RSC Adv.* **2018**, *8*, 32200–32210. doi:10.1039/c8ra04663h
157. Bhaumik, J.; Gogja, G.; Kirar, S.; Vijay, L.; Thakur, N. S.; Banerjee, U. C.; Laha, J. K. *New J. Chem.* **2016**, *40*, 724–731. doi:10.1039/c5nj02056e
158. Li, H.; Zhu, L.; Zhang, Y.; Yang, L.; Wu, W.; Yang, D. *J. Controlled Release* **2024**, *366*, 28–43. doi:10.1016/j.jconrel.2023.12.039
159. Li, J.; Wang, S.; Fontana, F.; Tapeinos, C.; Shahbazi, M.-A.; Han, H.; Santos, H. A. *Bioact. Mater.* **2023**, *23*, 471–507. doi:10.1016/j.bioactmat.2022.11.013
160. Zhang, X.; Wang, X.; Zhong, W.; Ren, X.; Sha, X.; Fang, X. *Int. J. Nanomed.* **2016**, 1643–1661. doi:10.2147/ijn.s101030
161. Palanikumar, L.; Al-Hosani, S.; Kalmouni, M.; Nguyen, V. P.; Ali, L.; Pasricha, R.; Barrera, F. N.; Magzoub, M. *Commun. Biol.* **2020**, *3*, 95. doi:10.1038/s42003-020-0817-4
162. Shi, X.; Yang, W.; Ma, Q.; Lu, Y.; Xu, Y.; Bian, K.; Liu, F.; Shi, C.; Wang, H.; Shi, Y.; Zhang, B. *Theranostics* **2020**, *10*, 11607–11621. doi:10.7150/thno.46228
163. Ding, L.; Wu, Y.; Wu, M.; Zhao, Q.; Li, H.; Liu, J.; Liu, X.; Zhang, X.; Zeng, Y. *ACS Appl. Mater. Interfaces* **2021**, *13*, 52435–52449. doi:10.1021/acssami.1c19096
164. Xu, X.; Cui, Y.; Bu, H.; Chen, J.; Li, Y.; Tang, G.; Wang, L.-Q. *J. Mater. Chem. B* **2018**, *6*, 1825–1833. doi:10.1039/c7tb03109b
165. Cai, X.; Xie, Z.; Ding, B.; Shao, S.; Liang, S.; Pang, M.; Lin, J. *Adv. Sci.* **2019**, *6*, 1900848. doi:10.1002/advs.201900848
166. Hou, X.; Tao, Y.; Li, X.; Pang, Y.; Yang, C.; Jiang, G.; Liu, Y. *Int. J. Nanomed.* **2020**, *15*, 10401–10416. doi:10.2147/ijn.s283515
167. Yin, J.; Cao, H.; Wang, H.; Sun, K.; Li, Y.; Zhang, Z. *Acta Pharm. Sin. B* **2020**, *10*, 2246–2257. doi:10.1016/j.apsb.2020.06.004
168. Wang, H.; Qu, R.; Chen, Q.; Zhang, T.; Chen, X.; Wu, B.; Chen, T. *J. Mater. Chem. B* **2022**, *10*, 5410–5421. doi:10.1039/d2tb00571a
169. Niu, N.; Zhang, Z.; Gao, X.; Chen, Z.; Li, S.; Li, J. *Chem. Eng. J.* **2018**, *352*, 818–827. doi:10.1016/j.cej.2018.07.049
170. Radi, R.; Cassina, A.; Hodara, R.; Quijano, C.; Castro, L. *Free Radical Biol. Med.* **2002**, *33*, 1451–1464. doi:10.1016/s0891-5849(02)01111-5
171. Beltrán, B.; Quintero, M.; García-Zaragozá, E.; O'Connor, E.; Esplugues, J. V.; Moncada, S. *Proc. Natl. Acad. Sci. U. S. A.* **2002**, *99*, 8892–8897. doi:10.1073/pnas.092259799
172. Ashton, T. M.; McKenna, W. G.; Kunz-Schughart, L. A.; Higgins, G. S. *Clin. Cancer Res.* **2018**, *24*, 2482–2490. doi:10.1158/1078-0432.ccr-17-3070
173. Lyu, C.; Lu, G.; Bao, W.; Li, F.; Wang, S.; Zhang, F.; Gao, X.; Kamiya, H.; Ma, G.; Wei, W. *Chem. Eng. J.* **2020**, *398*, 125453. doi:10.1016/j.cej.2020.125453
174. Pan, Y.; He, Y.; Zhao, X.; Pan, Y.; Meng, X.; Lv, Z.; Hu, Z.; Mou, X.; Cai, Y. *Adv. Healthcare Mater.* **2022**, *11*, 2200962. doi:10.1002/adhm.202200962
175. Liang, X.; Chen, M.; Bhattarai, P.; Hameed, S.; Dai, Z. *ACS Nano* **2020**, *14*, 13569–13583. doi:10.1021/acsnano.0c05617
176. Xavierselvan, M.; Cook, J.; Duong, J.; Diaz, N.; Homan, K.; Mallidi, S. *Photoacoustics* **2022**, *25*, 100306. doi:10.1016/j.pacs.2021.100306
177. Fang, H.; Gai, Y.; Wang, S.; Liu, Q.; Zhang, X.; Ye, M.; Tan, J.; Long, Y.; Wang, K.; Zhang, Y.; Lan, X. *J. Nanobiotechnol.* **2021**, *19*, 81. doi:10.1186/s12951-021-00827-2
178. Gao, S.; Zheng, P.; Li, Z.; Feng, X.; Yan, W.; Chen, S.; Guo, W.; Liu, D.; Yang, X.; Wang, S.; Liang, X.-J.; Zhang, J. *Biomaterials* **2018**, *178*, 83–94. doi:10.1016/j.biomaterials.2018.06.007
179. Min, H.; Wang, J.; Qi, Y.; Zhang, Y.; Han, X.; Xu, Y.; Xu, J.; Li, Y.; Chen, L.; Cheng, K.; Liu, G.; Yang, N.; Li, Y.; Nie, G. *Adv. Mater. (Weinheim, Ger.)* **2019**, *31*, 1808200. doi:10.1002/adma.201808200
180. Chen, H.; Zheng, D.; Pan, W.; Li, X.; Lv, B.; Gu, W.; Machuki, J. O.; Chen, J.; Liang, W.; Qin, K.; Greven, J.; Hildebrand, F.; Yu, Z.; Zhang, X.; Guo, K. *ACS Appl. Mater. Interfaces* **2021**, *13*, 19710–19725. doi:10.1021/acssami.1c03010
181. Zuo, H.; Tao, J.; Shi, H.; He, J.; Zhou, Z.; Zhang, C. *Acta Biomater.* **2018**, *80*, 296–307. doi:10.1016/j.actbio.2018.09.017
182. Li, X.; Wang, H.; Li, Z.; Li, D.; Lu, X.; Ai, S.; Dong, Y.; Liu, S.; Wu, J.; Guan, W. *Biomater. Res.* **2022**, *26*, 47. doi:10.1186/s40824-022-00296-0
183. Ren, H.; Liu, J.; Li, Y.; Wang, H.; Ge, S.; Yuan, A.; Hu, Y.; Wu, J. *Acta Biomater.* **2017**, *59*, 269–282. doi:10.1016/j.actbio.2017.06.035
184. Tang, Y.; Tang, T.; Li, Y.; Wu, J.; Liu, X.; Xiang, D.; Hu, X. *Int. J. Nanomed.* **2025**, *20*, 2743–2759. doi:10.2147/ijn.s508696
185. Li, C.; Yang, X.-Q.; An, J.; Cheng, K.; Hou, X.-L.; Zhang, X.-S.; Hu, Y.-G.; Liu, B.; Zhao, Y.-D. *Theranostics* **2020**, *10*, 867–879. doi:10.7150/thno.37930
186. Zhang, J.; Gu, B.; Wu, S.; Liu, L.; Gao, Y.; Yao, Y.; Yang, D.; Du, J.; Yang, C. *Pharmaceutics* **2023**, *15*, 2243. doi:10.3390/pharmaceutics15092243
187. Ke, Q.; Costa, M. *Mol. Pharmacol.* **2006**, *70*, 1469–1480. doi:10.1124/mol.106.027029
188. Broekgaarden, M.; Weijer, R.; van Gulik, T. M.; Hamblin, M. R.; Heger, M. *Cancer Metastasis Rev.* **2015**, *34*, 643–690. doi:10.1007/s10555-015-9588-7
189. Guo, R.; Sun, H.; Gobeze, H. B.; Jana, K.; Li, L.; Wu, Y.; Schanze, K. S.; Li, Z.; Song, F. *Nano Today* **2025**, *61*, 102596. doi:10.1016/j.nantod.2024.102596

190. Tada, D. B.; Baptista, M. S. *Front. Chem. (Lausanne, Switz.)* **2015**, *3*, 33. doi:10.3389/fchem.2015.00033
191. Udrea, A. M.; Smarandache, A.; Dinache, A.; Mares, C.; Nistorescu, S.; Avram, S.; Staicu, A. *Pharmaceutics* **2023**, *15*, 2124. doi:10.3390/pharmaceutics15082124
192. Alzeibak, R.; Mishchenko, T. A.; Shilyagina, N. Y.; Balalaeva, I. V.; Vedunova, M. V.; Krysko, D. V. *J. ImmunoTher. Cancer* **2021**, *9*, e001926. doi:10.1136/jitc-2020-001926
193. Krysko, D. V.; Garg, A. D.; Kaczmarek, A.; Krysko, O.; Agostinis, P.; Vandenabeele, P. *Nat. Rev. Cancer* **2012**, *12*, 860–875. doi:10.1038/nrc3380
194. Xi, Y.; Chen, L.; Tang, J.; Yu, B.; Shen, W.; Niu, X. *Immunol. Rev.* **2024**, *321*, 94–114. doi:10.1111/imr.13251
195. Garg, A. D.; Krysko, D. V.; Vandenabeele, P.; Agostinis, P. *Photochem. Photobiol. Sci.* **2011**, *10*, 670–680. doi:10.1039/c0pp00294a
196. Obeid, M.; Tesniere, A.; Ghiringhelli, F.; Fimia, G. M.; Apetoh, L.; Perfettini, J.-L.; Castedo, M.; Mignot, G.; Panaretakis, T.; Casares, N.; Métivier, D.; Larochette, N.; van Ender, P.; Ciccosanti, F.; Piacentini, M.; Zitvogel, L.; Kroemer, G. *Nat. Med.* **2007**, *13*, 54–61. doi:10.1038/nm1523
197. Kielbik, M.; Szulc-Kielbik, I.; Klink, M. *Cells* **2021**, *10*, 130. doi:10.3390/cells10010130
198. Elliott, M. R.; Chekeni, F. B.; Trampont, P. C.; Lazarowski, E. R.; Kadl, A.; Walk, S. F.; Park, D.; Woodson, R. I.; Ostankovich, M.; Sharma, P.; Lysiak, J. J.; Harden, T. K.; Leitinger, N.; Ravichandran, K. S. *Nature* **2009**, *461*, 282–286. doi:10.1038/nature08296
199. Martins, I.; Wang, Y.; Michaud, M.; Ma, Y.; Sukkurwala, A. Q.; Shen, S.; Kepp, O.; Métivier, D.; Galluzzi, L.; Perfettini, J.-L.; Zitvogel, L.; Kroemer, G. *Cell Death Differ.* **2014**, *21*, 79–91. doi:10.1038/cdd.2013.75
200. Yamazaki, T.; Hannani, D.; Poirier-Colame, V.; Ladoire, S.; Locher, C.; Sistigu, A.; Prada, N.; Adjemian, S.; Catani, J. P.; Freudenberg, M.; Galanos, C.; André, F.; Kroemer, G.; Zitvogel, L. *Cell Death Differ.* **2014**, *21*, 69–78. doi:10.1038/cdd.2013.72
201. Melcher, A.; Todryk, S.; Hardwick, N.; Ford, M.; Jacobson, M.; Vile, R. G. *Nat. Med.* **1998**, *4*, 581–587. doi:10.1038/nm0598-581
202. Korbek, M.; Sun, J.; Cecic, I. *Cancer Res.* **2005**, *65*, 1018–1026. doi:10.1158/0008-5472.1018.65.3
203. Rodríguez, M. E.; Cogno, I. S.; Sanabria, L. S. M.; Morán, Y. S.; Rivarola, V. A. *Photochem. Photobiol. Sci.* **2016**, *15*, 1090–1102. doi:10.1039/c6pp00097e
204. Mroz, P.; Hashmi, J. T.; Huang, Y.-Y.; Lange, N.; Hamblin, M. R. *Expert Rev. Clin. Immunol.* **2011**, *7*, 75–91. doi:10.1586/eci.10.81
205. Chou, W.; Sun, T.; Peng, N.; Wang, Z.; Chen, D.; Qiu, H.; Zhao, H. *Pharmaceutics* **2023**, *15*, 2617. doi:10.3390/pharmaceutics15112617
206. Tavakkoli Yarak, M.; Liu, B.; Tan, Y. N. *Nano-Micro Lett.* **2022**, *14*, 123. doi:10.1007/s40820-022-00856-y
207. Skovsen, E.; Snyder, J. W.; Lambert, J. D. C.; Ogilby, P. R. *J. Phys. Chem. B* **2005**, *109*, 8570–8573. doi:10.1021/jp051163i
208. Przygoda, M.; Bartusik-Aebischer, D.; Dynarowicz, K.; Cieślak, G.; Kawczyk-Krupka, A.; Aebischer, D. *Int. J. Mol. Sci.* **2023**, *24*, 16890. doi:10.3390/ijms242316890
209. Lennicke, C.; Rahn, J.; Lichtenfels, R.; Wessjohann, L. A.; Seliger, B. *Cell Commun. Signaling* **2015**, *13*, 39. doi:10.1186/s12964-015-0118-6
210. Bienert, G. P.; Chaumont, F. *Biochim. Biophys. Acta, Gen. Subj.* **2014**, *1840*, 1596–1604. doi:10.1016/j.bbagen.2013.09.017
211. Li, H.; Shen, J.; Zheng, C.; Zhu, P.; Yang, H.; Huang, Y.; Mao, X.; Yang, Z.; Hu, G.; Chen, Y. *Interdiscip. Med.* **2025**, *3*, e20240057. doi:10.1002/inmd.20240057
212. Gomes-da-Silva, L. C.; Zhao, L.; Bezu, L.; Zhou, H.; Sauvat, A.; Liu, P.; Durand, S.; Leduc, M.; Souquere, S.; Loos, F.; Mondragón, L.; Sveinbjörnsson, B.; Rekdal, Ø.; Boncompain, G.; Perez, F.; Arnaut, L. G.; Kepp, O.; Kroemer, G. *EMBO J.* **2018**, *37*, e98354. doi:10.15252/embj.201798354
213. Li, W.; Yang, J.; Luo, L.; Jiang, M.; Qin, B.; Yin, H.; Zhu, C.; Yuan, X.; Zhang, J.; Luo, Z.; Du, Y.; Li, Q.; Lou, Y.; Qiu, Y.; You, J. *Nat. Commun.* **2019**, *10*, 3349. doi:10.1038/s41467-019-11269-8
214. Turubanova, V. D.; Balalaeva, I. V.; Mishchenko, T. A.; Catanzaro, E.; Alzeibak, R.; Peskova, N. N.; Efimova, I.; Bachert, C.; Mitroshina, E. V.; Krysko, O.; Vedunova, M. V.; Krysko, D. V. *J. ImmunoTher. Cancer* **2019**, *7*, 350. doi:10.1186/s40425-019-0826-3
215. Chang, Q.; Wang, P.; Zeng, Q.; Wang, X. *Heliyon* **2024**, *10*, e28942. doi:10.1016/j.heliyon.2024.e28942
216. Huang, Y.; Li, X.; Zhang, Z.; Xiong, L.; Wang, Y.; Wen, Y. *Cancers* **2023**, *15*, 5043. doi:10.3390/cancers15205043
217. Wu, S.; Xing, D. J. *X-Ray Sci. Technol.* **2012**, *20*, 363–372. doi:10.3233/xst-2012-0344
218. Galluzzi, L.; Vitale, I.; Aaronson, S. A.; Abrams, J. M.; Adam, D.; Agostinis, P.; Alnemri, E. S.; Altucci, L.; Amelio, I.; Andrews, D. W.; Annicchiarico-Petruzzelli, M.; Antonov, A. V.; Arama, E.; Baehrecke, E. H.; Barlev, N. A.; Bazan, N. G.; Bernassola, F.; Bertrand, M. J. M.; Bianchi, K.; Blagosklonny, M. V.; Blomgren, K.; Borner, C.; Boya, P.; Brenner, C.; Campanella, M.; Candi, E.; Carmona-Gutierrez, D.; Cecconi, F.; Chan, F. K.-M.; Chandel, N. S.; Cheng, E. H.; Chipuk, J. E.; Cidlowski, J. A.; Ciechanover, A.; Cohen, G. M.; Conrad, M.; Cubillos-Ruiz, J. R.; Czabotar, P. E.; D'Angiolella, V.; Dawson, T. M.; Dawson, V. L.; De Laurenzi, V.; De Maria, R.; Debatin, K.-M.; DeBerardinis, R. J.; Deshmukh, M.; Di Daniele, N.; Di Virgilio, F.; Dixit, V. M.; Dixon, S. J.; Duckett, C. S.; Dynlacht, B. D.; El-Deiry, W. S.; Elrod, J. W.; Fimia, G. M.; Fulda, S.; García-Sáez, A. J.; Garg, A. D.; Garrido, C.; Gavathiotis, E.; Golstein, P.; Gottlieb, E.; Green, D. R.; Greene, L. A.; Gronemeyer, H.; Gross, A.; Hajnoczky, G.; Hardwick, J. M.; Harris, I. S.; Hengartner, M. O.; Hetz, C.; Ichijo, H.; Jäättelä, M.; Joseph, B.; Jost, P. J.; Juin, P. P.; Kaiser, W. J.; Karin, M.; Kaufmann, T.; Kepp, O.; Kimchi, A.; Kitsis, R. N.; Klionsky, D. J.; Knight, R. A.; Kumar, S.; Lee, S. W.; Lemasters, J. J.; Levine, B.; Linkermann, A.; Lipton, S. A.; Lockshin, R. A.; López-Otín, C.; Lowe, S. W.; Luedde, T.; Lugli, E.; MacFarlane, M.; Madeo, F.; Malewicz, M.; Malorni, W.; Manic, G.; Marine, J.-C.; Martin, S. J.; Martinou, J.-C.; Medema, J. P.; Mehlen, P.; Meier, P.; Melino, S.; Miao, E. A.; Molkenin, J. D.; Moll, U. M.; Muñoz-Pinedo, C.; Nagata, S.; Nuñez, G.; Oberst, A.; Oren, M.; Overholtzer, M.; Pagano, M.; Panaretakis, T.; Pasparakis, M.; Penninger, J. M.; Pereira, D. M.; Pervaiz, S.; Peter, M. E.; Piacentini, M.; Pinton, P.; Prehn, J. H. M.; Puthalakath, H.; Rabinovich, G. A.; Rehm, M.; Rizzuto, R.; Rodrigues, C. M. P.; Rubinsztein, D. C.; Rudel, T.; Ryan, K. M.; Sayan, E.; Scorrano, L.; Shao, F.; Shi, Y.; Silke, J.; Simon, H.-U.; Sistigu, A.; Stockwell, B. R.; Strasser, A.; Szabadkai, G.; Tait, S. W. G.; Tang, D.; Tavernarakis, N.; Thorburn, A.; Tsujimoto, Y.; Turk, B.; Vanden Berghe, T.; Vandenabeele, P.; Vander Heiden, M. G.; Villunger, A.; Virgin, H. W.; Vousden, K. H.; Vucic, D.; Wagner, E. F.; Walczak, H.; Wallach, D.; Wang, Y.; Wells, J. A.; Wood, W.; Yuan, J.; Zakeri, Z.; Zhivotovsky, B.; Zitvogel, L.; Melino, G.; Kroemer, G. *Cell Death Differ.* **2018**, *25*, 486–541. doi:10.1038/s41418-017-0012-4

219. Mishchenko, T.; Balalaeva, I.; Gorokhova, A.; Vedunova, M.; Krysko, D. V. *Cell Death Dis.* **2022**, *13*, 455. doi:10.1038/s41419-022-04851-4
220. Jin, K.; Luo, Z.; Zhang, B.; Pang, Z. *Acta Pharm. Sin. B* **2018**, *8*, 23–33. doi:10.1016/j.apsb.2017.12.002
221. Zhu, Z.; Scalfi-Happ, C.; Ryabova, A.; Gräfe, S.; Wiehe, A.; Peter, R.-U.; Loschenov, V.; Steiner, R.; Wittig, R. *J. Photochem. Photobiol., B* **2018**, *185*, 215–222. doi:10.1016/j.jphotobiol.2018.06.015
222. Ryabova, A.; Romanishkin, I.; Skobeltsin, A.; Markova, I.; Pominova, D.; Linkov, K.; Loschenov, V. *Photonics* **2022**, *9*, 961. doi:10.3390/photonics9120961
223. Jian, H.; Wang, X.; Song, P.; Wu, X.; Zheng, R.; Wang, Y.; Zhang, H. *Acta Biomater.* **2022**, *140*, 518–529. doi:10.1016/j.actbio.2021.12.014
224. Liu, H.; Lv, H.; Duan, X.; Du, Y.; Tang, Y.; Xu, W. *Int. J. Nanomed.* **2023**, *18*, 6915–6940. doi:10.2147/ijn.s430877
225. Kousis, P. C.; Henderson, B. W.; Maier, P. G.; Gollnick, S. O. *Cancer Res.* **2007**, *67*, 10501–10510. doi:10.1158/0008-5472.can-07-1778
226. Kabingu, E.; Vaughan, L.; Owczarczak, B.; Ramsey, K. D.; Gollnick, S. O. *Br. J. Cancer* **2007**, *96*, 1839–1848. doi:10.1038/sj.bjc.6603792
227. Gabrilovich, D. I.; Chen, H. L.; Girgis, K. R.; Cunningham, H. T.; Meny, G. M.; Nadaf, S.; Kavanaugh, D.; Carbone, D. P. *Nat. Med.* **1996**, *2*, 1096–1103. doi:10.1038/nm1096-1096
228. Brackett, C. M.; Gollnick, S. O. *Photochem. Photobiol. Sci.* **2011**, *10*, 649–652. doi:10.1039/c0pp00354a
229. Ashley, C. E.; Carnes, E. C.; Phillips, G. K.; Padilla, D.; Durfee, P. N.; Brown, P. A.; Hanna, T. N.; Liu, J.; Phillips, B.; Carter, M. B.; Carroll, N. J.; Jiang, X.; Dunphy, D. R.; Willman, C. L.; Petsev, D. N.; Evans, D. G.; Parikh, A. N.; Chackerian, B.; Wharton, W.; Peabody, D. S.; Brinker, C. J. *Nat. Mater.* **2011**, *10*, 389–397. doi:10.1038/nmat2992
230. Thirupathi, J.; Vijayan, V.; Park, I.-K.; Lee, S. E.; Rhee, J. H. *Front. Immunol.* **2024**, *15*, 1375767. doi:10.3389/fimmu.2024.1375767
231. Chen, C.; Song, M.; Du, Y.; Yu, Y.; Li, C.; Han, Y.; Yan, F.; Shi, Z.; Feng, S. *Nano Lett.* **2021**, *21*, 5522–5531. doi:10.1021/acs.nanolett.1c00818
232. Huang, X.; Wang, L.; Guo, H.; Zhang, W. *Bioact. Mater.* **2023**, *23*, 69–79. doi:10.1016/j.bioactmat.2022.09.027
233. Yoon, J.; Le, X. T.; Kim, J.; Lee, H.; Nguyen, N. T.; Lee, W. T.; Lee, E. S.; Oh, K. T.; Choi, H.-G.; Youn, Y. S. *J. Controlled Release* **2023**, *360*, 482–495. doi:10.1016/j.jconrel.2023.07.009
234. Dehaini, D.; Wei, X.; Fang, R. H.; Masson, S.; Angsantikul, P.; Luk, B. T.; Zhang, Y.; Ying, M.; Jiang, Y.; Kroll, A. V.; Gao, W.; Zhang, L. *Adv. Mater. (Weinheim, Ger.)* **2017**, *29*, 1606209. doi:10.1002/adma.201606209
235. Xu, L.; Gao, F.; Fan, F.; Yang, L. *Biomaterials* **2018**, *159*, 59–67. doi:10.1016/j.biomaterials.2017.12.028
236. Yang, Z.; Zhang, Y.; Wang, W.; Shi, X.; Cui, K.; Du, Y.; Ma, W.; Chen, Q. *Mater. Des.* **2025**, 114497. doi:10.1016/j.matdes.2025.114497
237. Zhang, Y.; He, Z.; Li, Y.; Xia, Q.; Li, Z.; Hou, X.; Feng, N. *Mater. Sci. Eng.: C* **2021**, *120*, 111670. doi:10.1016/j.msec.2020.111670
238. Cohen, B. A.; Bergkvist, M. J. *Photochem. Photobiol., B* **2013**, *121*, 67–74. doi:10.1016/j.jphotobiol.2013.02.013
239. Masarapu, H.; Patel, B. K.; Chariau, P. L.; Hu, H.; Gulati, N. M.; Carpenter, B. L.; Ghiladi, R. A.; Shukla, S.; Steinmetz, N. F. *Biomacromolecules* **2017**, *18*, 4141–4153. doi:10.1021/acs.biomac.7b01196
240. Wang, D.; Liu, C.; You, S.; Zhang, K.; Li, M.; Cao, Y.; Wang, C.; Dong, H.; Zhang, X. *ACS Appl. Mater. Interfaces* **2020**, *12*, 41138–41147. doi:10.1021/acsami.0c13169
241. Zhuang, W.-R.; Wang, Y.; Lei, Y.; Zuo, L.; Jiang, A.; Wu, G.; Nie, W.; Huang, L.-L.; Xie, H.-Y. *Nano Lett.* **2022**, *22*, 4491–4500. doi:10.1021/acs.nanolett.2c01280
242. Lan, Z.; Liu, W.-J.; Yin, W.-W.; Yang, S.-R.; Cui, H.; Zou, K.-L.; Cheng, G.-W.; Chen, H.; Han, Y.-H.; Rao, L.; Tian, R.; Li, L.-L.; Zhao, Y.-Y.; Yu, G.-T. *J. Nanobiotechnol.* **2024**, *22*, 174. doi:10.1186/s12951-024-02417-4
243. Liu, W.-L.; Zou, M.-Z.; Liu, T.; Zeng, J.-Y.; Li, X.; Yu, W.-Y.; Li, C.-X.; Ye, J.-J.; Song, W.; Feng, J.; Zhang, X.-Z. *Adv. Mater. (Weinheim, Ger.)* **2019**, *31*, 1900499. doi:10.1002/adma.201900499
244. Li, J.; Li, J.; He, J.; He, X.; Chen, D.; Dong, Z.; Xiong, L.; Bai, W.; Li, M.; Guo, R.; He, Q. *Nano Res.* **2024**, *17*, 9932–9941. doi:10.1007/s12274-024-6917-6
245. Zhou, Z.; Song, J.; Nie, L.; Chen, X. *Chem. Soc. Rev.* **2016**, *45*, 6597–6626. doi:10.1039/c6cs00271d
246. Qiu, H.; Kim, M. M.; Penjweini, R.; Finlay, J. C.; Busch, T. M.; Wang, T.; Guo, W.; Cengel, K. A.; Simone, C. B., II; Glatstein, E.; Zhu, T. C. *Photochem. Photobiol.* **2017**, *93*, 1115–1122. doi:10.1111/php.12719

License and Terms

This is an open access article licensed under the terms of the Beilstein-Institut Open Access License Agreement (<https://www.beilstein-journals.org/bjnano/terms>), which is identical to the Creative Commons Attribution 4.0 International License (<https://creativecommons.org/licenses/by/4.0>). The reuse of material under this license requires that the author(s), source and license are credited. Third-party material in this article could be subject to other licenses (typically indicated in the credit line), and in this case, users are required to obtain permission from the license holder to reuse the material.

The definitive version of this article is the electronic one which can be found at: <https://doi.org/10.3762/bjnano.17.27>